AD

Technical Report ARAEW-TR-08002

Incorporation of a Variable Discharge Coefficient for the Primary Orifice into the Benét Labs Recoil Analysis Model via Results from Quasi-Steady State Simulations Using Computational Fluid Dynamics

Ronald Gast
Steven Morris
Timothy Gedney

March 2008

ARMAMENT RESEARCH, DEVELOPMENT AND ENGINEERING CENTER
Armaments Engineering & Technology Center
Weapon Systems & Technology
Benét Laboratories

Approved for public release; distribution is unlimited.

The views, opinions, and/or findings contained in this report are those of the author(s) and should not be construed as an official Department of the Army position, policy, or decision, unless so designated by other documentation.

The citation in this report of the names of commercial firms or commercially available products or services does not constitute official endorsement by or approval of the U.S. Government.

Destroy this report when no longer needed by any method that will prevent disclosure of its contents or reconstruction of the document. Do not return to the originator.

REPORT DOCUMENTATION PAGE

Form Approved
OMB No. 0704-0188

1. REPORT DATE *(DD-MM-YYYY)*	2. REPORT TYPE	3. DATES COVERED *(From - To)*
xx-03-2008	Final	2008

4. TITLE AND SUBTITLE

Incorporation of a Variable Discharge Coefficient for the Primary Orifice into the Benét Labs Recoil Analysis Model via Results from Quasi-Steady State Simulations Using Computational Fluid Dynamics

5a. CONTRACT NUMBER

5b. GRANT NUMBER

5c. PROGRAM ELEMENT NUMBER

6. AUTHOR(S)

Gast, Ronald ; Morris, Steven ; Gedney, Timothy

5d. PROJECT NUMBER

5e. TASK NUMBER

5f. WORK UNIT NUMBER

7. PERFORMING ORGANIZATION NAME(S) AND ADDRESS(ES)

U.S. Army ARDEC, AETC
Benét Laboratories, AMSRD-AAR-AEW, B. 40
1 Buffington Street
Watervliet Arsenal, NY 12189-4000

8. PERFORMING ORGANIZATION REPORT NUMBER

ARAEW-TR-08002

9. SPONSORING/MONITORING AGENCY NAME(S) AND ADDRESS(ES)

U.S. Army ARDEC, AETC
Benét Laboratories, AMSRD-AAR-AEW, B. 40
1 Buffington Street
Watervliet Arsenal, NY 12189-4000

10. SPONSOR/MONITOR'S ACRONYM(S)

11. SPONSOR/MONITOR'S REPORT NUMBER(S)

12. DISTRIBUTION/AVAILABILITY STATEMENT

Approved for public release; distribution is unlimited.

13. SUPPLEMENTARY NOTES

14. ABSTRACT

The design and analysis of recoil systems for direct fire weapons has been conducted at Benét for the last 25 years. The model developed employs the Bernoulli Equation to establish the relationship between flow rate and back pressure within the internal paths and through the primary orifice of the recoil brake. This displacement varying orifice provides the throttling mechanism needed to generate back pressure which opposes the ballistic driving load and arrests the gun in recoil. An orifice is designed to maintain constant upstream pressure over the complete length of recoil, thus minimizing the load transferred to the gun support and vehicle. The equation which models this type of orifice requires an discharge coefficient (Cd) which 'lumps' all of the flow losses due to contraction and directional change of the fluid stream. This coefficient is constant regardless of fluid properties, flow regimes and geometries. Test data from firing tests and research experiments indicate that this may not be the case. This report presents the details of using an offline CFD analysis to establish the flow response characteristics of a typical recoil brake orifice and a methodology of incorporating these results via a lookup table of Cd values into the lumped parameter recoil analysis model.

15. SUBJECT TERMS

Recoil systems, Bernoilli equations, Ballistics, Recoil analysis

16. SECURITY CLASSIFICATION OF:			17. LIMITATION OF ABSTRACT	18. NUMBER OF PAGES	19a. NAME OF RESPONSIBLE PERSON
a. REPORT	b. ABSTRACT	c. THIS PAGE			19b. TELEPHONE NUMBER *(Include area code)*
U/L	U	U	U	95	

INSTRUCTIONS FOR COMPLETING SF 298

1. REPORT DATE. Full publication date, including day, month, if available. Must cite at least the year and be Year 2000 compliant, e.g. 30-06-1998; xx-06-1998; xx-xx-1998.

2. REPORT TYPE. State the type of report, such as final, technical, interim, memorandum, master's thesis, progress, quarterly, research, special, group study, etc.

3. DATES COVERED. Indicate the time during which the work was performed and the report was written, e.g., Jun 1997 - Jun 1998; 1-10 Jun 1996; May - Nov 1998; Nov 1998.

4. TITLE. Enter title and subtitle with volume number and part number, if applicable. On classified documents, enter the title classification in parentheses.

5a. CONTRACT NUMBER. Enter all contract numbers as they appear in the report, e.g. F33615-86-C-5169.

5b. GRANT NUMBER. Enter all grant numbers as they appear in the report, e.g. AFOSR-82-1234.

5c. PROGRAM ELEMENT NUMBER. Enter all program element numbers as they appear in the report, e.g. 61101A.

5d. PROJECT NUMBER. Enter all project numbers as they appear in the report, e.g. 1F665702D1257; ILIR.

5e. TASK NUMBER. Enter all task numbers as they appear in the report, e.g. 05; RF0330201; T4112.

5f. WORK UNIT NUMBER. Enter all work unit numbers as they appear in the report, e.g. 001; AFAPL30480105.

6. AUTHOR(S). Enter name(s) of person(s) responsible for writing the report, performing the research, or credited with the content of the report. The form of entry is the last name, first name, middle initial, and additional qualifiers separated by commas, e.g. Smith, Richard, J, Jr.

7. PERFORMING ORGANIZATION NAME(S) AND ADDRESS(ES). Self-explanatory.

8. PERFORMING ORGANIZATION REPORT NUMBER. Enter all unique alphanumeric report numbers assigned by the performing organization, e.g. BRL-1234; AFWL-TR-85-4017-Vol-21-PT-2.

9. SPONSORING/MONITORING AGENCY NAME(S) AND ADDRESS(ES). Enter the name and address of the organization(s) financially responsible for and monitoring the work.

10. SPONSOR/MONITOR'S ACRONYM(S). Enter, if available, e.g. BRL, ARDEC, NADC.

11. SPONSOR/MONITOR'S REPORT NUMBER(S). Enter report number as assigned by the sponsoring/ monitoring agency, if available, e.g. BRL-TR-829; -215.

12. DISTRIBUTION/AVAILABILITY STATEMENT. Use agency-mandated availability statements to indicate the public availability or distribution limitations of the report. If additional limitations/ restrictions or special markings are indicated, follow agency authorization procedures, e.g. RD/FRD, PROPIN, ITAR, etc. Include copyright information.

13. SUPPLEMENTARY NOTES. Enter information not included elsewhere such as: prepared in cooperation with; translation of; report supersedes; old edition number, etc.

14. ABSTRACT. A brief (approximately 200 words) factual summary of the most significant information.

15. SUBJECT TERMS. Key words or phrases identifying major concepts in the report.

16. SECURITY CLASSIFICATION. Enter security classification in accordance with security classification regulations, e.g. U, C, S, etc. If this form contains classified information, stamp classification level on the top and bottom of this page.

17. LIMITATION OF ABSTRACT. This block must be completed to assign a distribution limitation to the abstract. Enter UU (Unclassified Unlimited) or SAR (Same as Report). An entry in this block is necessary if the abstract is to be limited.

Title: Incorporation of a Variable Discharge Coefficient for the Primary Orifice into the Benét Labs Recoil Analysis Model via Results from Quasi-Steady State Simulations Using Computational Fluid Dynamics

Authors: Ronald Gast, Steven Morris, Timothy Gedney

ABBREVIATIONS & ACRONYMS

C_d	Discharge Coefficient
CFD	Computational Fluid Dynamics
DOE	Design of Experiments
fea	Finite Element Analysis
fem	Finite Element Methods
in	Inches
ms	Milliseconds
NASA	National Aeronautics and Space Administration
psi	Pounds per Square Inch
sec	Seconds

LIST OF FIGURES

LIST OF TABLES

ABSTRACT

The design and analysis of recoil systems for direct fire weapons has been conducted at Benét Labs for the last 25 years. The model developed employs the Bernoulli Equation to establish the relationship between flow rate and back pressure within the internal paths and through the primary orifice of the recoil brake. This displacement varying orifice provides the throttling mechanism needed to generate back pressure which opposes the ballistic driving load and arrests the gun in recoil. An orifice is designed to maintain constant upstream pressure over the complete length of recoil, thus minimizing the load transferred to the gun support and vehicle. The equation which models this type of orifice requires an discharge coefficient (C_d) which 'lumps' all of the flow losses due to contraction and directional change of the fluid stream. For the model developed at Benét Labs, this coefficient is constant regardless of fluid properties, flow regimes and geometries. Test data from firing tests and research experiments indicate that this may not be the case.

This report presents the details of using an offline CFD analysis to establish the flow response characteristics of a typical recoil brake orifice and a methodology of incorporating these results via a lookup table of C_d values into the lumped parameter recoil analysis model developed at Benét Labs. Although CFD analysis usually requires a considerable amount of time and cost to conduct, we have discovered that similarities and trajectories in the solutions allow the use of a reduced number of analysis conditions between flow rates and geometries. For our case, this type of CFD analysis should become a cost competitive method for use in hardware design and system analysis when the conduction of a large number of parametric studies is required.

Although the report presented herein is complete in terms of the intent of the research proposal, a considerable amount of follow on studies has been proposed to further advance the use of these methodologies.

Introduction

Recoil Analysis at Benét Labs: Historical Perspective and Modeling Features

In the early 1980's Benét Labs was given the mission to design and develop tank mounts and recoil systems for future weapons which would be much lighter than their predecessors. Several concepts, computer aided routines and other procedures were developed to fulfill this requirement. The first program to which this design philosophy was applied was the LW105mm EX35 Weapon (type classified M35 in 1995). Since then, there have been several developmental weapons to which Benét's recoil design and analysis technique has been applied. Currently, Benét Labs is responsible for the design of the primary weapon for Future Combat System (FCS). It is a 120mm smooth bore gun tube, a multi-lug breech and a box-type mount which envelopes two recoil brake and two recuperator assemblies. A solid body representation is found in Figure 1. Figure 2 presents an exploded view of the mount components. The two green components are the recoil brakes. These brakes are of the Schneider-type design the characteristics of which may be found in [1] and [3].

The function of a recoil system is to transform high intensity interior ballistic force acting in the axial direction on the gun tube for a short period of time (5 to 20 ms), into much lower recoil forces acting on the support structure for a longer period of time (100 to 300 ms). The objective is the attenuation of short duration high peak loads into longer duration loads whose peak values are much lower. In addition, the recoil system must provide for the storage of enough energy such that the recoiling parts may be returned to their 'home' position ready for the next firing. Figure 3 contains a schematic diagram of a weapon, vehicle and the recoil system. There are three components shown in the upper part of the figure: 1- recoiling parts; 2- stationary parts; 3- recoil system. The recoil system may be further separated into a recoil brake and recuperator. Relative force distributions in time which drive and resist are shown below the components.

The function of the recoil brake is to provide the bulk of the retarding forces. This is accomplished by metering flow through a travel dependent orifice. The metering process causes upstream pressure to develop, which opposes the forces on and momentum of the recoiling mass. The orifice is designed such that the force response is rather constant over time and operating stroke. The energy absorbed during

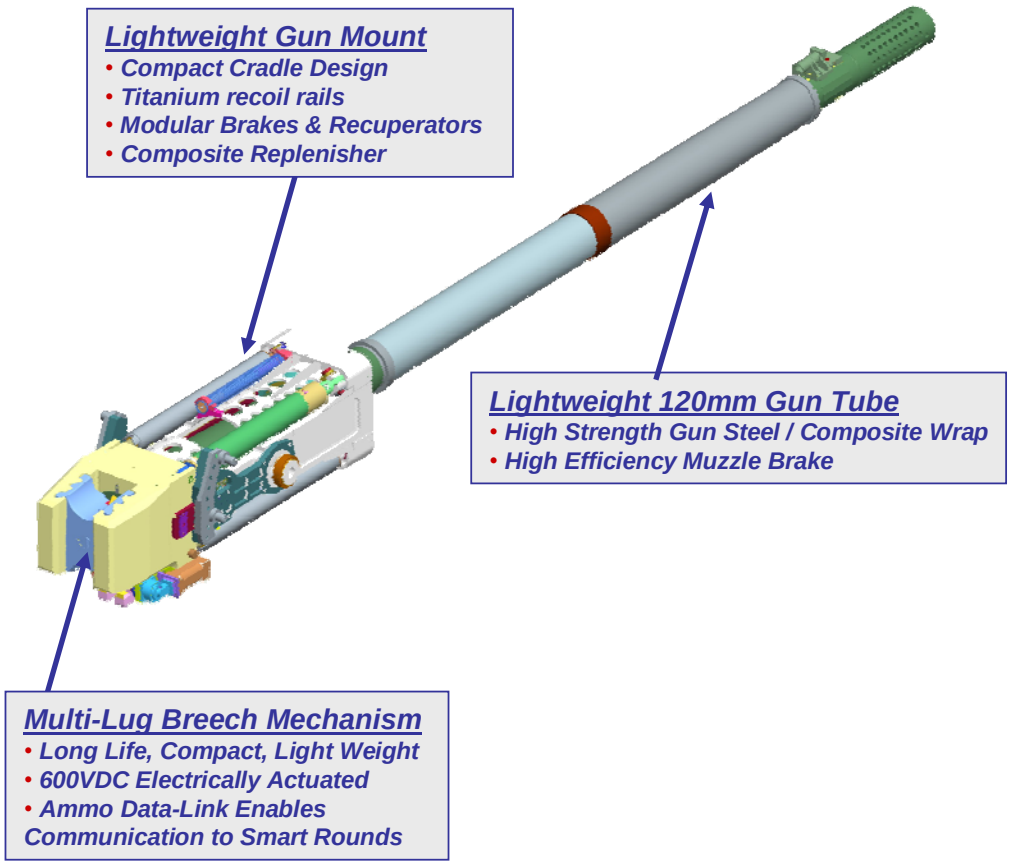

Figure 1. 120mm XM360 Primary Weapon Assembly

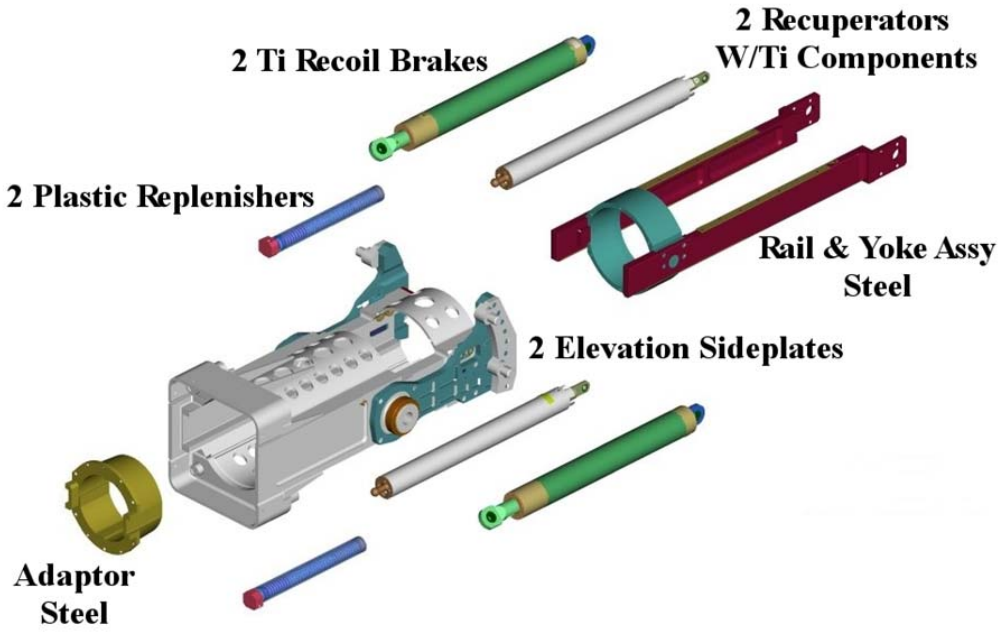

Figure 2. Mount Components

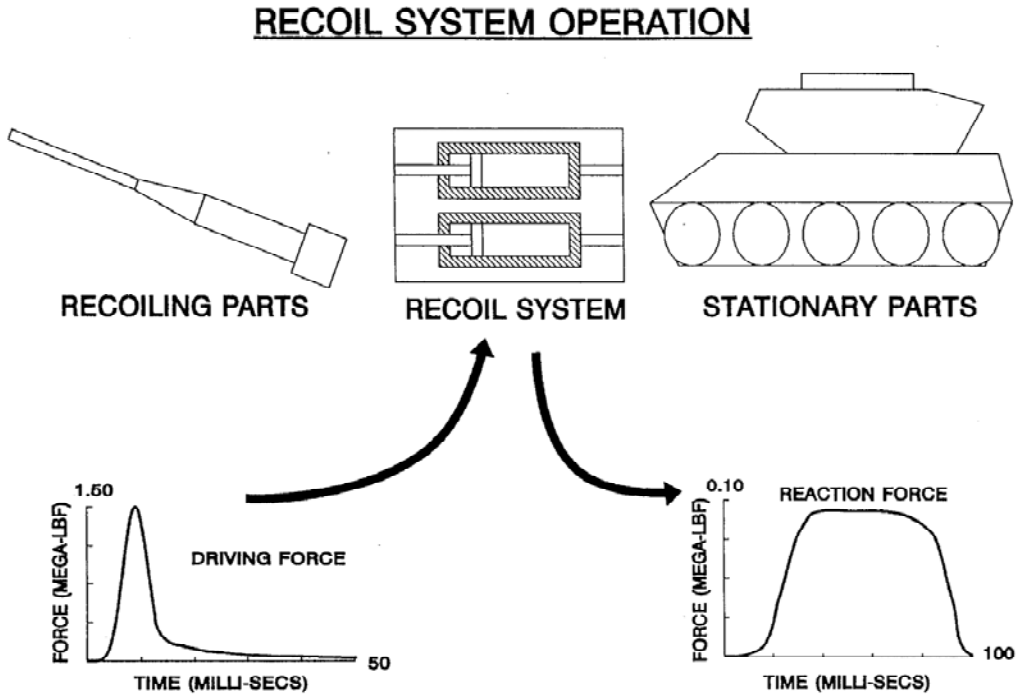

Figure 3. Recoil System Schematic

this process is converted into heat, which is manifest by a temperature rise in the brake fluid and structure. A schematic of a generic Schneider-type recoil brake in its static state is shown on Figure 4. The main components of the assembly are called out on the figure. Hydraulic fluid fills the internal volume. As the brake is extended due to ballistic force at the breech, the breech end cap, cylinder, control rod and buffer valve move as a unit in the recoil direction. Fluid from the annular chamber between the outer diameter (OD) of the recoil rod and the inner diameter (ID) of the cylinder is driven along the OD of the recoil rod and through the annular opening between the orifice and control rod. The restricted area between the orifice and control rod provides the impetus for the development of the upstream pressure which opposes the ballistic driving force and eventually arrests the gun's recoiling parts. This pressure is a function of this resreictor area and the flow rate of the fluid. As shown, the control rod is profiled such that the pressure distribution in this chamber remains relatively constant as the velocity of the recoiling parts continually change as the gun approaches and reaches full extension in recoil. In addition, some of the fluid flows back over the buffer valve into the counter recoil buffer chamber remaining in reserve to decelerate the brake as it returns to its static position. Figure 5 contains three views of the brake during the recoil operation. The curved arrows indicate the flow directions from the main annular chamber, through the annular area between the control rod and the orifice and back over the buffer plug and into the buffering chamber for counter recoil control.

Recoil analysis at Benét labs is accomplished using the computer code RECOILA. This code written in FORTRAN was initially developed in 1982 and has continually been improved through several modifications. It employs a time marching integration scheme using Adams & Bashfort Four Step Method [4] during which the derivatives from three preceding time steps are used to calculate the integral solution at the current time step. Using the applied force (ballistic pressure) and the resisting forces (brake pressure, recuperator pressure and friction) the equation of motion is solved the results of which are reported in output files at user selected time steps. The heart of the program revolves around determining back pressure on the upstream side of the flow within the brake cylinder to determine the resistance force applied to the recoiling parts. This quantity is computed at every time step in the analysis. Figure 6 contains a schematic of flow through the main orifice along with the modeling equations used to determine the relationship between flow speed and back pressure. It is a rather simple relationship

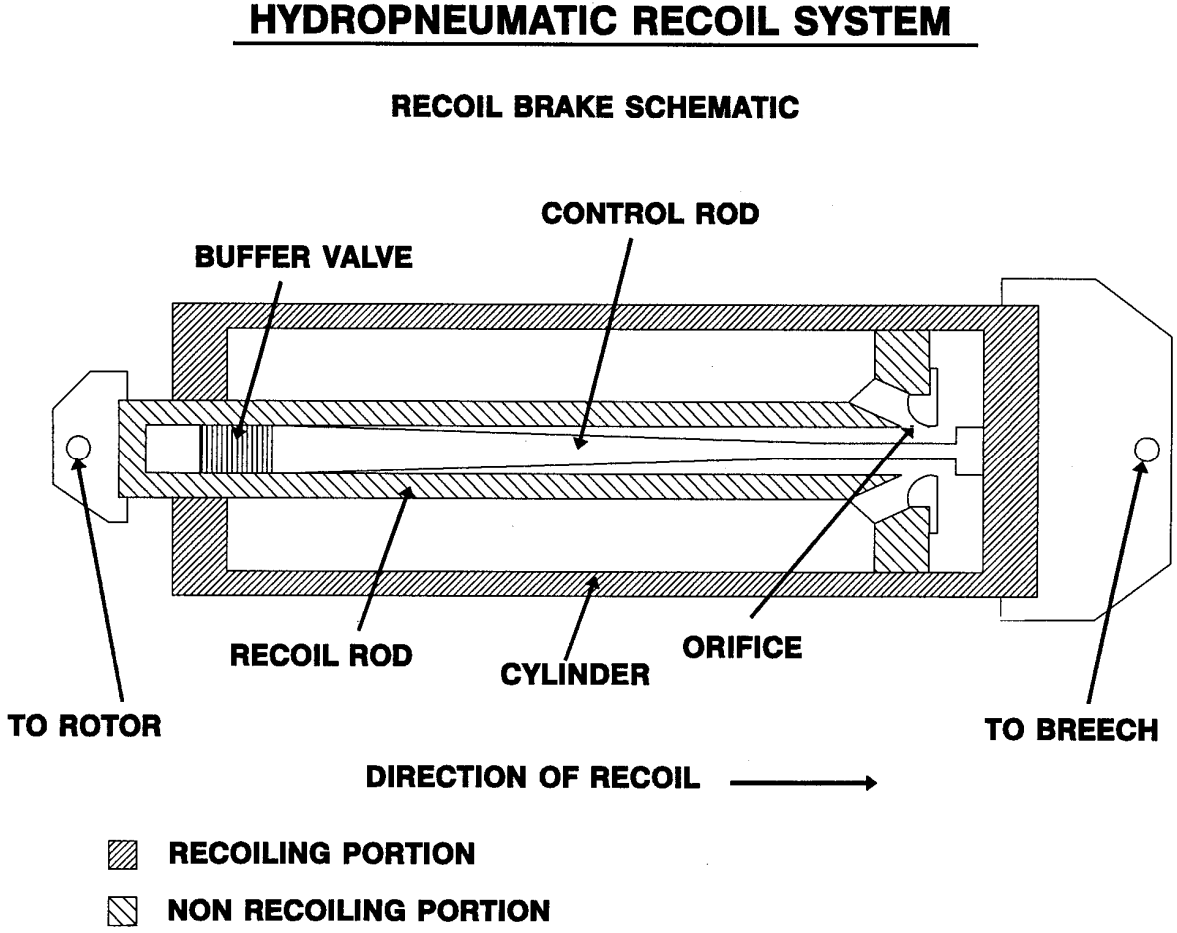

Figure 4. Schneider Recoil Brake Schematic with Components

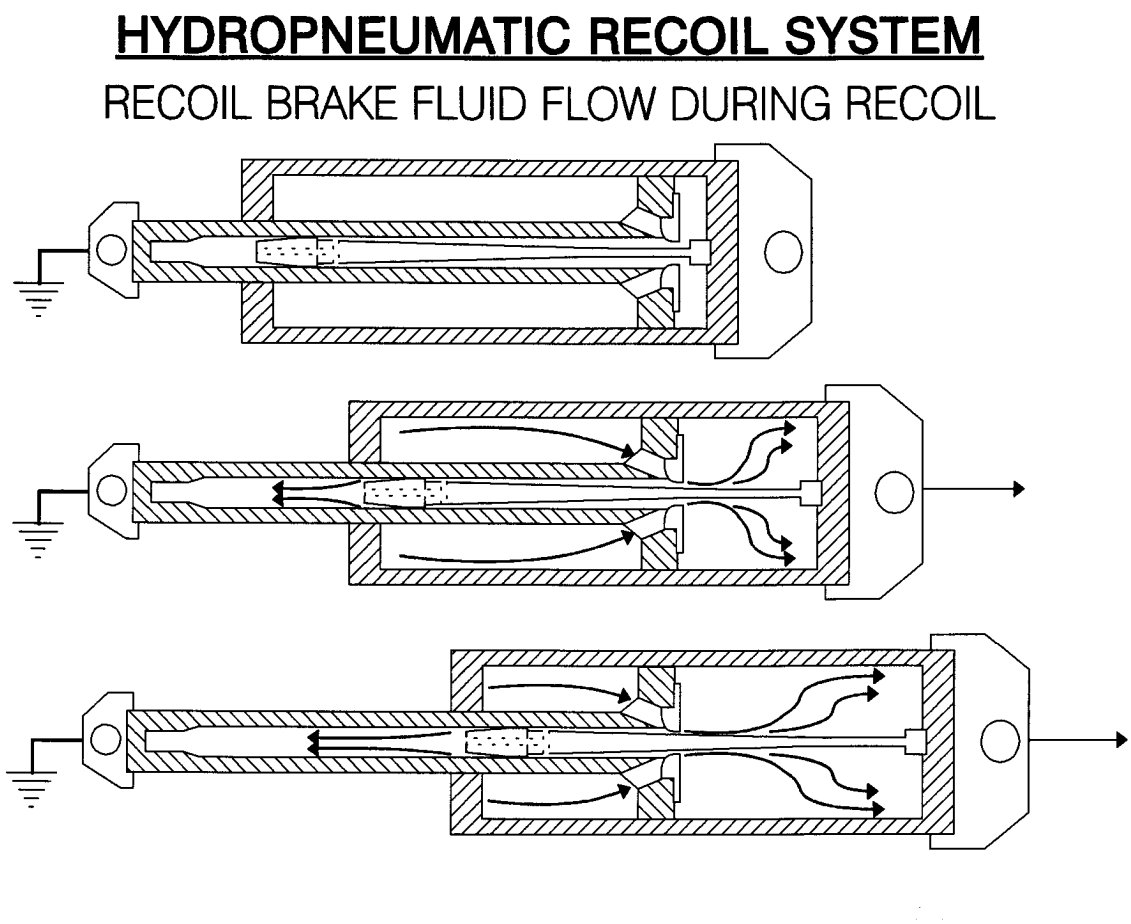

Figure 5. Quasi Static Operation of a Generic Recoil Brake

EQUATIONS GOVERNING FLUID FLOW THROUGH RECOIL ORIFICE

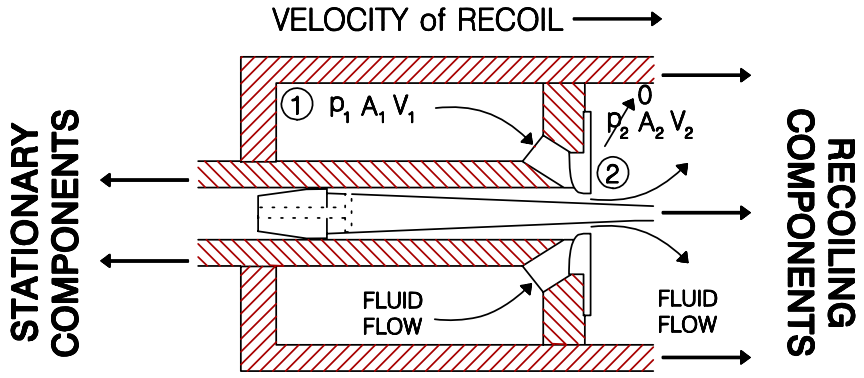

Bernoulli Flow Equation

$$\frac{p_1}{\rho} + \frac{V_1^2}{2g} = \frac{V_2^2}{2gC_d^2}$$

Continuity Equation

$$A_1V_1 = A_2V_2$$

Pressure vs Flow Equation

$$p_1 = \frac{\rho V_1^2}{2g}\left(A_r^2 - 1\right)$$

where $A_r = \dfrac{A_1}{C_d A_2}$

Figure 6. Model and Equations Governing Fluid Flow in Recoil

derived from the Bernoulli equation for flow through a pipe with restrictors. Coupling this equation with the continuity equation for incompressible flow yields the upstream pressure equation (p_1) which is a function of recoil speed (V_1), area ratio ($A_r = A_1/A_2$), fluid density (ρ) and the orifice coefficient (C_d). The current version of the code uses a constant value for the discharge coefficient (C_d) based solely upon textbook values for a round-edge orifice. Published values for this configuration are about 0.95 [5]. It is the feeling of the authors that this parameter is a strong function of the flow geometry as well as fluid properties and kinematics of the flow. The modeling version being proposed herein will have the capability of using a variable coefficient for flow through the main orifice during recoil. We expect that this coefficient will be a function of recoil velocity (V_1), area ratio (A_r) and possibly fluid temperature.

Current Analysis Techniques Applied to XM360 Weapon

Since the inception of the recoil design and analysis mission at Benét Labs, thousands of analysis runs have been conducted and compared against live fire test data. As our knowledge regarding the nuances of fluid dynamics within damper-type components grew, modifications to the analysis algorithms were developed as well as additional flow features. The latest version (release date: October 2006) incorporates fluid compressibility, where the density is treated as a function of pressure through the bulk modulus of the fluid. It proved to be a minor contributor to the brake pressure response (typically a few hundred psi for a nominal pressure of 4000 psi). However, the use of a constant C_d for flow through the main orifice has been a feature of this code since the first release. Discussion of a dedicated laboratory test [6] led to a very complicated and expensive test rig which may or may not have generated the data needed for variable C_d confirmation. This avenue was abandoned and to this day we are still using a constant C_d value that provides acceptable results as we shall subsequently present in some detail.

We have applied the current analysis methodology to test data generated during the LW120mm XM360 ATD-4 Test Program. The brake pressure results (data and simulation) for Shot #108 from the fall of 2006 are shown on figures 7 and 8. Figure 7 shows pressure data (red line) and simulation response (blue line) for both brakes plotted against time. For the simulation, the measured control rod profile for

LW120 XM36 ATD-4 RECOIL SYSTEM TEST RESPONSE SHOT #108 (9/18/06) TEST RESPONSE & SIMULATION @ NOMINAL Cd

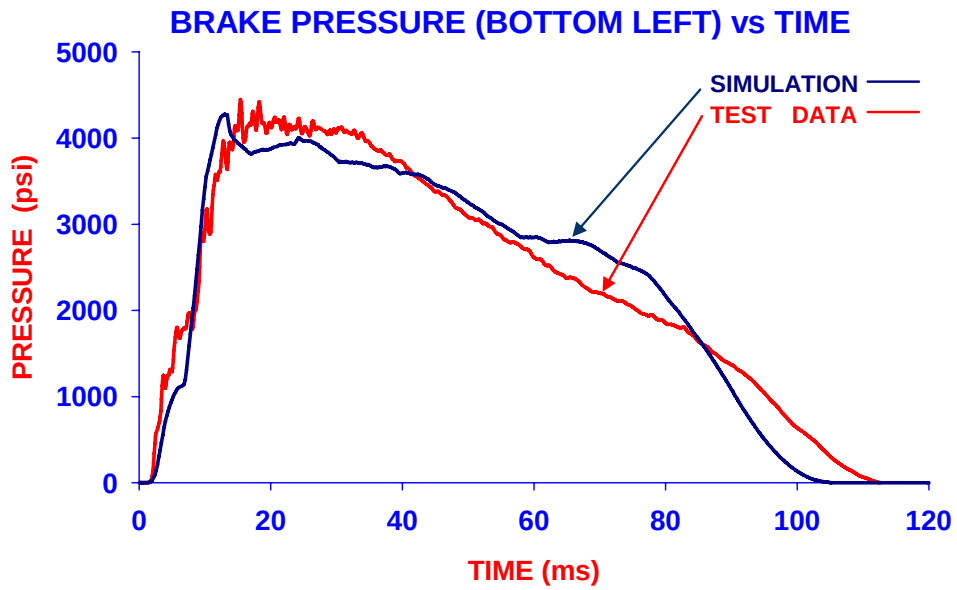

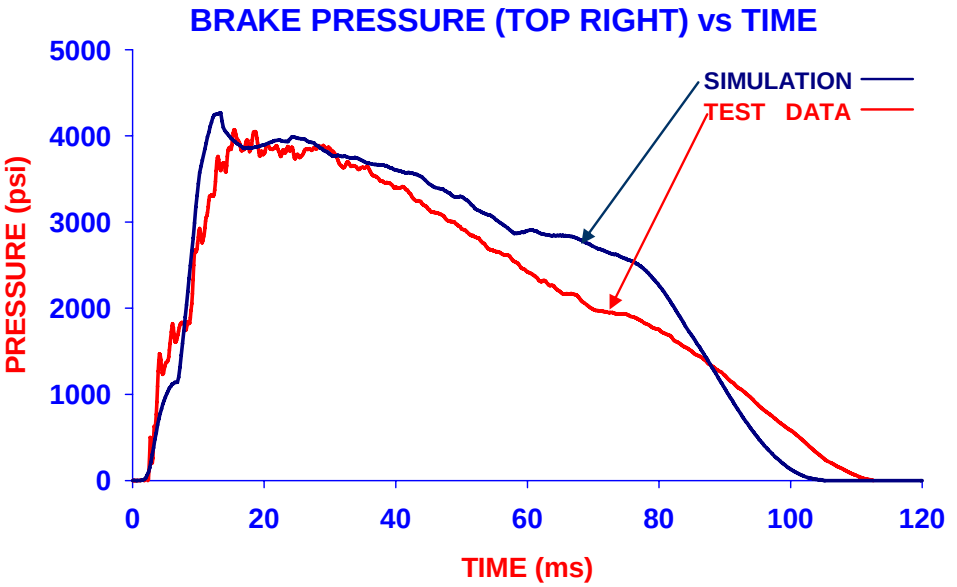

Figure 7. Brake Pressure vs Time for Round #108 (Nominal Cd Value)

LW120 XM36 ATD-4 RECOIL SYSTEM TEST RESPONSE SHOT #108 (9/18/06) TEST RESPONSE & SIMULATION @ NOMINAL Cd

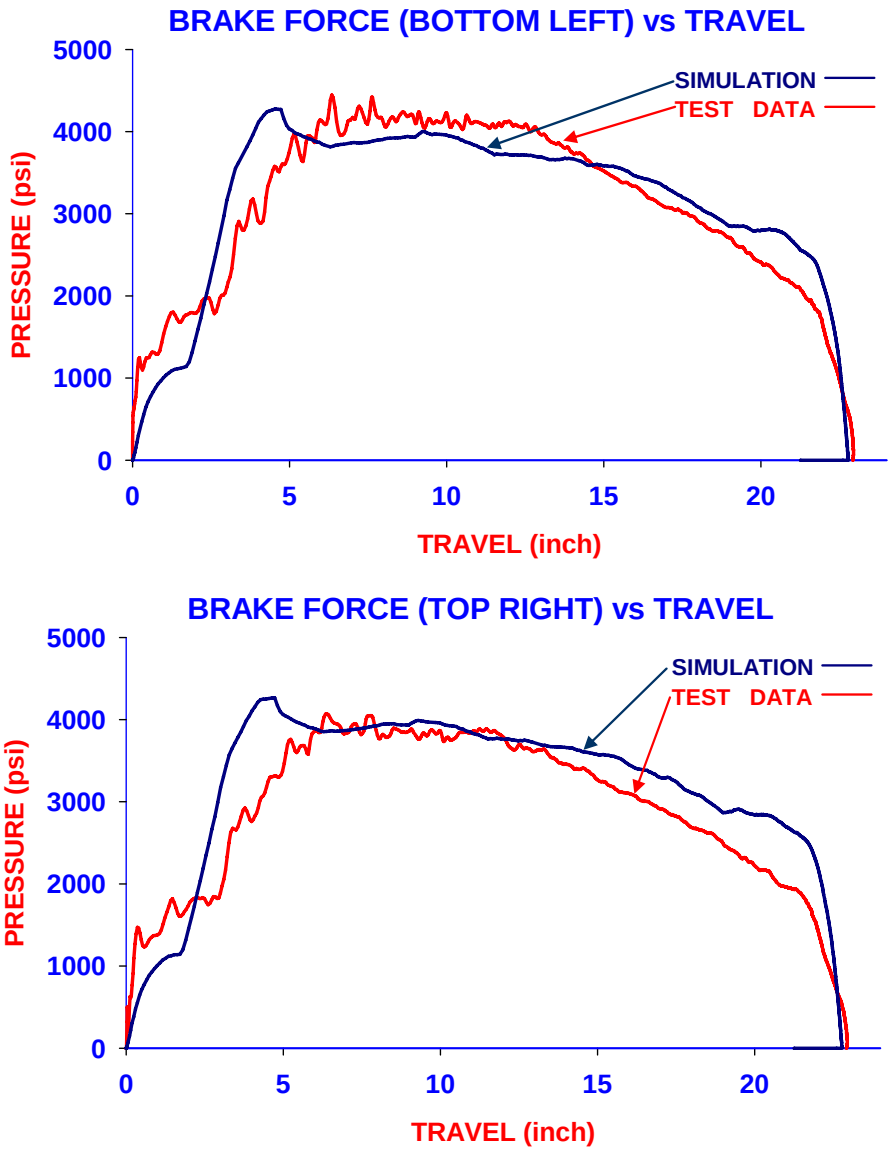

Figure 8. Brake Pressure vs Travel for Round #108 (Nominal Cd Value)

each brake was used with a nominal C_d of 0.95 for the orifice. For both brakes, the data indicates a very similar response. The peak pressure for the left brake is slightly greater than the same for the right brake. Pressure decay after peak is very similar in distribution. For the simulated response, slight deviations are shown. Early in the cycle (0 to 10 ms) the simulation under-predicts the data however, the pressure rise (10 to 15 ms) is quite steep achieving a sharp peak value that is slightly earlier than the data indicates. The decrease in pressure after peak is very quick. This is most likely due to the muzzle brake model used in the simulation. Muzzle brake parameters are simply the time of exit of the projectile and the Beta value of the brake. The Beta value abruptly decreases the gun's driving load (i.e. ballistic pressure) subsequent to exit. So, a 'step-like' reduction in the force occurs at time of projectile exit resulting in an abrupt change in recoil dynamics. After peak, the response settles down and tracks the data until approximately 30 ms. Beyond this point, the simulation deviates significantly from the data meandering above and below. Towards the end of the recoil cycle the simulation response indicates pressure values that are several hundred psi greater than the data until the very end when the simulated pressure response quickly drops below the data and terminates about 10 ms earlier. On figure 8, the same data and responses are plotted against recoil travel. When viewed in this manner the deviations between the data and simulation are quite clear. From 0 to 2.5 inches, the simulated response is less than the data by 300 to 500 psi. The abrupt rise in the simulation response at 2.5 inches is very clearly shown. At its peak value, the simulation predicts a pressure response that is 1000 to 1200 psi greater than the data indicates at that location. From 5 to about 15 inches, simulation and data track each other. From 15 to 23 inches, the simulated pressure response is greater than the data by 200 to 500 psi.

To indicate the sensitivity of the discharge coefficient we conducted a series of simulations of Shot #108 using various values for C_d and compared the results to each other and the test data. Figures 9 and 10 contain graphical representations of this analysis. We have used four values for C_d (0.85, 0.90, 0.95, and 1.00). Pressure plotted against time is shown on figure 9. As indicated, for low values of C_d the simulated pressure tracks the data for about 5 ms then rises sharply to a peak which surpasses the data by about 1000 psi. It returns and tracks the data from 40 to 60 ms to the end of the cycle. For large values of C_d the early portion of the cycle is matched quite well, however, towards the end the simulation value surpasses the data by as much as 1200 psi. The distribution in time from 60 to 110 ms is very different as

LW120 XM36 ATD-4 RECOIL SYSTEM TEST RESPONSE SHOT #108 (9/18/06) TEST RESPONSE & SIMULATION @ VARIOUS Cd VALUES

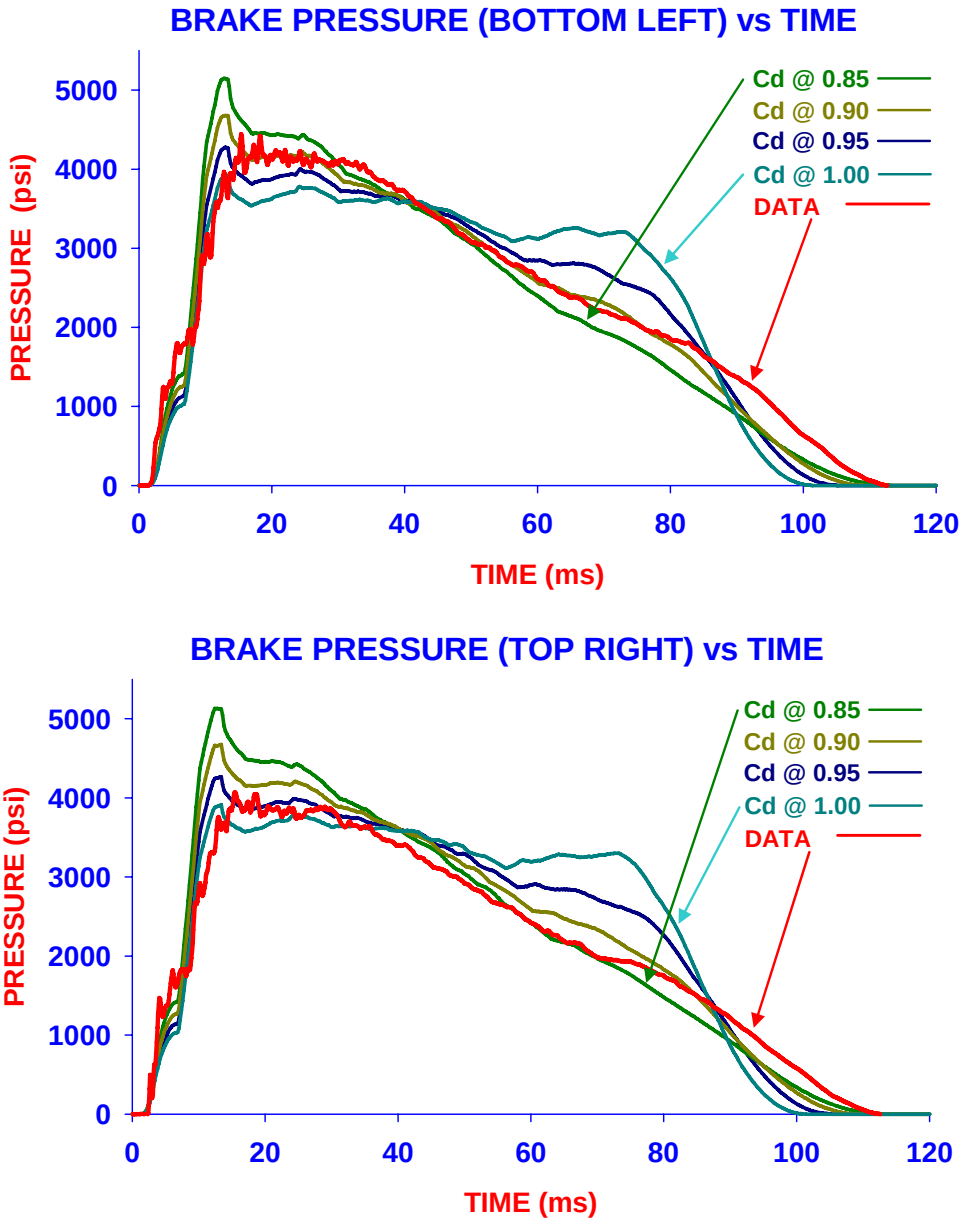

Figure 9. Brake Pressure vs Time for Round #108 (Various Cd Values)

LW120 XM36 ATD-4 RECOIL SYSTEM TEST RESPONSE SHOT #108 (9/18/06) TEST RESPONSE & SIMULATION @ VARIOUS Cd VALUES

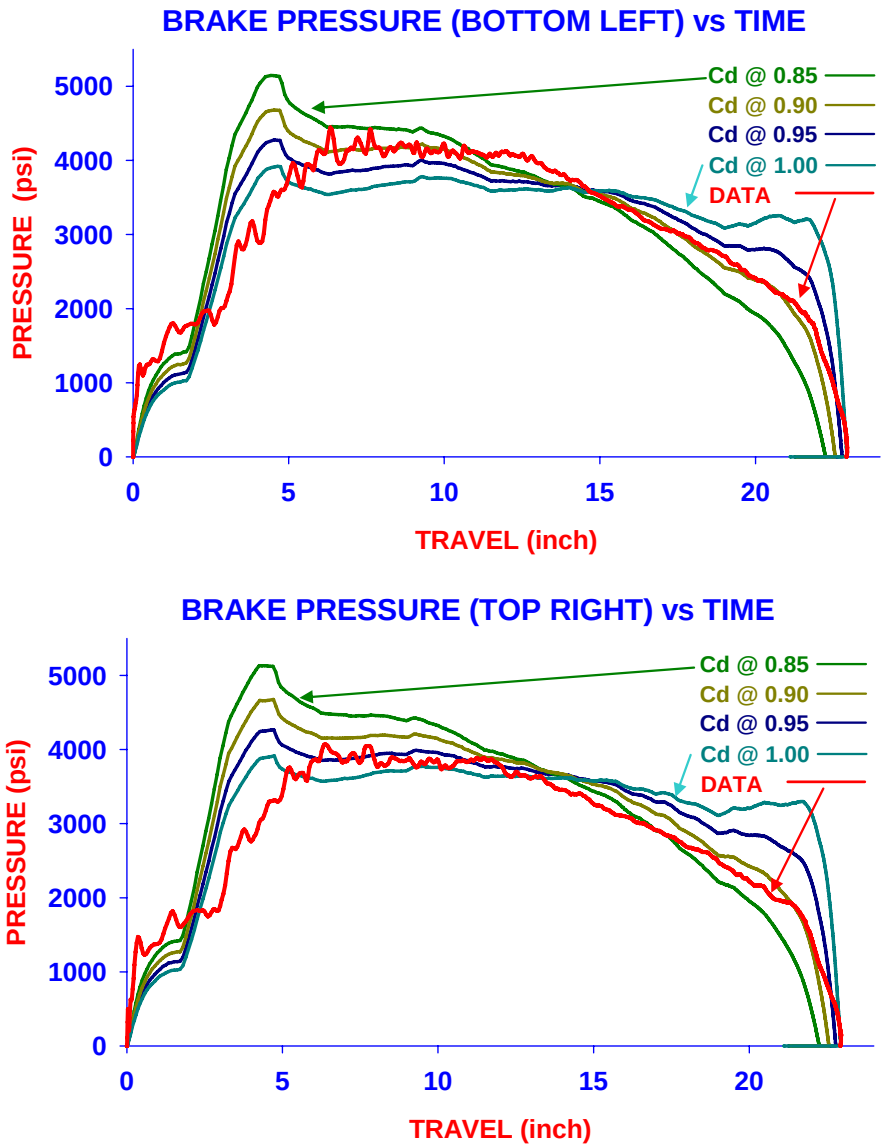

Figure 10. Brake Pressure vs Travel for Round #108 (Various Cd Values)

well. Pressure plotted against travel is shown on figure 10. The differences between the various C_d values and the data are easy to discern when viewed in this manner. It is quite obvious that there is no single value for C_d that best matches the data. Early in the cycle (0 to 2.5 inches) a C_d value of 0.85 is evident. As travel progresses (from 2.5 to 10 inches) a C_d value of approximately 0.95 provides the best fit. Towards the end of travel (15 to 24 inches) C_d values of 0.85 to 0.90 seem to best match the data. Although only one particular shot has been reported herein, this trend is repeated for all of the data we have simulated to date.

Attempt to Extract Discharge Coefficients from Test Data

As our data collection methods matured especially during the various XM36 and XM360 programs, we have been able to get a much better and more accurate reporting of the recoil system responses. In addition, there are several computer programs that have rendered data collection and analysis a nearly turnkey operation. There is one caveat, however, data analysis and review should be conducted by a trained professional who knows the expected values and the errors associated with the measurement transducers and reporting hardware. In this section, we attempt to reproduce via assumptions and calculations a measure of the instantaneous C_d value by using test data from the aforementioned ATD-4 test.

If we are to assume that fluid flow within the internal chamber of the brake during a recoil cycle follows the flow laws of Bernoulli, we may pick any two points in the flow and write the momentum and continuity equations as shown in figure 6 and repeated in figure 11. Note that C_d is buried on the right side of the flow equation. It may be extracted as shown in the final equation on figure 11. Per this equation, C_d is directly proportional to the ratio of the main flow area (A_1) to the area at the throat (A_2), inversely proportional to the pressure with fluid density and flow speed in both numerator and denominator within the radical. Essentially, knowing the pressure, recoil velocity and flow areas (orifice flow area is a function of travel) we may in theory calculate values for this coefficient using the time dependent data collected during the recoil portion of any shot in a firing test. We have routinely collected pressure and travel data as a part of all previous XM36 and XM360 firings, however, the use of this data to calculate C_d is problematic. First, since a parallel flow path exists to the buffer pocket we do not know

EQUATIONS GOVERNING FLUID FLOW THROUGH RECOIL ORIFICE

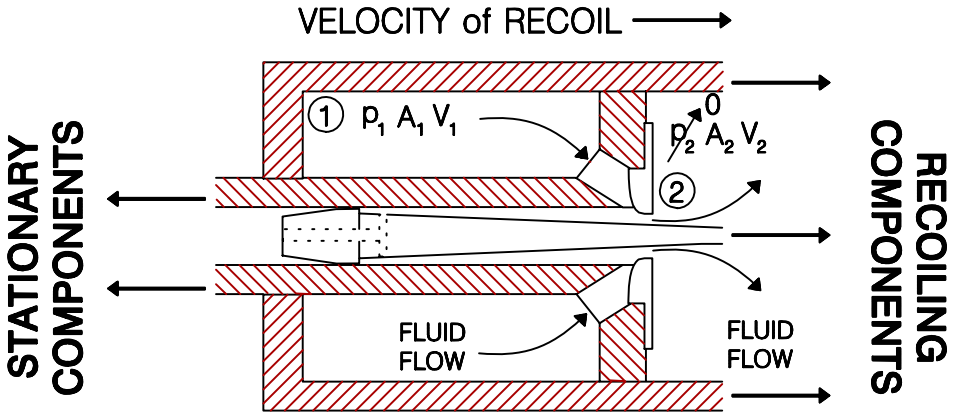

Bernoulli Flow Equation

$$\frac{p_1}{\rho} + \frac{V_1^2}{2g} = \frac{V_2^2}{2gC_d^2}$$

Continuity Equation

$$A_1V_1 = A_2V_2$$

Discharge Coefficient Equation

$$C_d = \frac{A_1}{A_2}\sqrt{\frac{\rho V_1^2}{2gp_1 + \rho V_1^2}}$$

Figure 11. Extraction of C_d from Firing Data

how the flow is apportioned between the path to the buffer pocket and through the main orifice. Therefore, the continuity equation on the figure may not apply as shown. A potential solution to this problem would be to 'calculate' flow to the buffer using a backflow orifice equation (as a flow restriction along this path) along with the pressure data. Once this flow rate to the buffer pocket is estimated the remaining fluid must pass through the main orifice. Second, although the travel is globally representative of the gun's position it is not smooth enough to yield an accurate recoil velocity using a point by point differentiation algorithm. A potential solution to this problem would be to fit the travel data to a function using a least squares method and then differentiate the function to determine velocity. Both MatLab© and Sigma Plot© have several standard functions to use in a least squares fit algorithm. After several tries of both algebraic and transcendental functions the existence of 3 sigmoidal-type functions within the Sigma Plot regression library seems to best fit the data and expected velocity profiles.

The first is the 3 parameter Logistic function, which is depicted on Figure 12 for Shot #104. This figure contains 2 plots and the relevant fitting equations. The upper plot contains travel data from the test with the logistic fitting function superimposed. On the lower plot, the velocity as derived from an analytic differentiation of the function is shown. As indicated in the equation, the travel (***x***) is a function of time which appears only in the denominator of the function along with the parameters a, b and t_o. The residuals (the difference between the data and the fit function) are on the order of ±0.2 inches. The meandering nature of the data is observed through the slight oscillation about the smoother fit function. As mentioned earlier, this is most likely due to the transducer used for travel determination and is not unlike other data that has been collected before. In the velocity function (***v***) shown on in the lower plot, the independent variable (***t***) appears in both the numerator and denominator along with combinations of the other parameters. We expect a velocity response of this type; however, the actual shape of the tail end (i.e. the decay portion) is unknown. The second is the 3 parameter Chapman function, which is depicted on Figure 13 for Shot #104. As indicated in the equation, the travel (***x***) is a strong function of the exponential (***e***). Since the exponential appears in both the numerator and denominator of the velocity function, its value at zero time is indeterminate; however, by using techniques of calculus, it is found to be zero. The third is the 3 parameter Hill function, which is depicted on Figure 14 for Shot #104. As indicated

LW120 XM36 ATD-4 RECOIL SYSTEM TEST RESPONSE
TEST ROUND #104 (3 PARAMETER LOGISTIC FIT)

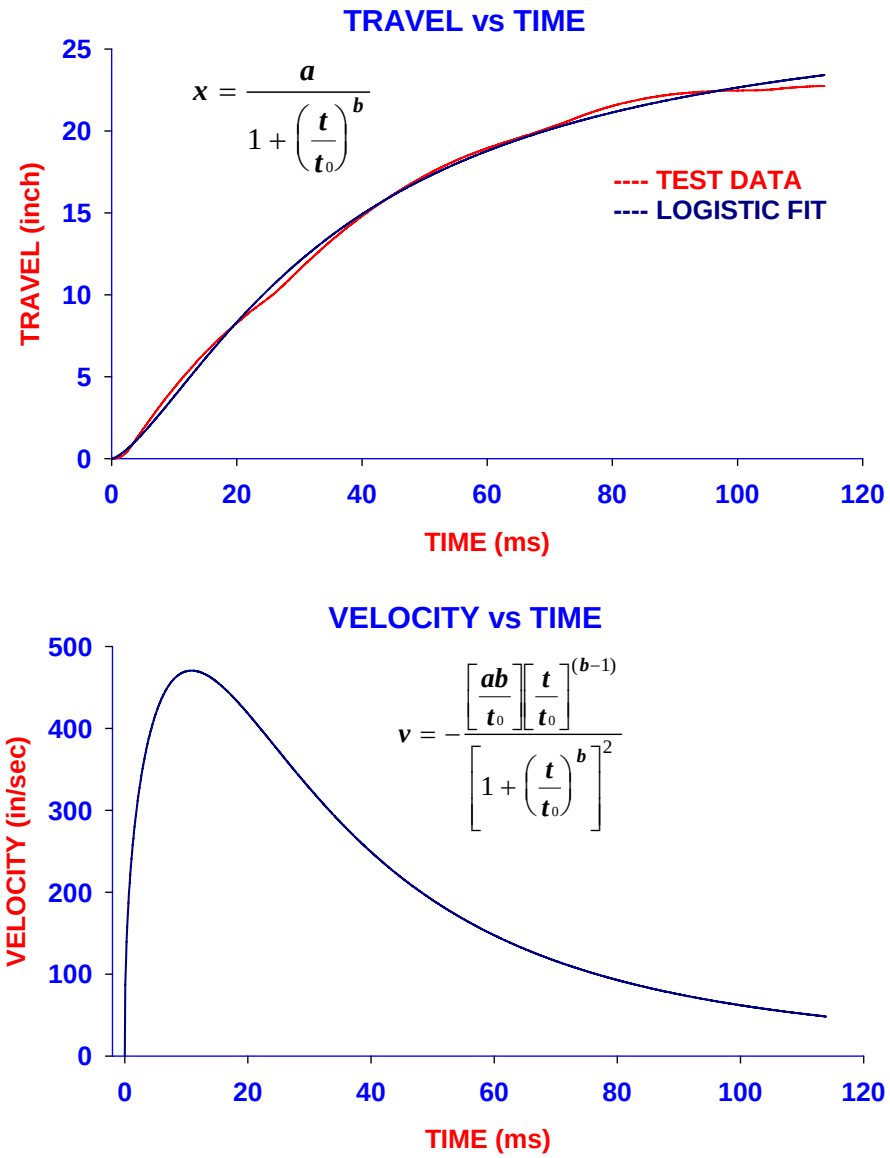

Figure 12. Data and Logistic Fit of Recoil Travel for ATD-4 Shot #104

LW120 XM36 ATD-4 RECOIL SYSTEM TEST RESPONSE
TEST ROUND #104 (3 PARAMETER CHAPMAN FIT)

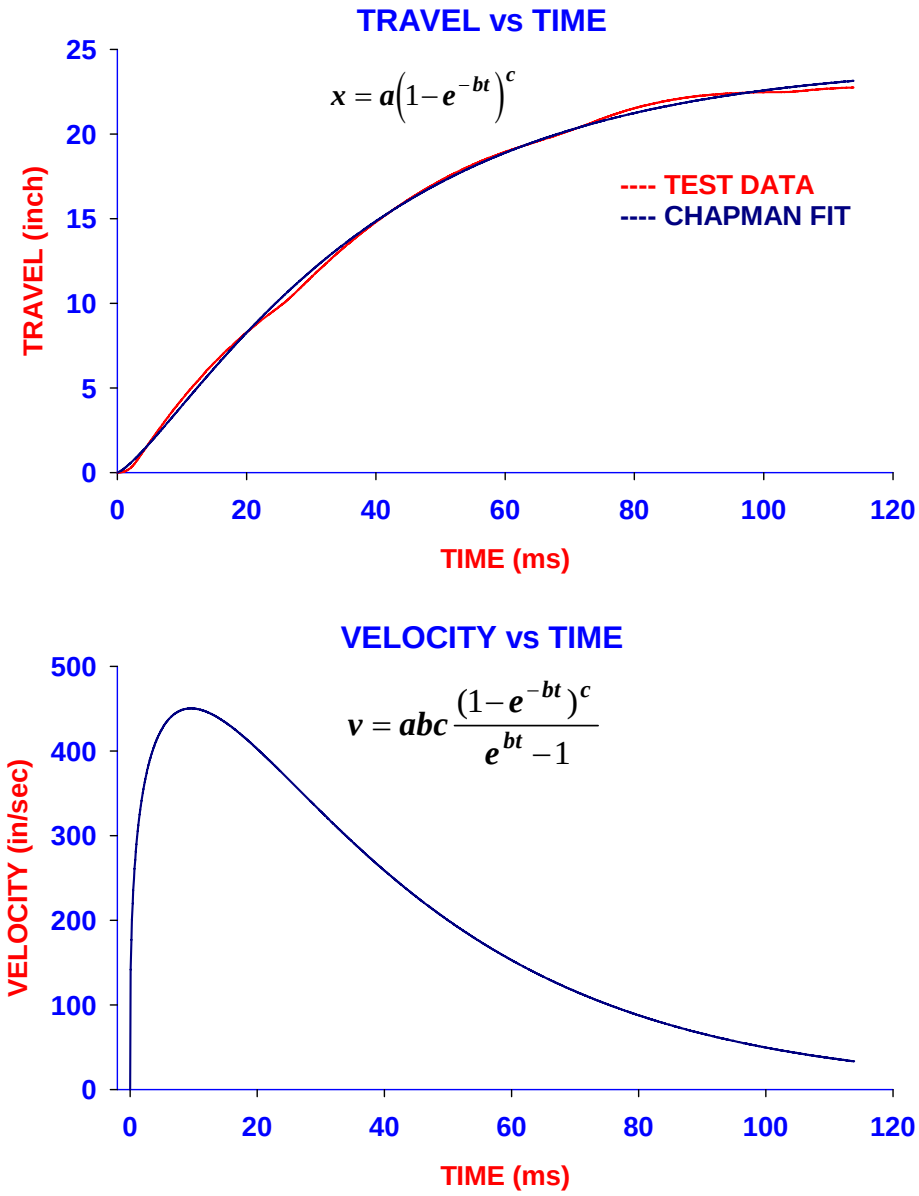

Figure 13. Data and Chapman Fit of Recoil Travel for ATD-4 Shot #104

LW120 XM36 ATD-4 RECOIL SYSTEM TEST RESPONSE
TEST ROUND #104 (3 PARAMETER HILL FIT)

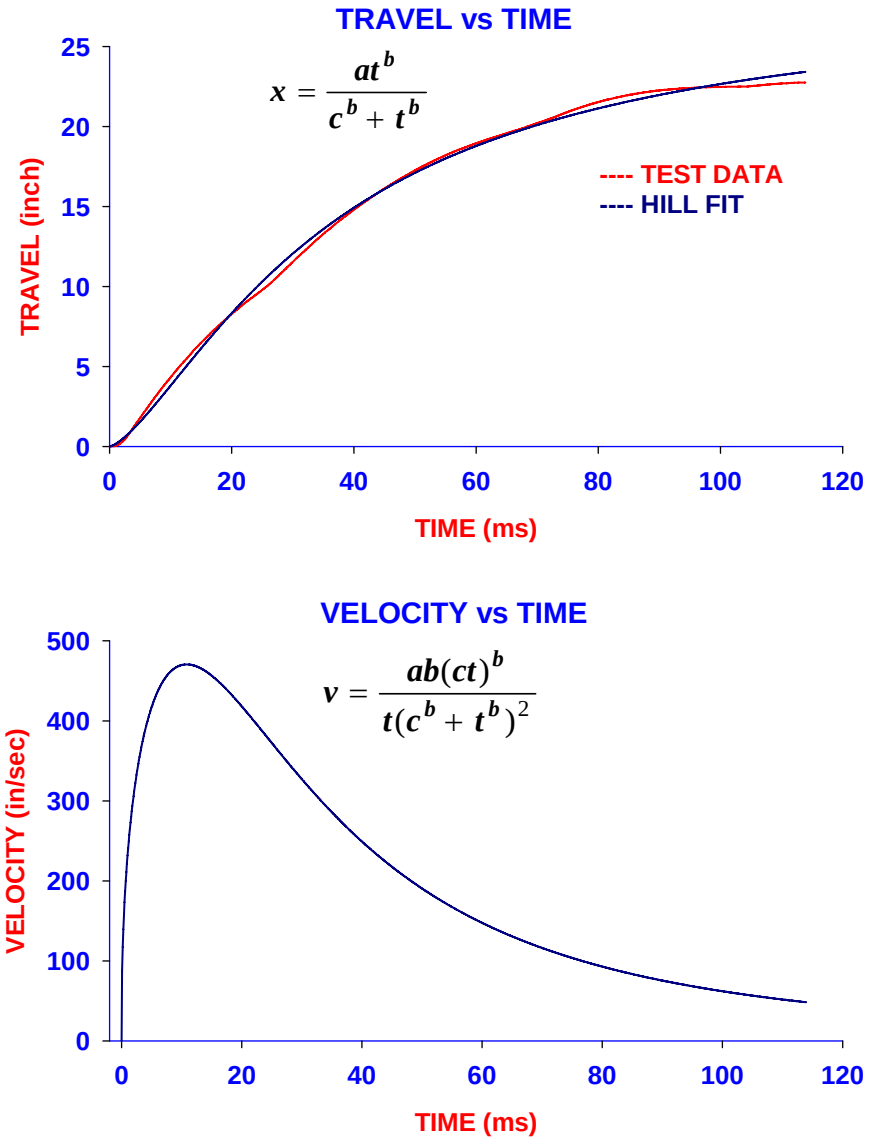

Figure 14. Data and Hill Fit of Recoil Travel for ATD-4 Shot #104

in the equation the travel (***x***) and velocity (***v***) are rational functions of (***t***). The form of the velocity equation admits a value of zero at zero time. In summary, all three fitting methods produced travel and velocity data that are nearly identical. We shall proceed using all three methods to analyze the firing data in the C_d equation from figure 11.

A MatLab© script (see Appendix A) was developed and used for processing the recoil pressure, brake geometry, travel and velocity fitting functions to generate the dynamic C_d values. Each data set contained about 1100 points for each variable. We shall discuss in some the detail the results for this processing of Round #104 and highlight the remaining 10 rounds in this series. As mentioned earlier, in order to use firing data for this process, it must be rather smooth and continuous. As shown, the raw travel data did not possess this characteristic; therefore, a smoothing technique had to be implemented to determine recoil velocity. Additionally, the brake pressure data which comprises a term in the C_d calculation was rather oscillatory as well, especially early in the cycle, therefore a smoothing process had to be applied. Since we only needed the data and not its derivative, a polynomial function would be good enough for its representation. On Figure 15, the raw data and its 15 term polynomial fitting function is shown for Round #104. The red line is the data and as shown it contains low amplitude oscillations up to about 35 ms. The fitting function (blue line) yields a very good representation of the data, smoothing the initial transients very well.

On Figure 16, the result for the C_d calculation is shown for the Logistic fit of the travel data. This coefficient is plotted against recoil travel using the pressure data for the left and right brakes independently. The upper plot contains the results for left brake while the result for the right brake is shown on the lower plot. The result for either brake is nearly the same. Up to about 2.5 inches of travel the C_d value is low (~0.60 to 0.70). During this portion of travel, the speed is slowly rising and the throat area is constant, however, C_d rises quickly, reaching a maximum value of slightly above 1.1 at 5 inches of travel. Obviously a value of 1.1 is not physically possible since C_d values should be between 0 and 1. However, during this portion of recoil, the speed and pressure are increasing rapidly, whereas, the throat area is decreasing, so the calculated value (since a straightforward equation is being used) could rise above 1.0 although this is ambiguous. Maximum recoil velocity and pressure are shown to occur at about

LW120 XM36 ATD-4 RECOIL SYSTEM TEST RESPONSE
TEST ROUND #104 (15 TERM POLYNOMIAL FIT)

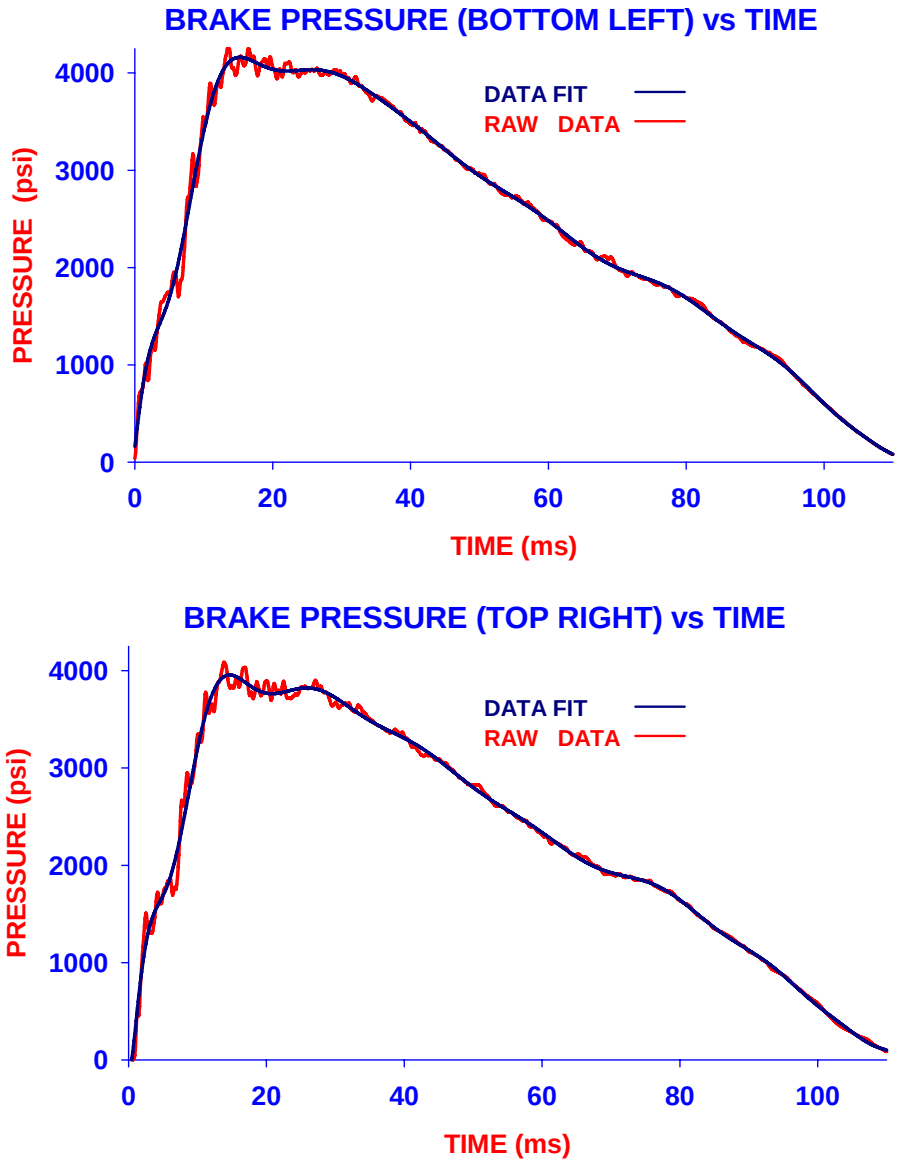

Figure 15. Data & Polynomial Fit of Brake Pressure for ATD-4 Shot #104

LW120 XM36 ATD-4 RECOIL SYSTEM TEST RESPONSE
TEST ROUND #104 (3 PARAMETER LOGISTIC FIT)

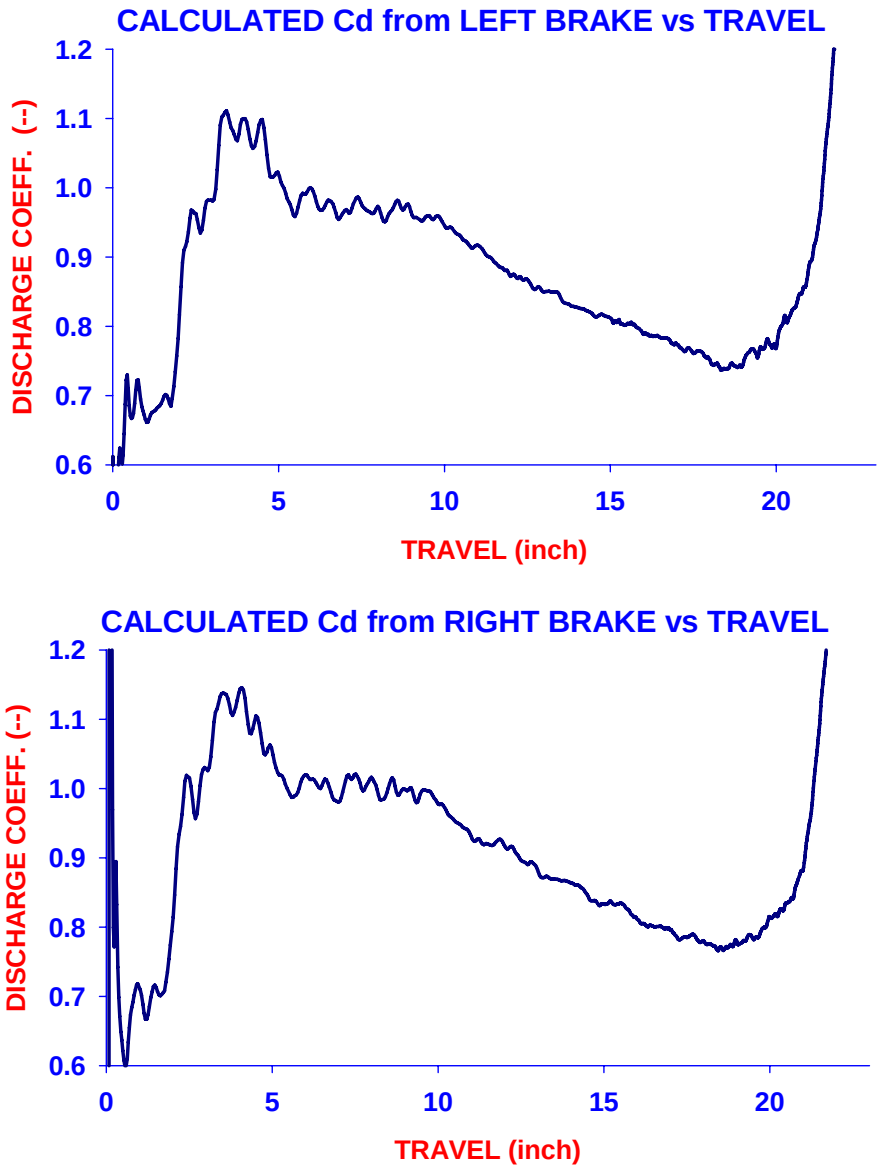

Figure 16. C_d Calculation Using Logistic Data Fit for ATD-4 Shot #104

5 inches. The C_d value reverses after the 5 inch location reducing to values slightly less than 1.0 up to about the 10 inch travel location. From 10 to about 20 inches of travel, the C_d value monotonically drops to less than 0.8. Beyond the 20 inch location, the value rises rapidly to values in excess of 1.2. During this phase of the cycle, pressure, velocity and throat area are decreasing quickly, therefore, the transient nature of the variables involved in the calculation may render its result meaningless. Bottom line, once flow is established and the variables are changing slowly (from 5 to 20 inches of travel) the calculation of C_d is probably quite good. Nearly the same results and comments may be made for the Chapman and Hill fit which are shown on Figures 17 and 18. This similarity in response carries throughout the remaining 10 rounds of this test. This analysis lends credence to the premise that C_d is variable and probably a function of flow speed and the ratio of upstream chamber area to the throat area.

Use of Alternate Methodologies for Calculating Discharge Coefficient Values

The idea that C_d values are dependent upon various fluid and geometry parameters for flow around the circumference of plates mounted within a cylinder was shown experimentally by Bell and Bergelin [7]. The basic test fixture was a long cylinder with an inner diameter of 5.2541 inches within which individual plates of sizes between 5.0251 to 5.2325 inches in diameter of varying edge configurations and thickness were mounted both concentrically and tangentially. Three configurations of the plates' outer circumference were tested. They were square edge with measurable flow length, sharp edge and rounded entrance edge. Both oil and water were used and as it was pumped through the test section (after thermal and flow equilibrium was reached), pressure and flow rate data was collected. The orifice coefficients for each trial was calculated based upon the test data and a standard equation from a Bernoulli flow analysis similar to that explained in the last section. Additionally, the Reynolds number of all experimental trials was calculated using orifice and cylinder diameters as the length parameter along with the fluid's density, viscosity and flow rate.

The results are presented in the form of log-log plots of C_d as a function of Reynolds Number. Basically two distinct responses developed; one for the sharp edge orifice and another for the square and round edge orifice. These are presented in two forms on figures 5 through figure 8 of the referenced report. In addition, several empirical equations relating the test parameters (i.e. orifice geometry and

LW120 XM36 ATD-4 RECOIL SYSTEM TEST RESPONSE
TEST ROUND #104 (3 PARAMETER CHAPMAN FIT)

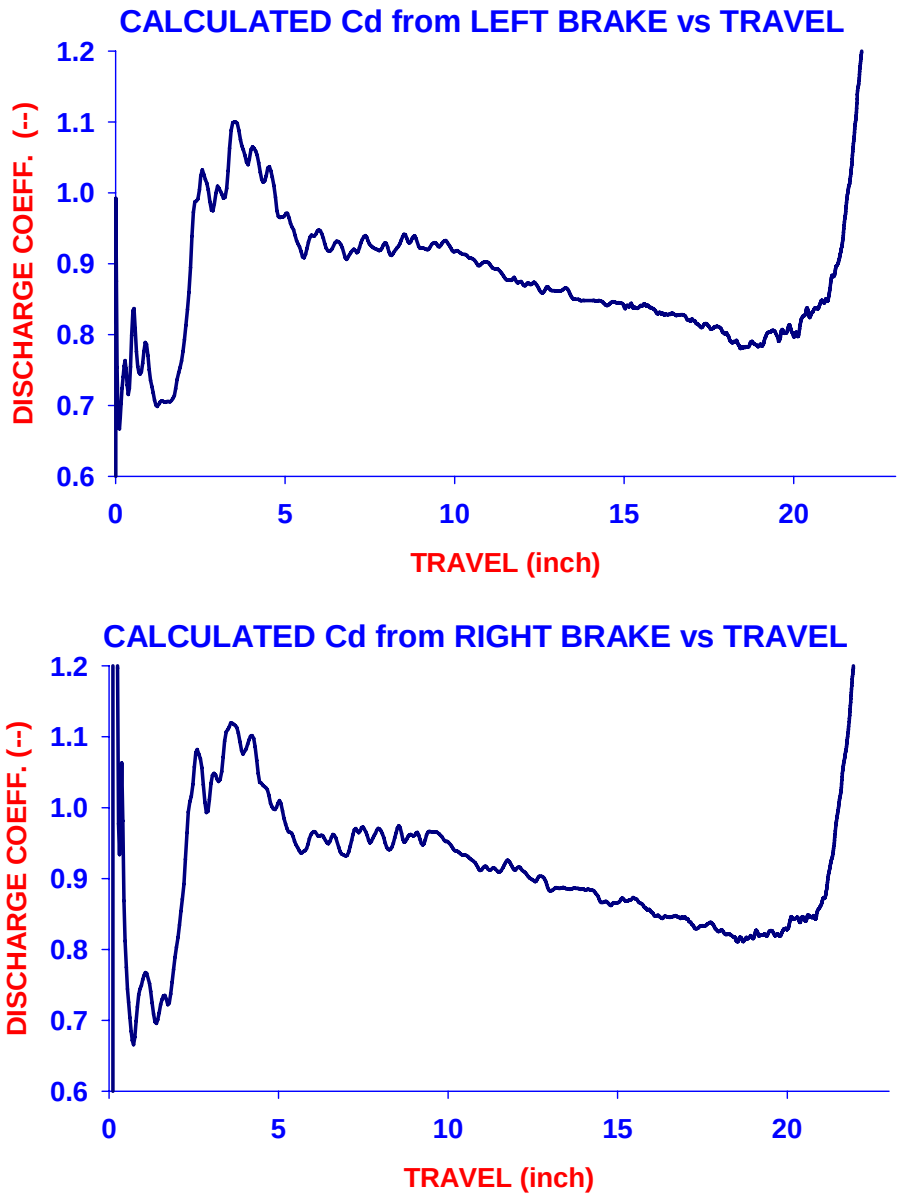

Figure 17. C_d Calculation Using Chapman Data Fit for ATD-4 Shot #104

LW120 XM36 ATD-4 RECOIL SYSTEM TEST RESPONSE
TEST ROUND #104 (3 PARAMETER HILL FIT)

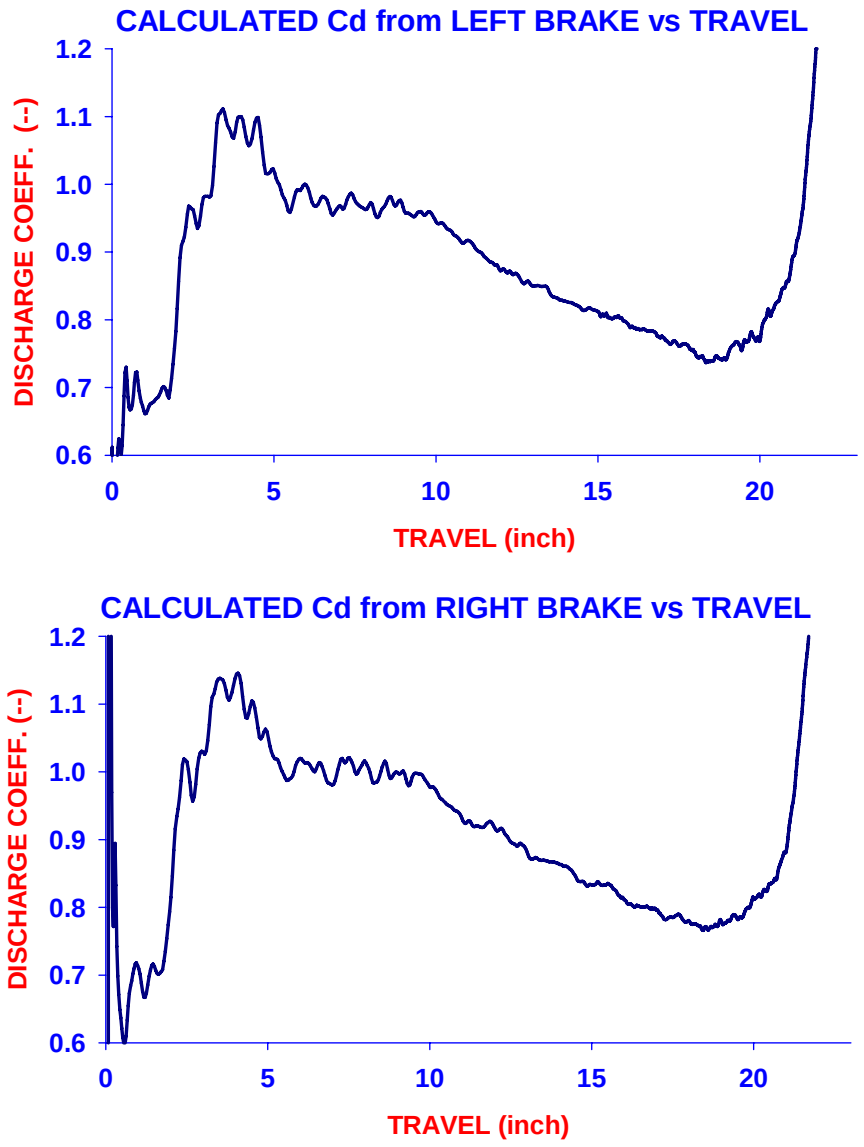

Figure 18. C_d Calculation Using Hill Data Fit for ATD-4 Shot #104

Reynolds number) to C_d were developed, the graphs of which were superimposed on the abovementioned plots. To summarize, C_d tends to increase monotonically with increasing Reynolds Number (within a 2 to 20,000 range) and asymptotically approaching a limiting value dependent upon the edge geometry of the disk.

Although this work is of great value for the geometries that were tested we could not apply these results to the problem at hand. Our flow restrictor was much smaller in size than that of the test and contains a moving part (Control Rod) which has a variable outer diameter and moves through the orifice at a varying speed. Additionally, the orifice is fed from 5 ports in the piston head each of which has a 90° shoulder of 0.31 inch at the leading edge of the entrance and a diverter angle of approximately 50°. In the past, discussions regarding laboratory testing of the orifice configuration was discussed [6], but as mentioned earlier, the parameters needed to conduct experiments in the flow regime of a live fire test could not be achieved. Additionally, a first cut at an experimental setup seemed to be quite pricey and was eventually abandoned.

In the late 1990's, Benét Labs began using dedicated computational fluid dynamics (CFD) codes for analysis of gas flow through muzzle brakes to predict overpressure fields in close proximity to the muzzle end of the gun. These fields were the result of expulsion and expansion of the propellant gases after the projectile has exited the muzzle. This type of flow is highly complicated in that gas compression, shock wave development and composition changes occur in a highly transient environment. These analyses were applied to several gun systems, including the XM360. Informal results indicate that the correlation between analysis and test data is good (although costly in terms of execution times). In addition, CFD was applied to an unsteady simplified 2-D axisymmetric model of a recoil cylinder buffer plug, control rod, and orifice inlet [8]. This model utilized dynamic meshing to simulate motion of the recoil cylinder. This unsteady model utilized oil as a medium, but also simulated the multi-phase flow environment to account for cavitation and collapse of the fluid. Based on these results, it makes sense that the application of CFD modeling for an incompressible Newtonian fluid flow in the absence of heat transfer, phase changes, etc. should be relatively low cost. Additionally, if a representative axisymmetric version of the flow path could be conceived this would render the problem to be two-dimensional, further

reducing run times. The combination of these three distinct bodies of work cited above was the motivation to conduct detailed CFD analysis of fluid flow within the brake during the recoil cycle. We would attempt to conduct 'numerical experiments' in a manner similar to the experimental work of Bell and Bergelin. The result would be a table of C_d values as a function of one or several parameters of the flow.

Incompressible Flow Modeling Using CFD Methodology

Description of CFD in General and the Code CFdesign©

Finite element analysis methods (fea) have been used to analyze elastic structures for several decades. In general, fea models partition the analysis domain into many 'nodes' at which displacements are calculated and reported. The areas or volumes between the nodes are filled in with elements throughout which these nodal displacements are approximated by basis functions using the values at adjacent nodes for their 'data'. The displacements vector and element formulation are assembled into a matrix expression which is equated to a vector of know forces much like a standard system of algebraic equations. The difference is that the solution vector (nodes) is quite long whereas the matrix representing the element formulation is the square of the length of the nodal vector. Solution to a problem formulated in this manner is accomplished through the use of clever numerical techniques. Once the displacement vector has been solved, the basis functions and the known values for the mechanical properties of the material are used to determine strains and stresses at any location in the structure. This is a field variable problem where the stresses are the field variables. One may liken this to a series of rings attached to each other by springs. If one or many of the rings are displaced, the springs will either extend or compress. The extension or compression will determine the internal force within each spring. The elastic energy in each spring is directly proportional to these forces. Stress and strain is directly proportional to these forces. For the types of structures and loads imparted to components designed by engineers and technicians at Benét Labs, the use of fea analysis is crucial to the success of weapons' systems. We have been using fea methods for design for nearly 4 decades. The initial code used was NASTRAN developed by NASA for the aerospace industry. During the early 1980's, we acquired the more comprehensive and adaptable code called ABAQUS which contains more features than NASTRAN. Also, there are several other specialty fea codes that have been developed in-house or acquired commercially

for desktop use.

Finite element analysis methods are not limited to structural problems only. A growing field of interest is in computational fluid dynamics (CFD) in which the methodology of finite elements has been incorporated into finite-volume problems. CFD uses setup procedures that are similar to the structural models. The fluid contained in a spatial domain is discretized into small cells (elements) the intersections of which are the nodes. A suitable algorithm to solve the Navier-Stokes equations of motion is then applied. These equations describe the changes in momentum within an infinitesimal volume of fluid as simply the product of changes in pressure and dissipative viscous forces acting inside the fluid. These equations are differential equations which describe the relationships among the rates of change of the variables.

CFdesign© is one such CFD code that can be run locally on a high powered PC. Its analysis method is based upon the finite-element method, unlike other fluid flow analysis packages that utilize a finite-volume approach. This method lends itself to a more flexible representation of the geometry and the physical properties of the fluid and components in the analysis. Additionally, it derives the geometric data from several commercial CAD packages (at Benét Labs Pro/Engineer© is used). Regarding flow modeling, it has the ability to simulate transient and steady state, compressible or incompressible, laminar or turbulent, internal or external, and relative motion of walls [9]. For the problem at hand (i.e. pipe flow within a recoil brake) we chose a steady state, incompressible analysis with the possibility of both laminar and turbulent zones.

Application to the Current Problem via Simplified Axisymmetric Geometry

The current Benét Labs recoil analysis code uses a lumped flow resistor to model the effects of the shoulder, angular paths and restricted area of the orifice with no requirement to calculate the detailed pressure or flow distributions throughout these volumes. On Figure 19, the assembly view of a recoil brake is shown. The cylinder and control rod move to the right driven by the pressure in the breech which accelerates the gun in recoil. The orifice which is attached to the throttling sleeve and piston head remain stationary. Fluid is forced through the annular area between the control rod profile and orifice. The path through the 6 feed ports in the piston head and the restricted area between the orifice and control rod are

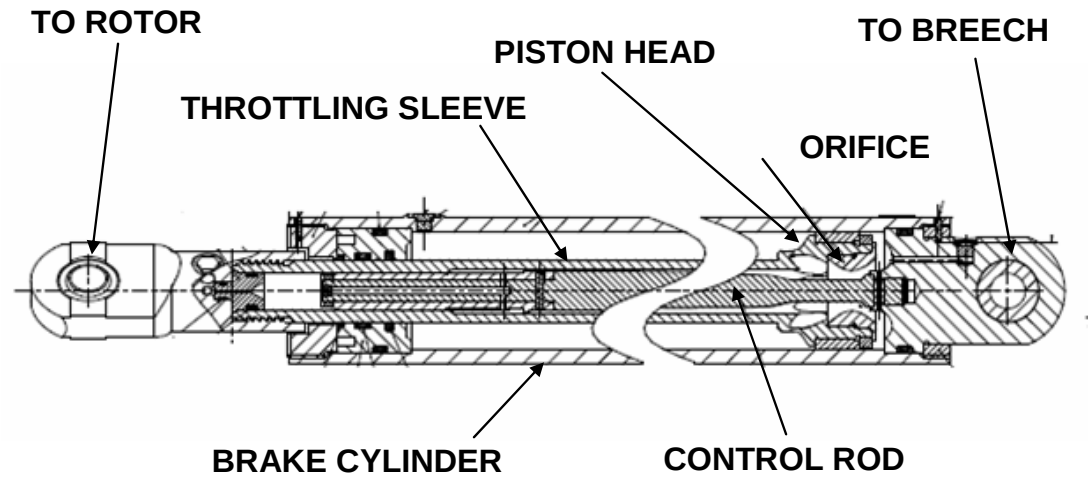

Figure 19. Assembly View of XM360 Recoil Brake

the areas of concern. As such, the actual flow is forced around shoulders and diverted through angular paths as well as a possible swirling motion as the fluid is driven circumferentially towards one of the ports.

Although we have always treated this as axisymmetric pipe flow, the exclusion of the 3D component through the six ports in the piston head should not compromise the required accuracy of the model. Therefore, flow representation for our CFD analysis will be axisymmetric.

A simplified model of the process detailed above is shown on Figure 20. It is comprised of two solid boundaries (heavy dark blue line) which envelopes the fluid (light blue fill). The model is axisymmetric and the given radial dimensions best represent the actual specifications for the current recoil brake. The variable dimension is the rod diameter, shown on the right side of the lower boundary. A constant rod diameter was utilized rather than a taper to simulate the control rod. This constant diameter varies from 0.375 to 0.5625 inches. We choose increments of 0.010 inches (ending at 0.555 in due to run time constraints as will be detailed later) yielding 19 distinct geometric models. The length of the model is only 4.75 inches which encompasses a small portion of the total flow within the brake. (When fully compressed, the actual length of the fluid column in the high pressure volume is 24 inches.) Unlike the physical component, the solid boundaries are immobile whereas the fluid is fed from left to right within the enclosure. The fluid entering the left boundary is given a flow rate or velocity which simulates a given recoil speed whereas the fluid exiting at the right boundary is in a zero pressure state which is the assumed state in the recoil simulation model. The CFD model calculates back pressure near the entrance. Using back pressure as the first independent variable and the input flow speed as the second independent variable the reformulated Bernoulli equation (Figure 11) is solved for C_d. We choose speeds from 5 to 700 in/sec in varying increments as our inlet flow condition. The full matrix of geometries and flow speeds yielded 627 runs of the CFD code.

The element density is a function of the location within the fluid and the clearance between the boundaries. Prior to developing this model, we conducted convergence studies on a similar flow regime and concluded that a minimum of 8 triangular elements within the core of flow and 3 prismatic boundary layer elements at each surface was sufficient to produce convergent results as a function of element

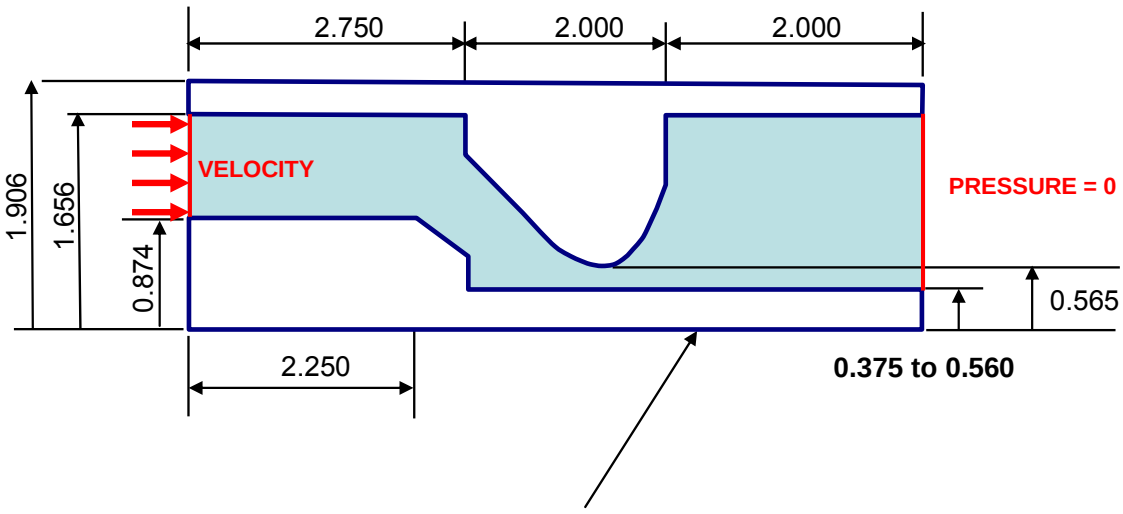

Figure 20. CFD Model of Axisymmetric Flow Area

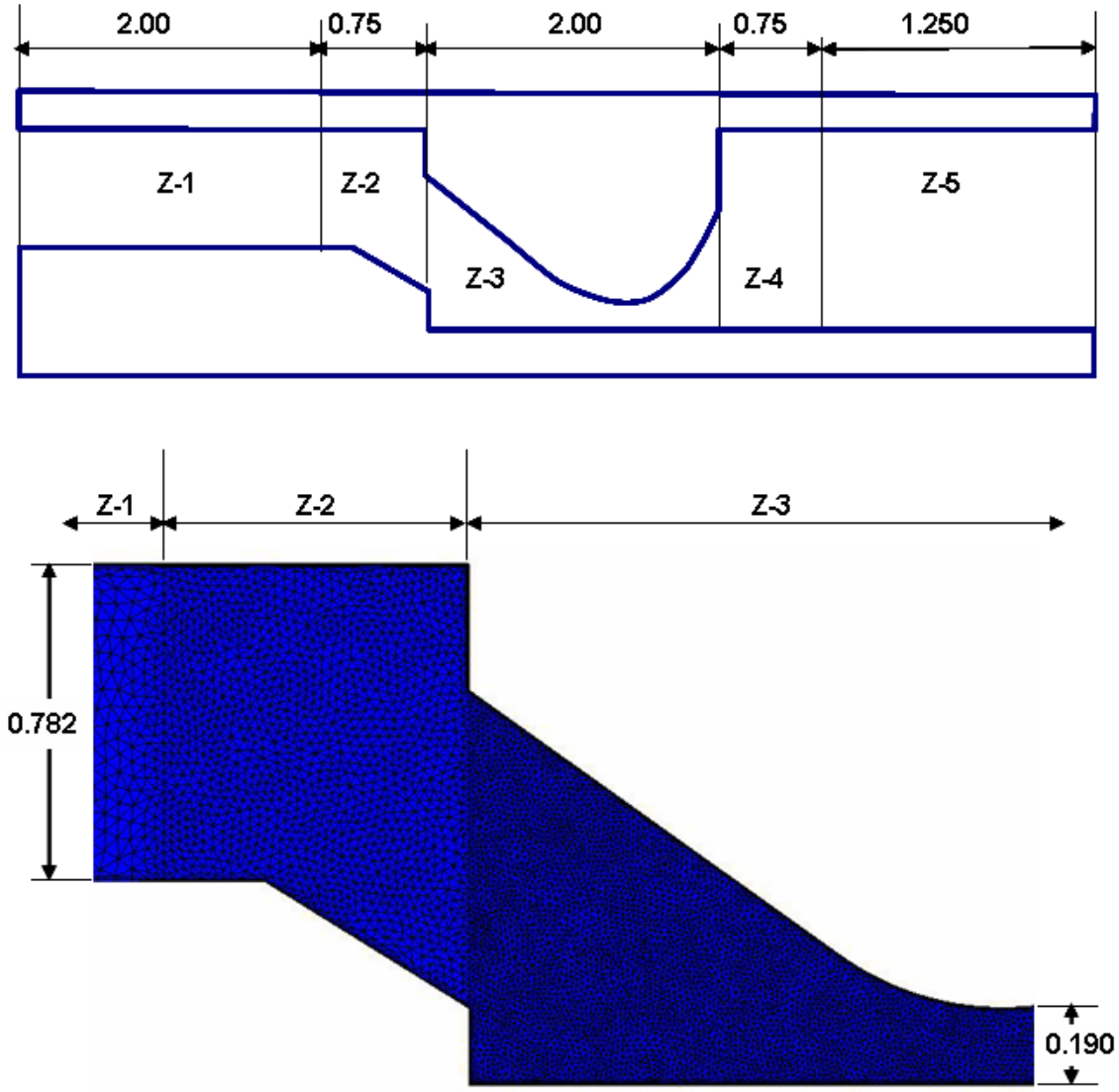

Figure 21. Zones of the CFD Model with Typical Meshing Density

density. Given that clearance values would be as small as 0.010 inches for a tight fitting control rod, we had the model divided into 5 zones within which the element density could be independently specified. These zones are depicted on Figure 21 as Z-1 through Z-5. The zones Z-1 and Z-5 at the extreme end of the fluid volume are, for the most part, independent of throat clearance; therefore, element density within these two zones was is always set to about 20 triangular and 3 each rectangular boundary layer elements at the solid surfaces. Nodal spacing was between 0.035 to 0.040 inches. For zones Z-2 and Z-4, which must merge with the elements within the throat area, there is some dependence upon clearance. Nodal spacing was 0.0175 to 0.025 inches dependent upon the throat clearance. Spacing in this range yielded

element densities of 32 to 40 triangular elements along with the usual boundary layer elements. Within the throat zone (Z-5), nodal spacing varied from 0.0025 to 0.015 inches, dependent upon clearance. This range always kept the element number to at least 8 triangular elements, the condition needed for convergence. For the looser fitting control rod diameters, the number of fluid elements was approximately 20,000 whereas for the tightest fit the number of elements increased to 234,000. For the mesh shown in the figure, there are 11,349 nodes and 21,970 elements. The nodal density change from Zones 1 to 3 is quite evident. Several hundred iterations were needed for convergence irrespective of number of elements. The actual run times for a single analysis ranged from 10 minutes for coarser element models to over 8 hours for the denser element models. Several weeks were needed to complete the full range of simulations.

Representative Results from the CFD Steady State Flow Model

As mentioned, we conducted approximately 627 individual runs to generate the pressure and flow speed data needed to calculate C_d. We shall report in detail the results from one geometric model. The chosen configuration is the one in which the rod diameter is 1.010 inches (0.505 inches radial). This geometric configuration needed a total of 43,450 elements for convergence. At this element density, the compilation time per iteration was 2.6 seconds. For the 33 runs the total number of iterations was 18,950 which convert to about 14 hours of run time. Since batch processing and overnight runs are possible, all 33 including post processing were completed in a few days. All the numerical data required to determine C_d was ported to a Sigma Plot© worksheet and processed via a user developed transform. (A transform is merely a set of instructions for manipulating and processing data that reside in Sigma Plot spreadsheet files.)

On Figure 22, the calculated values for C_d are shown in two plots. The upper reports C_d as a function of flow velocity which is the inlet condition used in the CFD model, whereas the lower plot shows C_d as a function of volumetric flow rate. (Velocity and flow-rate at any point in the fluid are directly proportional via the continuity equation for incompressible flow.) These plots are typical in shape for all rod profiles; however, the C_d values are shifted vertically as a function of rod diameter. From these plots it

CFD ANALYSIS OF RECOIL CYLINDER / ORIFICE FLOW
FLUID: INCOMPRESSIBLE HYDRAULIC BRAKE @ 75°F

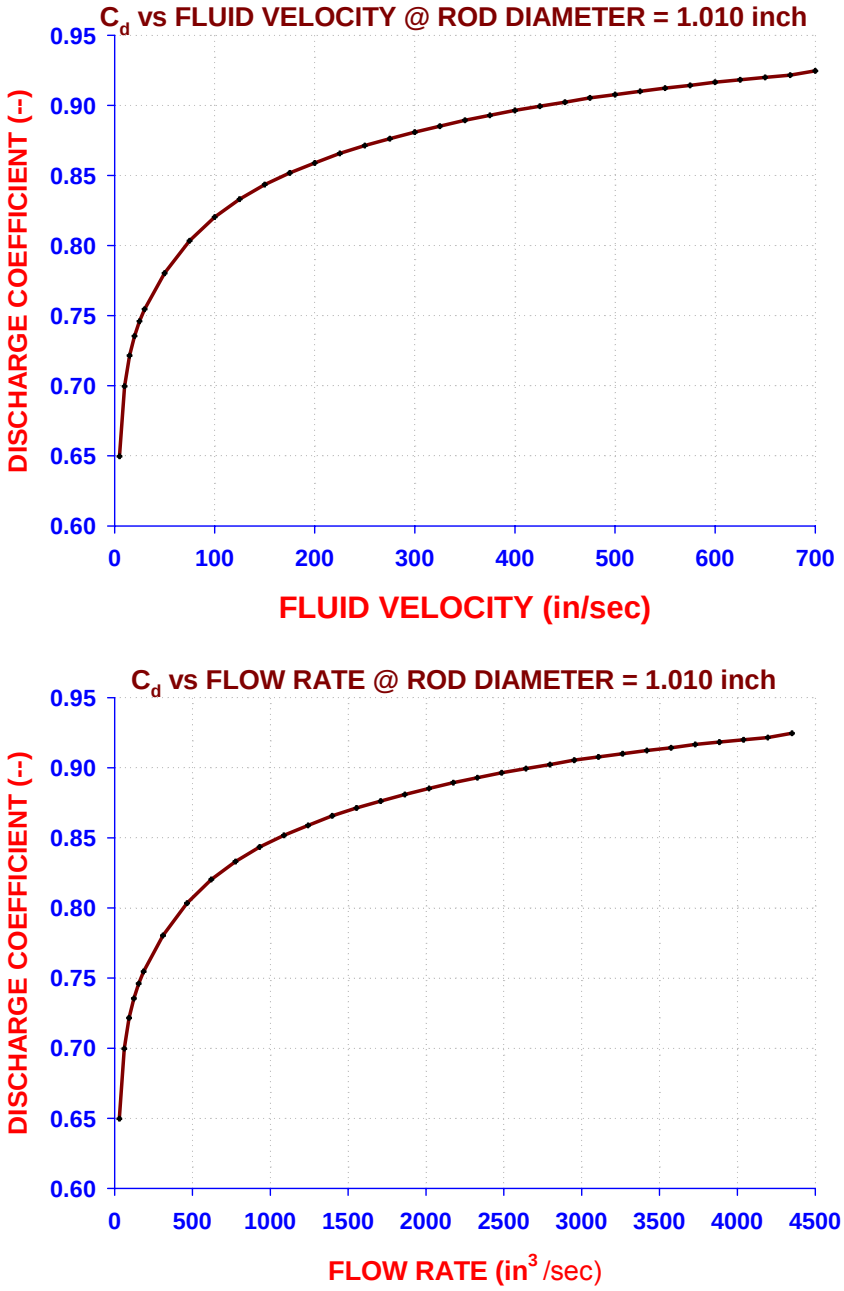

Figure 22. Discharge Coefficient vs Velocity & Flow Rate

is apparent that C_d is a strong function of flow speed. At low flow speeds (0 to 100 in/sec) the rate of change is quite large from 0.65 to 0.82. From this point it rises at a much slower rate, finally achieving its highest value of 0.925 at a flow speed of 700 in/sec. It is, as expected, a well behaved response, void of singularities and inflection points. The data needed for the recoil analysis code will be derived from the lower plot. We expect to set up tables of C_d versus flow rate, since this is the value that is iterated in the recoil model when attempting to calculated correct distribution of flow rate and pressure.

Figures 23 and 24 contain more detailed information regarding the flow. On Figure 23, we show the axial velocity profile from the entrance to the exit of the orifice. The range of values as shown on the color bar is from 0 to 1000 in/sec with the value of 700-1000 within the fluid's core at the throat. The flow speed at the inlet is only 25 in/sec, so a speedup of nearly 40 to 1 is indicated based upon the maximum flow speed in the throat. By using the continuity relationship, the average speed increase should be about 30 to 1 for this orifice which is the case if we were to calculate an average velocity at the throat. On figure 24, we show the pressure drop through the orifice. Left of the shoulder the pressure is rather constant between 30 and 35 psi. Pressure drop does not occur until the flow becomes quite restricted just to the left of the throat, finally exiting on the right at about 0 psi. The data on these two plots represent a classical result for orifice flow, the rapid speed up and pressure drop as the flow path becomes more restricted.

In the following section, we shall discuss the details involved in compiling these results into a form which in amendable to incorporation into the Benét Labs recoil analysis code. Additionally, we shall delve into the logic used in the code to implement a variable C_d for the main orifice.

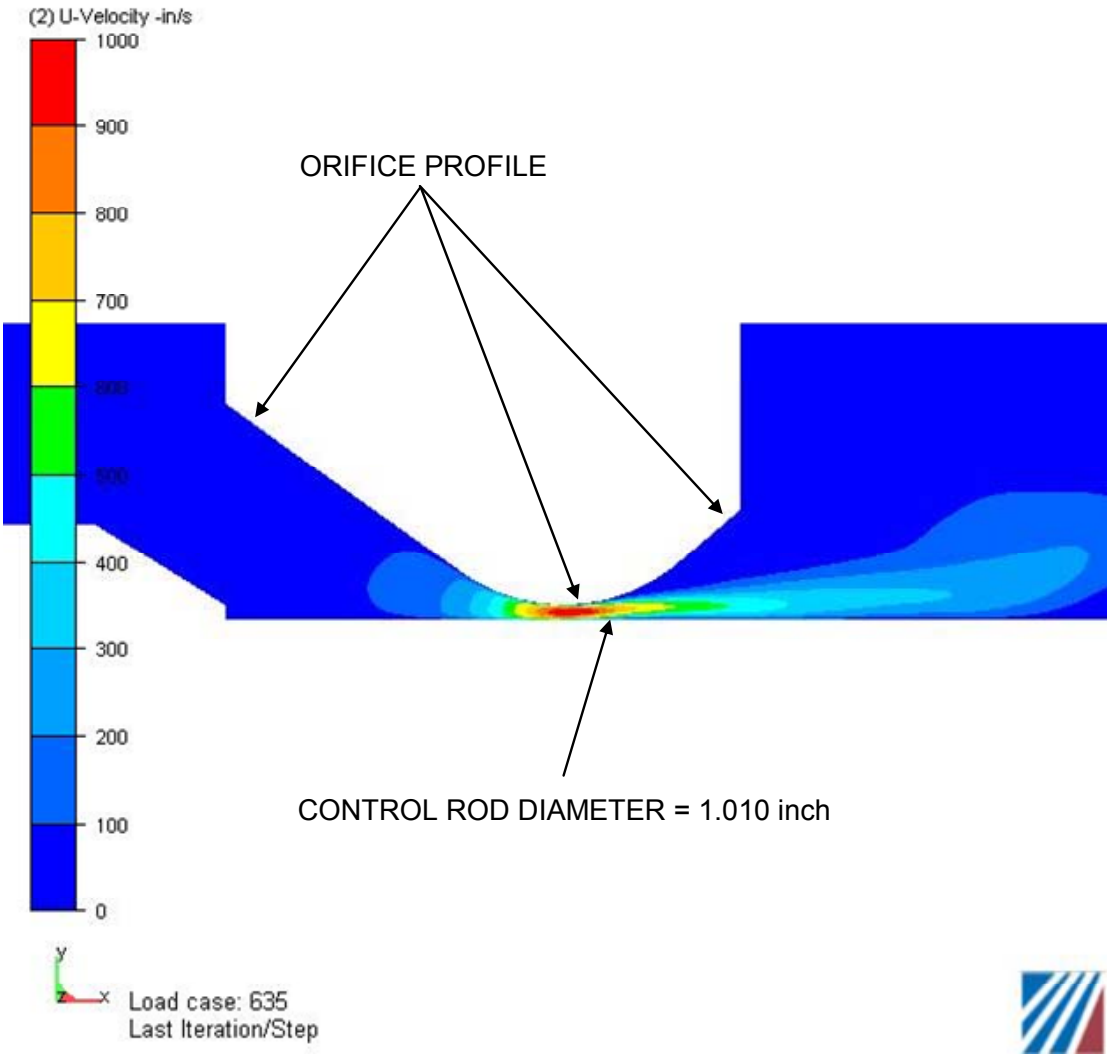

Figure 23. Velocity Profile Through Orifice 505 @ 25 in/sec Boundary

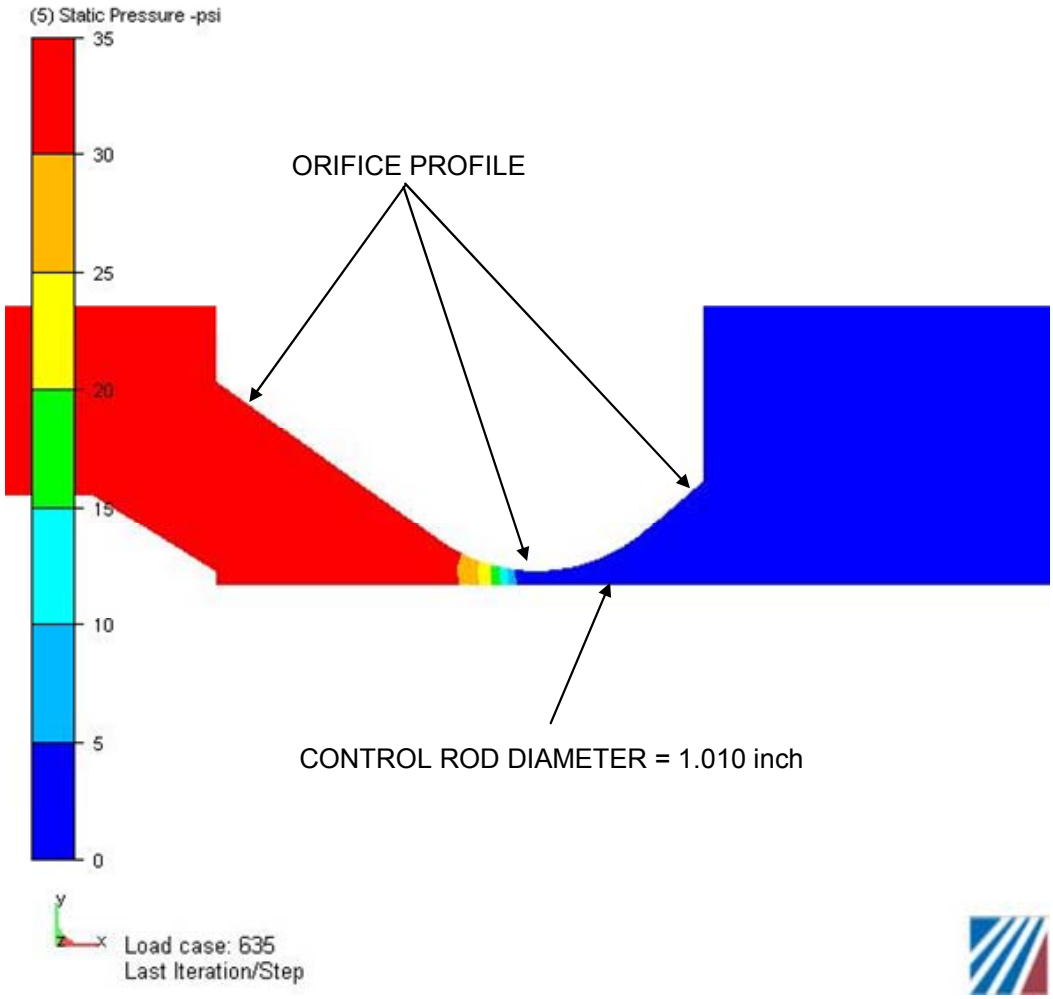

Figure 24. Static Pressure Profile Through Orifice 505 @ 25 in/sec Boundary

Application of Results to the Benét Labs Recoil Analysis Model

Extraction of Discharge Coefficient Values from CFD Results

We have conducted 627 independent runs using CFdesign© code for 19 geometry configurations and 33 flow speed conditions. Total CPU time for the conduction of these analyses was 485 hours with a total number of iterations of approximately 320,000. In the last section, we discussed in some detail the 'raw' data results from the model as well as the method of determining the parameter of concern which is the discharge coefficient of the restrictive flow path. Reiterating, the Benét Labs recoil analysis code uses the Bernoulli equation for all its pressure versus flow rate calculations, therefore, any restrictive areas must be rated for their efficiency (orifice coefficients) with respect to pressure enhancement due to contraction of the flow stream. Handbooks have a plethora of data regarding these coefficients with such parameter features as the lead in and exit angle of the constriction. The orifice type used in brakes designed at Benét Labs utilizes a spherical boundary on the orifice surface and a gentle taper on the control rod profile.

From the results cited in the previous section, we decided that the best way to attack the problem was to develop a two-parameter dataset to represent the C_d values. The parameters chosen are the flow rate in cubic inches per second (in^3/sec) and a parameter called the area ratio. The range of flow rate values used in the CFD analysis was 31 to 4340 (in^3/sec) which bounds the expected recoil velocities. The area ratio is the ratio of the flow area in the main chamber to the area across the throat of the restrictor. The range of this value in the actual brake is 11 to 702. When the area ratio is at a low value the throat area is open and vice versa when the ratio is large. Results for 7 of the 19 separate area ratio models are shown on Figures 25 and 26 using color coded lines to indicate the area ratio. The 'data' presented is the calculated C_d values as a function of flow rate with the various area ratio values as parameters of each trajectory. Four flow rate zones were established based on the corresponding recoil velocities. In Zone 1 the flow rate range is 0 to 400 in^3/sec. For Zone 2 the flow rate is 400 to 1000 in^3/sec. Results for these two flow rates are shown on Figure 25. Zone 3 flow rate is 1000 to 2600 in^3/sec. whereas Zone 4 flow rate is 2600 to 4400 in^3/sec. Results for these rates are shown on Figure 26.

The upper plot on Figure 25 contains results for Zone 1 flow rates. The range of flow rate values

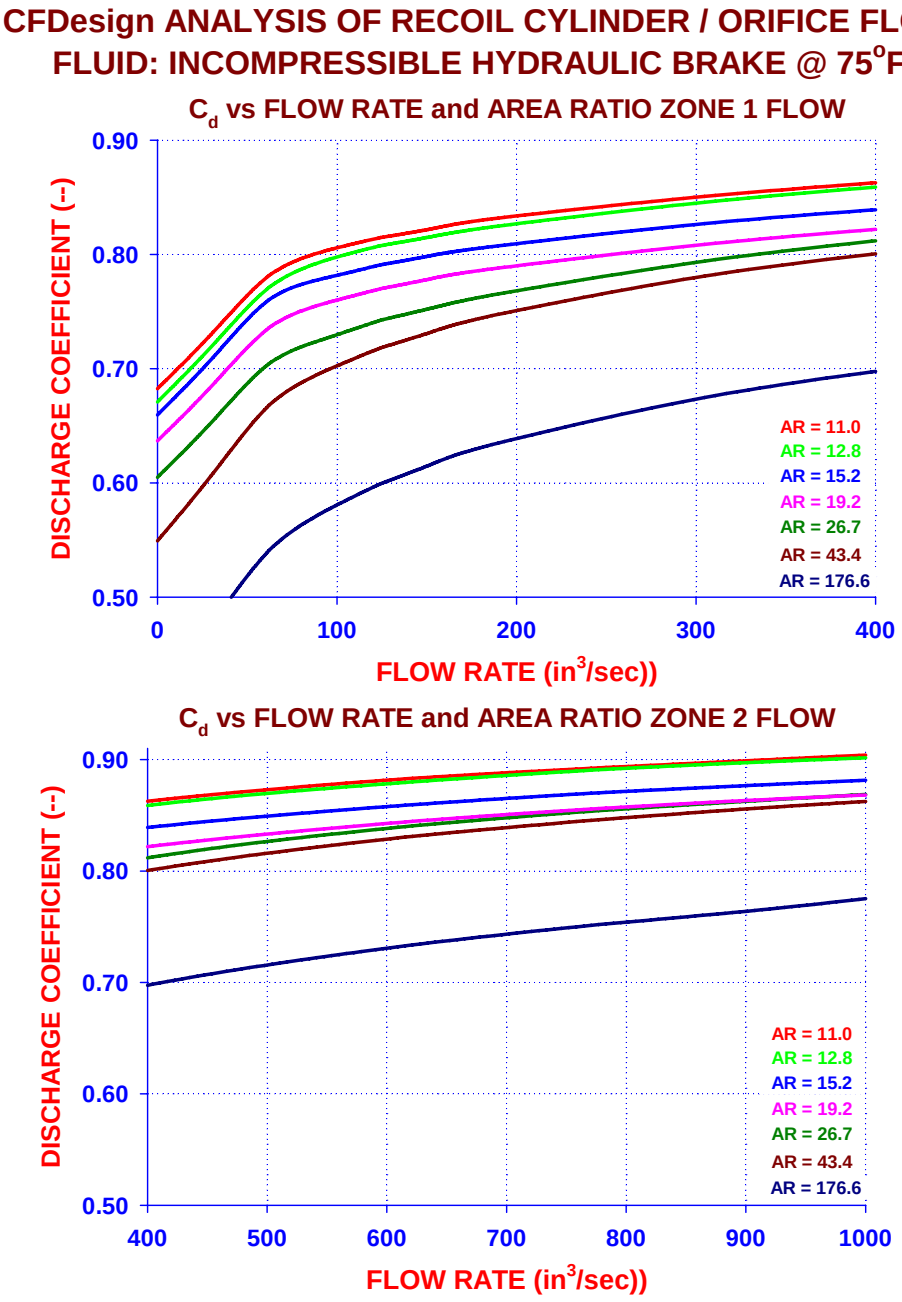

Figure 25. C_d Results for Flow Rate Zones 1 & 2

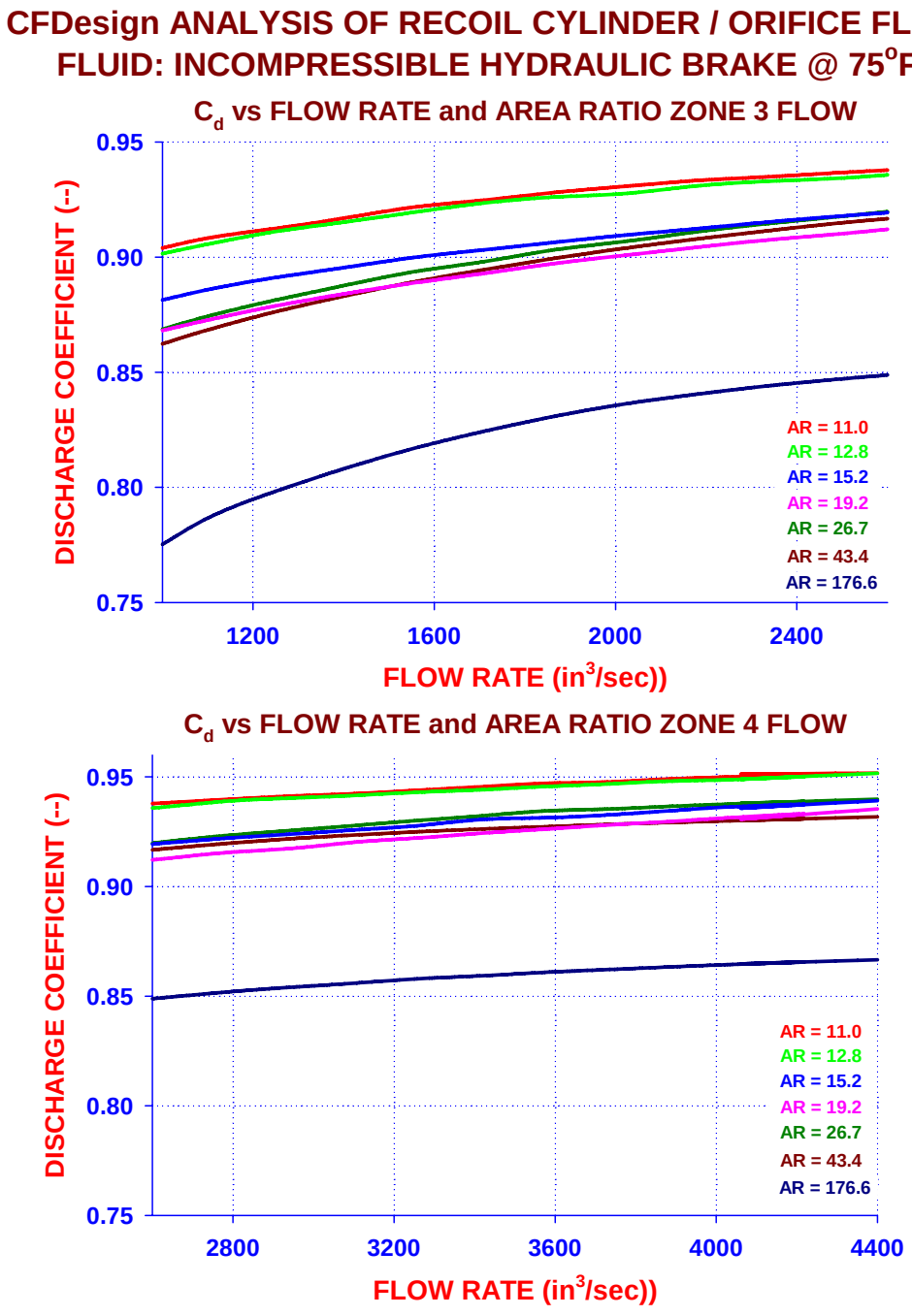

Figure 26. C_d Results for Flow Rate Zones 3 & 4

is 0 to 400 in^3/sec which corresponds to a recoil velocity range of 5 to 70 in/sec. These flow rates would be achieved very early in the recoil cycle when the initial acceleration causes a ramp up in speed and again at the termination of the cycle when deceleration reduces recoil speed. The smaller area ratios would be the case in the early portion of the cycle and the larger for the final portion of recoil cycle. The C_d range for these conditions is 0.40 to 0.86. As indicated, the data trajectories are smooth and monotonic with respect to both flow rate and area ratio. A substantial 'ramp up' is shown for very low flow rates (0 to 150 in^3/sec). The C_d trajectories decrease with increasing area ratio with a several point decrease for the largest area ratio but remain rather typical in shape. The lower plot on Figure 25 contains results for Zone 2 flow rates. The range of flow rate values is 400 to 1000 in^3/sec which corresponds to a recoil velocity range of 70 to 170 in/sec. The C_d range for these conditions is 0.70 to 0.90. The trajectories are monotonic and show signs of approaching asymptotic values without the presence of the 'knee' as shown for Zone 1 results. As before, the trajectory for the largest are ratio is far removed form the rest.

The upper plot on Figure 26 contains results for Zone 3 flow rates. The range of flow rate values is 1000 to 2600 in^3/sec which corresponds to a recoil velocity range of 170 to 420 in/sec. The C_d range for these conditions is 0.78 to 0.94. Response trajectories are as before, increasing with increasing flow rate, with a downward shift as the area ratio is increased. The lower plot on Figure 26 contains results for Zone 4 flow rates. The range of flow rate values is 2600 to 4400 in^3/sec which corresponds to a recoil velocity range of 420 to 700 in/sec. The C_d range for these conditions is 0.85 to 0.96. Comments regarding the responses in this zone are the same as above.

To sum up the entire CFD analysis, we are presenting all of the results on a single plot. This is presented in Figure 27. The flow rate range is 0 to 4400 in^3/sec whereas the C_d range is 0.50 to 0.95. For high speed flow rates (i.e.>2000 in^3/sec) the C_d range is between 0.85 and 0.95. For the slower flow rates (500 to 2000 in^3/sec) the C_d range is between 0.75 and 0.92. For slow flow rates (< 500 in^3/sec) the C_d range is between 0.50 and 0.87. When the trajectories are viewed in this expanded range it is quite clear that a strong relationship between C_d and flow rate exists containing a discernible 'knee' around the 500 in^3/sec flow rate. Since the range of flow rate values exercised in this model envelope the entire range of

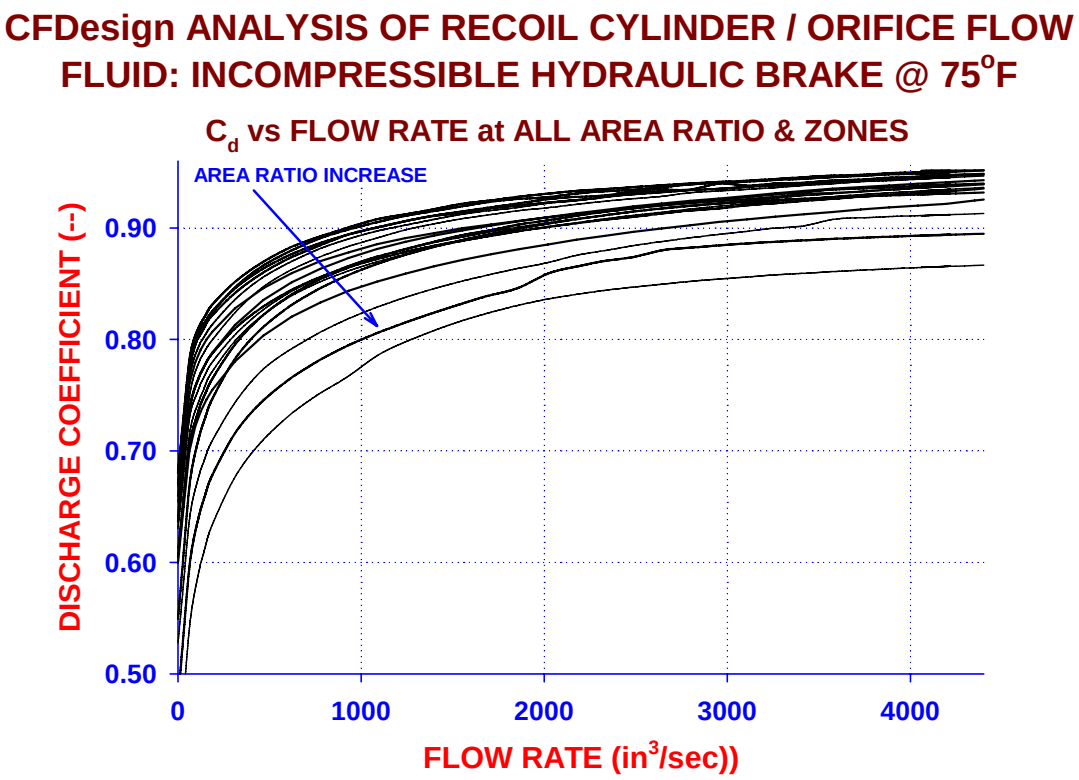

Figure 27. C_d Results for all Calculations

expected values and enough structure has been demonstrated for each area ratio, a linear interpolation of C_d between flow rate values is warranted.

Although the dependence upon area ratio is not as severe, it is quite clear that as this value increases, the entire range of C_d values decreases. Unfortunately, we could not conduct CFD simulations for the very large area ratios since the time and cost burden would be prohibitive. The table below presents a breakout of the costs for each area ratio exercised in these simulations. The first column contains the model number running consecutively from 1 to 19. The second column contains the radial values of the control rod profile whereas the third contains the area ratio for each of these radial values. The fourth column contains the CPU time in hours for the 33 simulations (flow rate is the independent variable) for these area ratios with the total number of iterations is in the fifth column. The last column contains the time per iteration in seconds.

GEOMETRIC MODEL NUMBER	CONTROL ROD RADIUS (in)	AREA RATIO	CPU TIME (hrs)	NUMBER OF ITERATIONS	ITERATION RATE (secs / iter)
1	0.375	11.08	4.02	14010	1.03
2	0.385	11.57	6.38	15575	1.47
3	0.395	12.12	5.81	14740	1.42
4	0.405	12.75	6.69	16872	1.43
5	0.415	13.46	4.39	16657	0.95
6	0.425	14.27	5.55	15555	1.28
7	0.435	15.22	8.02	16519	1.75
8	0.445	16.32	7.88	16101	1.76
9	0.455	17.63	6.73	14074	1.72
10	0.465	19.21	9.48	15776	2.16
11	0.475	21.14	8.61	15933	1.95
12	0.485	23.55	6.40	14468	1.59
13	0.495	26.66	8.54	15087	2.04
14	0.505	30.82	13.71	18957	2.60
15	0.515	36.64	18.24	19136	3.43
16	0.525	45.38	12.83	18304	2.52
17	0.535	59.95	35.95	23023	5.62
18	0.545	89.12	38.26	15466	8.91
19	0.555	176.65	277.53	23610	42.32

Table 1. Summary of Cost Burden for CFD Analysis

As we examine these results it is quite clear that the larger area ratios are quite burdensome in regard to execution time. In addition the trend is non-linear in that the time increases by a factor of 70 from the smallest to the largest ratio and the iteration rate increases by 40. The final ratio reported is 176.65 which correspond to a control rod radius of 0.555 in. The CPU time required for these simulations was over 11 days! The greatest radius of the current control rod is 0.5625 which occurs at the very end of recoil stroke. The area ratio for this rod would be ~700 and the number of elements and the time needed to analyze this configuration would be unfathomable. So, we decided to use an extrapolation method to approximate the C_d results out to the area ratio of 700.

Figure 28 presents the calculations (scatter plots) for C_d as a function of area ratio for 6 of the 33 flow rate values used in the CFD analysis. Color coding is used to distinguish between different flow rates. In the upper plot the results are presented on Cartesian coordinates whereas in the lower plot a semi-log graph is employed with the common logarithm of the area ratio as the independent variable. The range of flow rates presented bound a recoil speed of 5 to 600 in/sec. The area ratio axis range is 0 to 200 for the upper plot and 10 to 700 for the lower plot. The trend as a function of area ratio is similar for all flow rates with a decreasing dependence as the flow rate increases. For example, in the upper plot the results for a flow rate of 31 in^3/sec are the lowest set of 'data' points which range from 0.75 to 0.49. The upper set of 'data' ranging from 0.95 to 0.88 is for flow rate of 3726 in^3/sec. The dependence upon area ratio becomes less severe as the flow rate ratio increases. In the upper plot the indicated trend is exponential as a function of area ratio. When the common logarithm of the area ratio is used as the independent variable the points tend to become linear. This is indicated in the lower plot. The lines drawn within each set of 'data' merely indicate that an approximate linear trend could be employed to extrapolate the results out to the largest area ratio value. As is indicated by these lines, the C_d values at an area ratio of 700 could be reduced by as much as 0.15 from the lowest calculated value at area ratio of 176. This response characteristic will be exploited when the interpolation algorithm is developed for the recoil analysis code.

Brief Explanation of the Current Recoil Analysis Code

As mentioned earlier, the current Benét Labs Recoil Analysis Code employs a fixed value for the

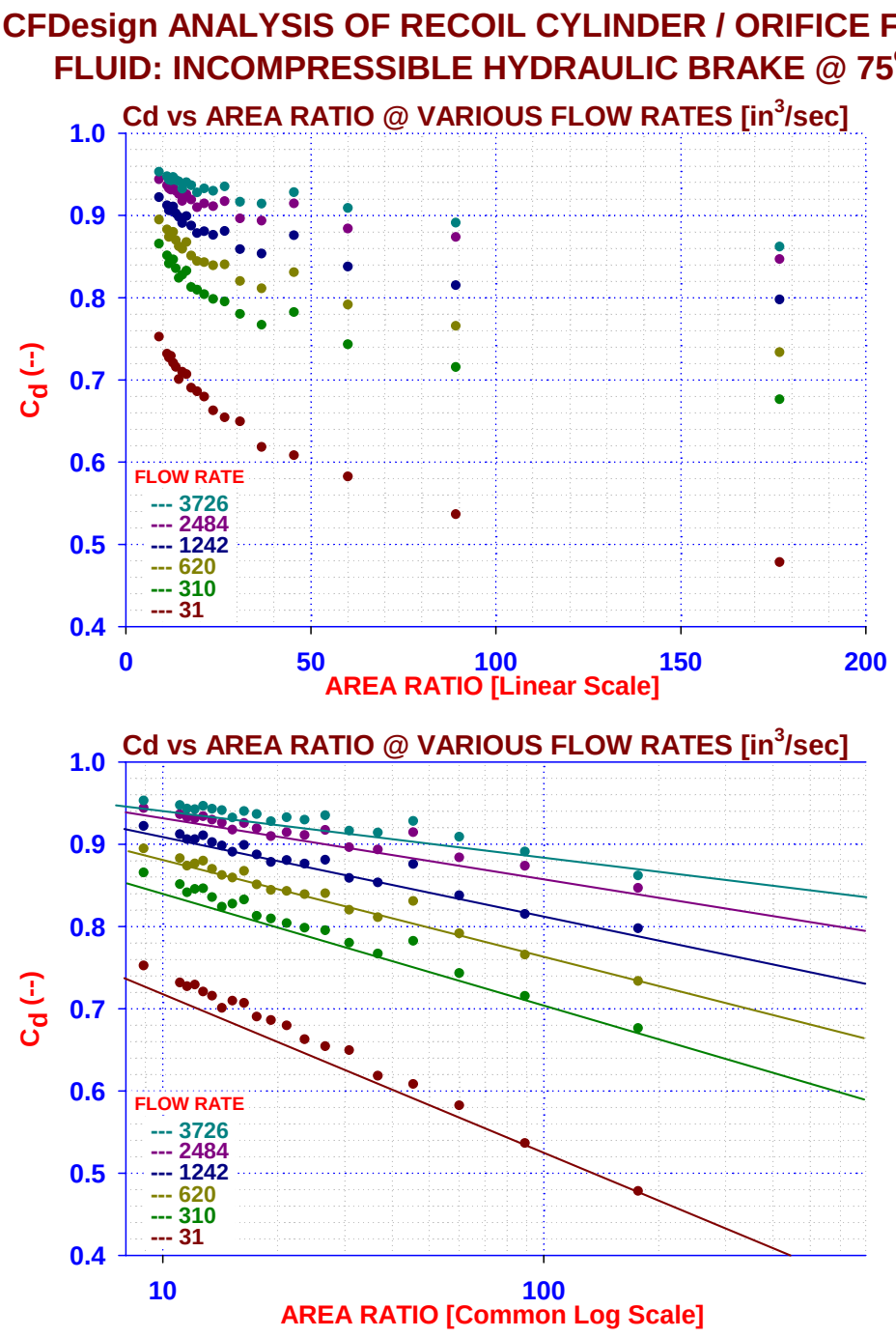

Figure 28. C_d Results for Various Area Ratios

discharge coefficient across the main orifice. Its value has been based upon those published in technical literature as well as empirical results based upon firing data. The most applicable values are usually between 0.90 and 0.95. In order to explain the implementation of the variable C_d feature, a brief 'tour' of the code's structure and logic flow is warranted. The initial release of this code occurred in 1981. Since then, it has been modified to include additional features and more elaborate modeling techniques. A complete rewrite of the code was completed in the early 1990's, after which several other modifications were made and features added.

Figure 29 contains a skeletal and simplified view of the overall code via standard flowchart terminology. The INPUT DATA block reads overall system data including number of brakes and recuperators, weight of recoiling parts, bore area, friction coefficients, muzzle brake characteristics, integration and output time steps as well as total analysis time. A tabular file of bore pressure versus time is input as well. An initial call is made to the RECUPERATOR and RECOIL BRAKE subroutines to read data for these components. Up to 6 input files are available for each. The recoil brake data includes diameter specifications for the brake cylinder and throttling sleeve, orifice diameter, temperature and bulk modulus of the fluid, several discharge coefficients for both recoil and counter recoil, as well as ramp up distribution features for partially filled fluid chambers. In separate tabular files, the diameter profile of the control rod and the characteristics of the backflow restrictive areas are input as function of the axial location of the recoiling parts. A file containing friction factor data as a function of Reynolds Number (i.e. Moody Chart) is input and is used in calculating the pressure drop along the flow length to and from the buffer chamber. Additionally, files for the density and viscosity of the fluid are input as a function of fluid temperature. The temperature value in the brake input file will determine the values of density and viscosity to be used during the analysis. The recuperator data includes relevant diameter and length specifications for the cylinder and rod, preload pressure and ratio of specific heats for the working gas. Subsequently, several initial values within the SET INITIAL VALUES block are set. An example would be the values of the integrator coefficients for the Adams-Bashfort multistep method and the initial values for recoil velocity and location.

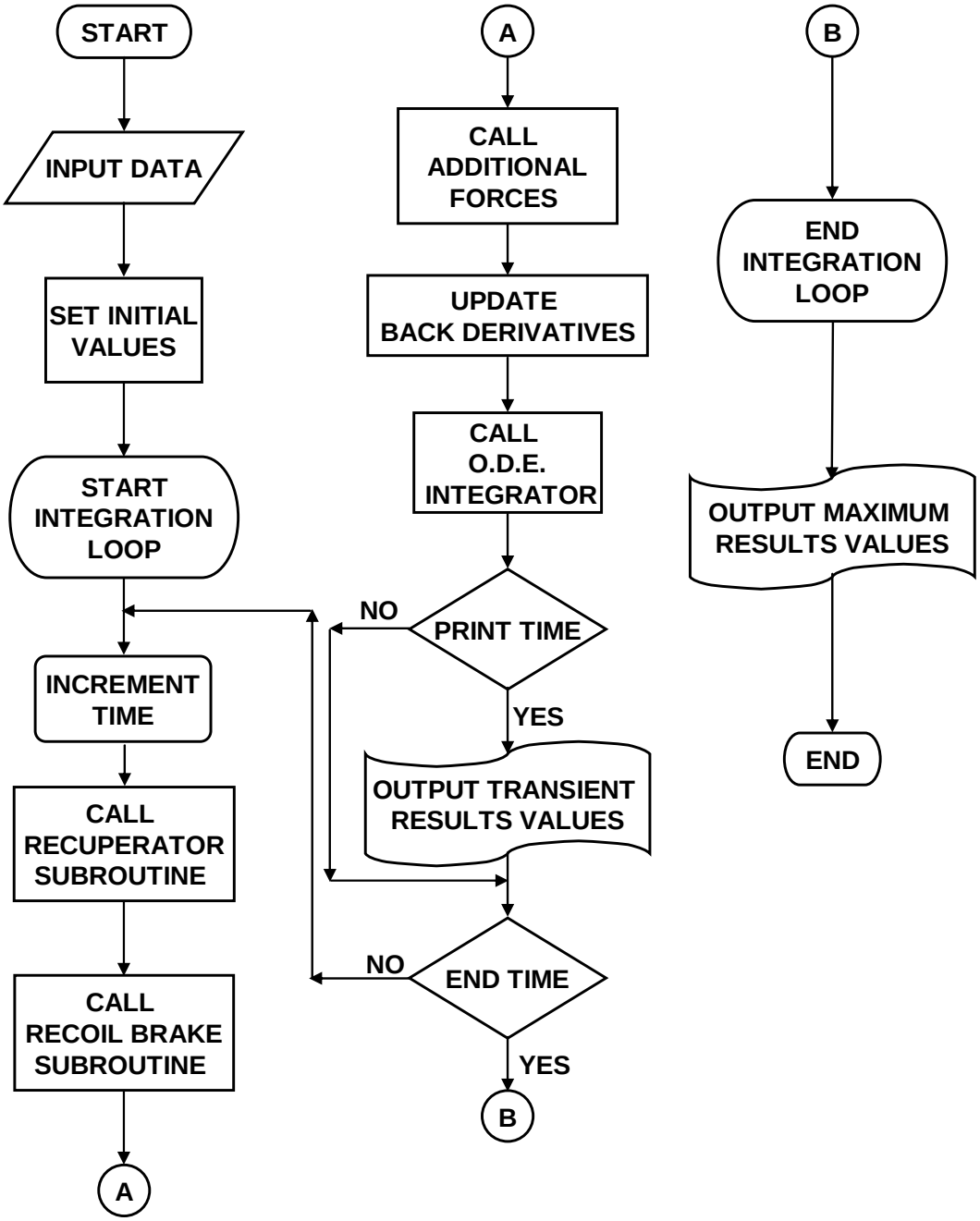

Figure 29. Overview Flowchart of Benet Labs Recoil Analysis Code

The dynamic analysis commences in the START INTEGRATION LOOP. The ballistic driving force is determined based upon the current time in the analysis and separate calls to the recuperator and brake subroutines are made for each component yielding values for the brake and recuperator forces at the current time step. Additional forces are then determined (e.g. friction, etc) from which the recoil acceleration for the current time step is calculated. The back derivatives are updated in the UPDATE BACK DERIVATIVES block and a call is made to the ODE integrator (CALL ODE INTEGATOR), yielding the current values for recoil velocity and travel. The PRINT TIME decision test yields transient values for output variables when applicable. The END TIME decision test either returns control to the integration loop for continuation of another time step or ends the analysis. Upon analysis termination, maximum values for selected output variables are reported to a maximum values file.

Figure 30 contains a simplified view of the flow within the recoil brake subroutine. There would be multiple calls to this routine within each time step dependent upon the number of brakes used in the analysis. Upon initial entry the parameter values for brake 'n' are placed in local variables. These values include brake specification dimensions, current flow rates, etc. The RECOIL OR C'RECOIL decision diamond determines the direction of travel. There are separate calculation equations for each direction. Dependent upon the recoil direction, forces and pressures are determined via the two CALCULATE blocks. Fluid flow rate states are reset for the current brake and the subroutine returns control to the main program.

Development of Variable Discharge Coefficient Capability in the Recoil Analysis Code

Figure 31 contains details of the logic within the branch flow portion of the recoil phase calculation block. As mentioned earlier, the flow within the brake during recoil follows two paths. During any time step the value of the outflow rate (in^3/sec) from the main chamber is known and is based upon the multiplication of recoil speed and cross section area of the main fluid chamber of the brake cylinder. A portion of the fluid flows through the annular restrictor defined by the control rod and the main orifice while the rest flows back over the buffer plug into the buffer chamber. However, a closed form solution to the equations yielding pressure for these flows is not possible since one branch requires the use of friction factors derived from a Moody Chart. So one must resort to estimating the flow rate split (automatically

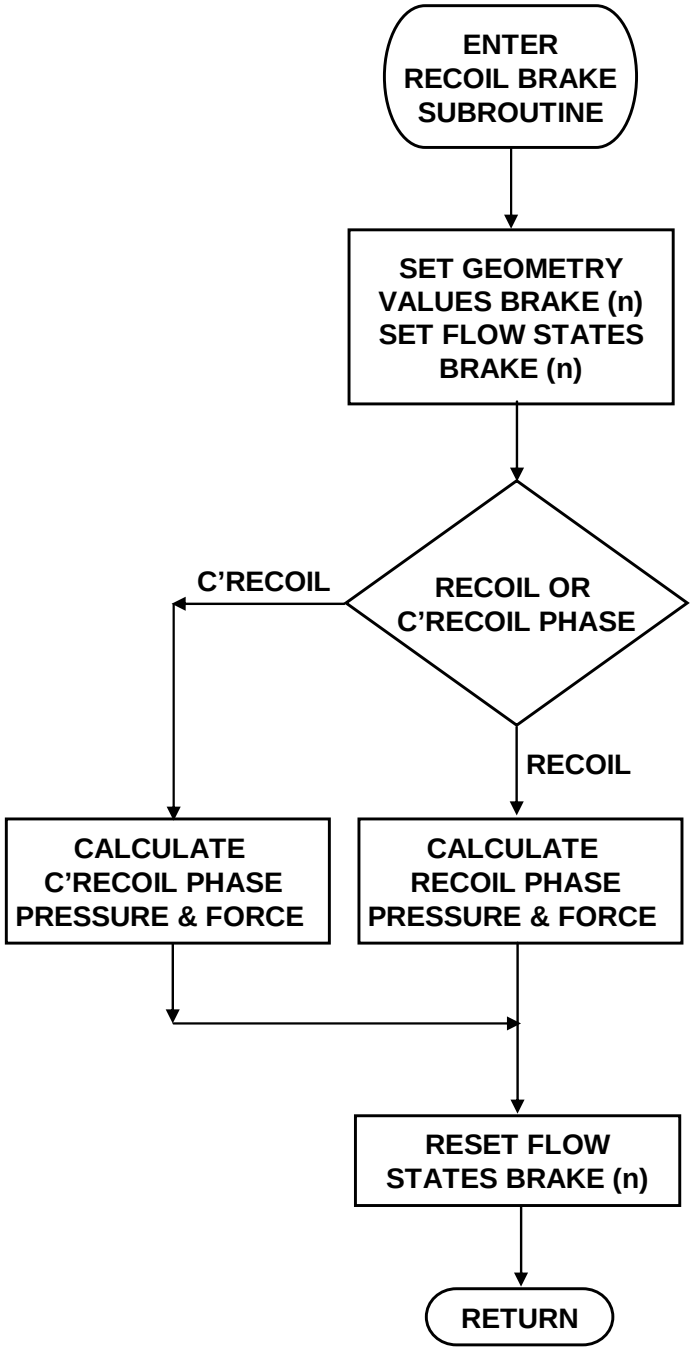

Figure 30. Overview Flowchart of Recoil Brake Subroutine

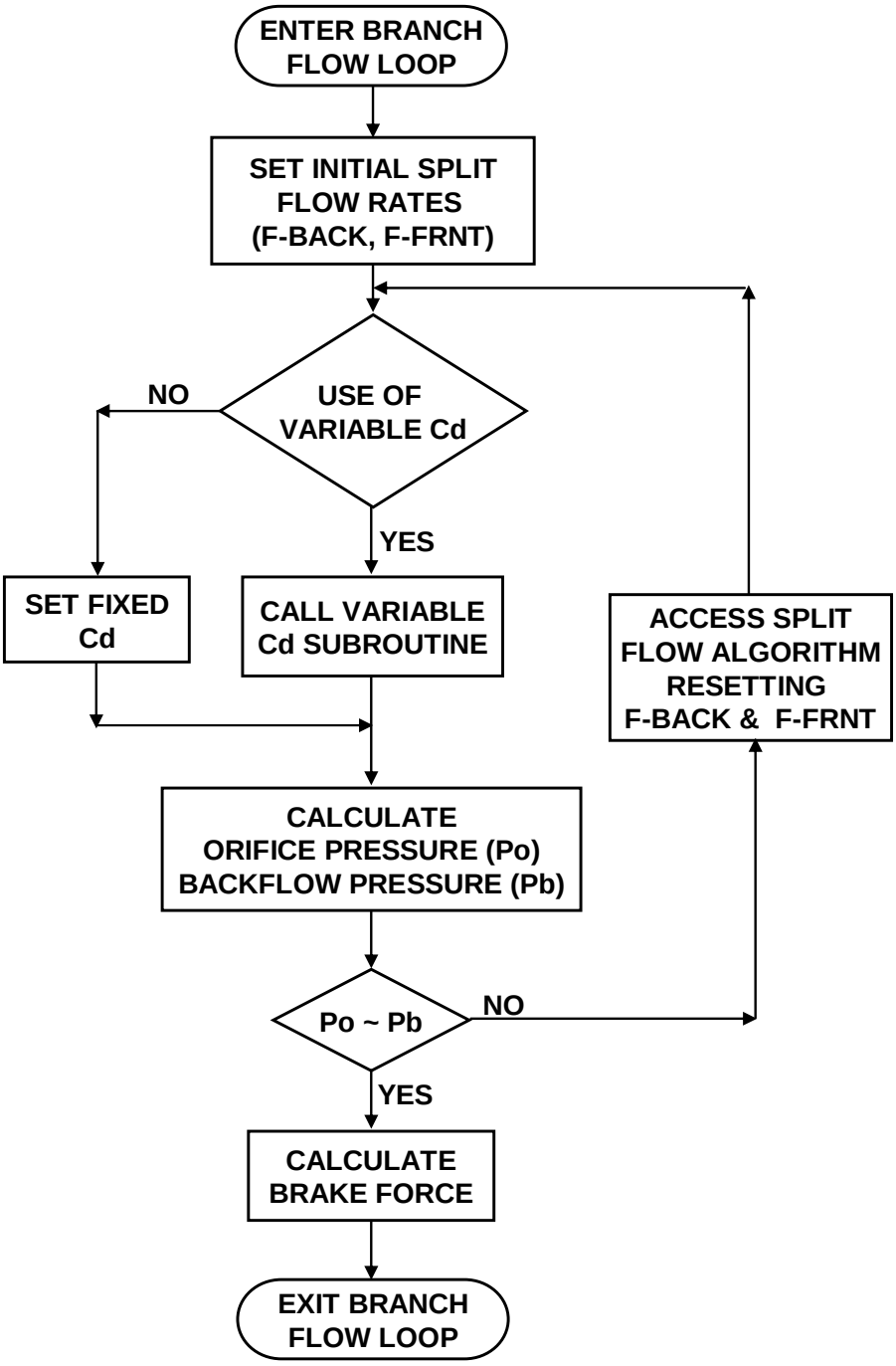

Figure 31. Detail Flowchart of Recoil Pressure/Force Calculations

done within the routine) and calculate the resulting pressures based upon these individual flow rates. Thus the initial setting of an expected flow rate split within the SET INITIAL SPLIT FLOW RATES block is accomplished. The logic portion USE OF VARIABLE C_d has been added to the latest version of the recoil model. Previous versions used only a fixed C_d which was input through the brake data file. In the current model, one has the option of using either. When the variable C_d option is exercised, the VARIABLE C_d SUBROUTINE is called and returns the current value for C_d based upon expected flow rate through the orifice and the area ratio, which is a function of the location of the recoiling parts. It is essentially a two parameter lookup table using linear interpolation for the flow rate and linear interpolation of the common logarithm of the area ratio to calculate values between data points. Upstream fluid pressure is calculated using each flow rate and the appropriate equations for the flow along that path yielding two values for the brake pressure. However, the physics of the problem dictates that both pressures must be the same. Thus the two are compared within the Po ~ Pb decision diamond. If both are approximately equal (a small residual is used for control) then the flow rates along each path are correct and brake force is calculated. If not, then the FLOW SPLIT ALGORITHM block is accessed and based upon the difference in pressure, the flow rate along each path the is adjusted and the pressure calculations are run again. This loop is traversed until the difference between the two pressures is within the residual value, after which the brake forces are determined and the flow volumes within both the front and buffer chambers are updated.

Figure 32 contains the flowchart for the variable C_d subroutine. The data passed to this routine is the expected flow rate and the area ratio at the current location of the recoiling parts. Upon entry a test is made to determine if this is the first pass through the routine (INITIAL ENTRY decision diamond). If true, the empirical data is input from the file relating C_d to flow rate and area ratio. Subsequently, the entered values (Q-in & A-in) are located within bounding pairs of the independent variables. From here, a simple linear interpolation is conducted to determine the C_d value to be used. Control is returned to the recoil brake subroutine with the applicable value for C_d. A listing of the FORTRAN code used to determine the C_d value may be found in the appendix.

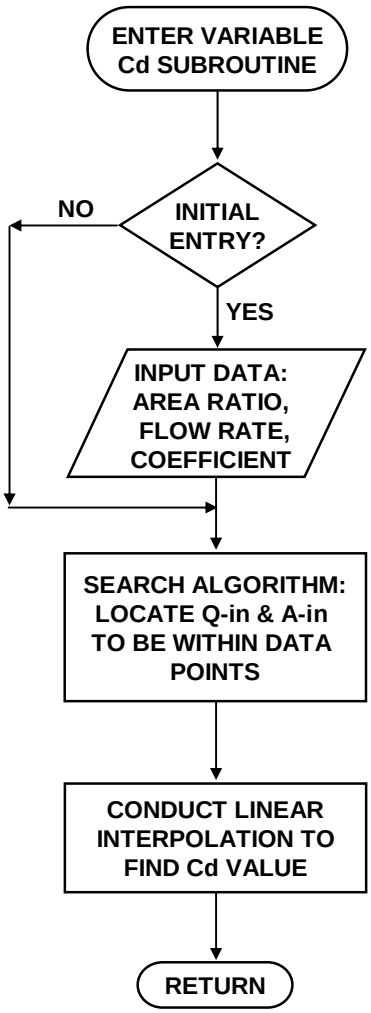

Figure 32. Detail Flowchart of Variable C_d Subroutine

Results Applied to Current Data from XM360 Firing Tests

Comparison of Simulations Using Fixed and Variable Discharge Coefficients

As an initial estimate of the effect of the variable coefficient feature, we shall conduct simulations using a fixed and variable C_d and compare the brake pressure results. The data generated in the CFD analysis at a fluid temperature of 75^{o}F will be used as C_d input. The ballistic pressure data from three 120mm rounds will be used; namely M829A3, M831A1 and M865. The control rod is the as-designed version for a recoil travel of 23.5 inches, which is being developed for the Future Combat System (FCS). Results of this analysis will be reported in pressure versus time and travel plots as well as C_d values plotted against time and travel.

Brake pressures for the M829A3 round are shown on Figure 33. The upper plot shows pressure versus time whereas the lower plot presents pressure versus travel. The blue line is the response for a fixed value of C_d , whereas the red line is the response for variable C_d values. Peak pressure values for both are about 4200 to 4500 psi. During the initial state of recoil (time < 15ms; travel < 4 inches) both responses track each other. From this point, the variable C_d model diverges quickly and overshoots the fixed model by about 300 psi. This occurs just short of 20 ms at a travel value of 5 inches. This response separation continues up to about 60 ms and 17.5 inches of travel. At this point, the pressure responses cross each other and the variable model predicts pressure values that are up to 500 psi lower than the fixed model. Total recoil stroke for the variable model is about 0.5 inches shorter than the same for the fixed model whereas the timing has only a 3 ms difference. C_d values are plotted against time and travel for the M829A3 round on Figure 34. The fixed value of 0.95 is shown along with the values determined within the dynamics analysis loop in the recoil analysis routine. The variable C_d response starts quite low but then rises quickly to its peak value of 0.94 within 10 ms of shot initiation and 2 inches of travel. At its peak, the C_d variation between fixed and variable is only 0.01. The C_d reduces slightly at 15 ms (5 inches of travel) and remains at this level until about 30 ms (10 inches of travel). From this time and travel location, the Cd reduces very slowly to about 0.86 at 60 ms and 19 inches of travel. It then reduces rapidly eventually to a value of 0.45 at 110 ms which is not shown on the plot.

LW120 XM36 RECOIL SYSTEM SIMULATED RESPONSE
RECOIL STROKE: 23.5 inch; ROUND: M829A3 (AMB)
FIXED and VARIABLE Cd

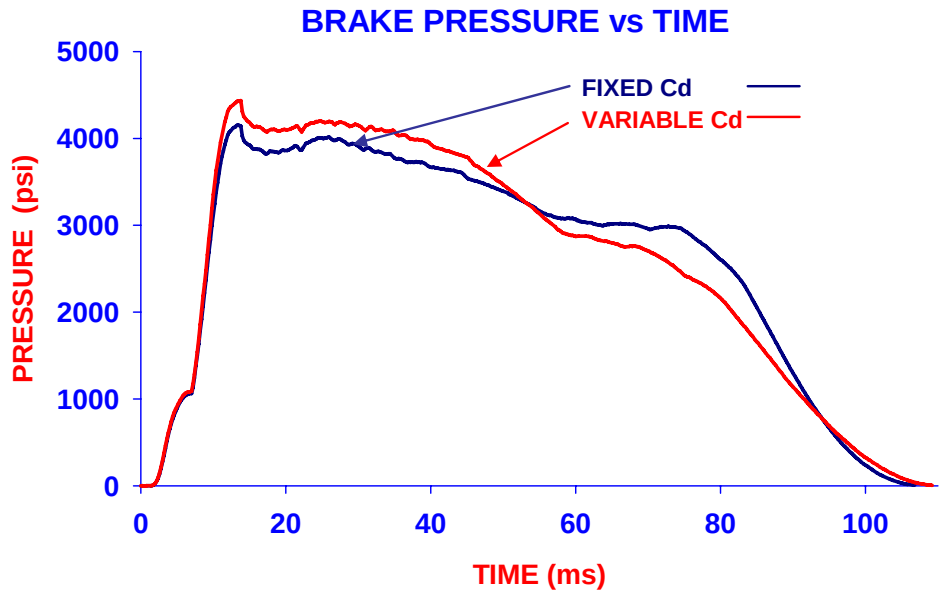

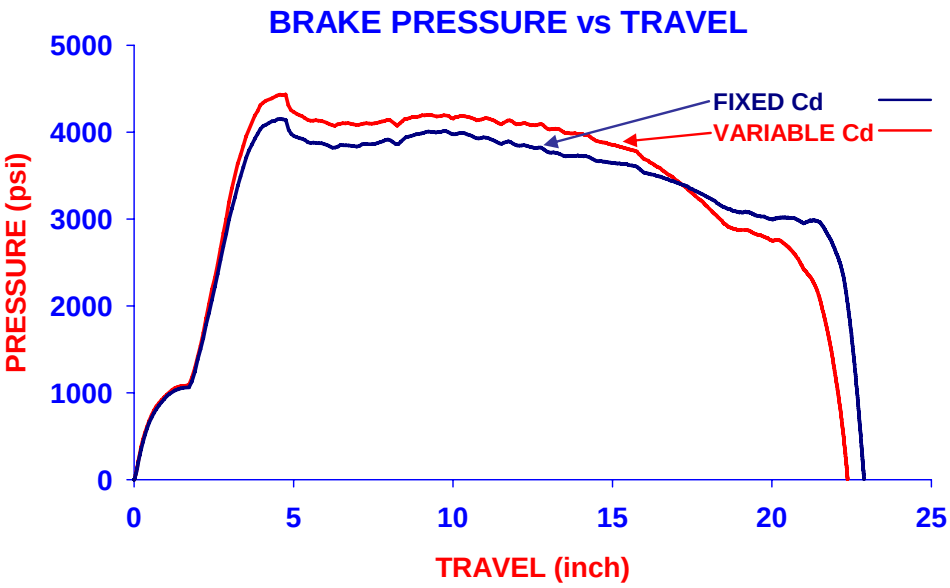

Figure 33. Simulated Brake Pressure Comparison for M829A3 Round

LW120 XM36 RECOIL SYSTEM SIMULATED RESPONSE
RECOIL STROKE: 23.5 inch; ROUND: M829A3 (AMB)
FIXED and VARIABLE Cd

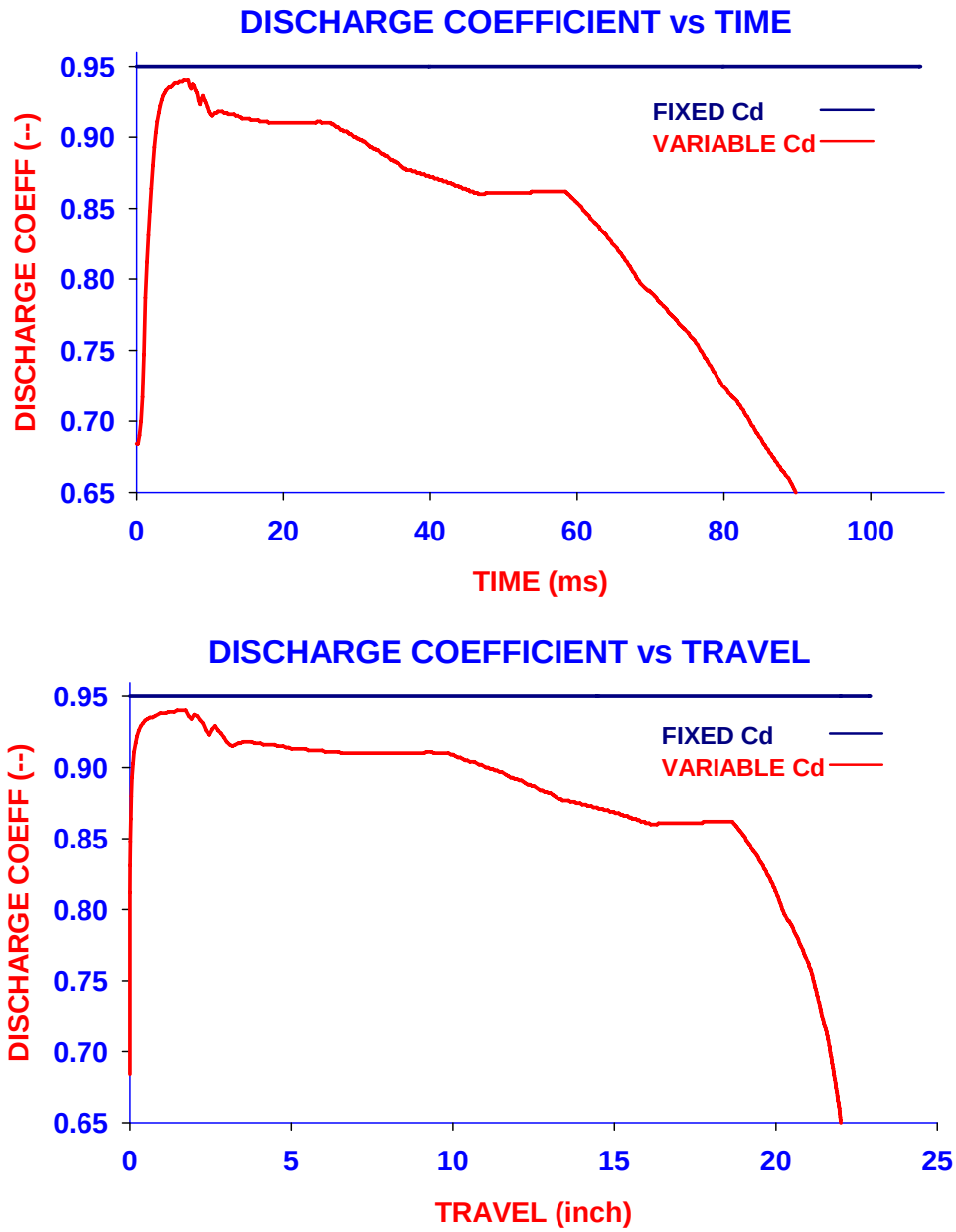

Figure 34. Simulated Discharge Coefficient Comparison for M829A3 Round

LW120 XM36 RECOIL SYSTEM SIMULATED RESPONSE
RECOIL STROKE: 23.5 inch; ROUND: M831A1 (AMB)
FIXED and VARIABLE Cd

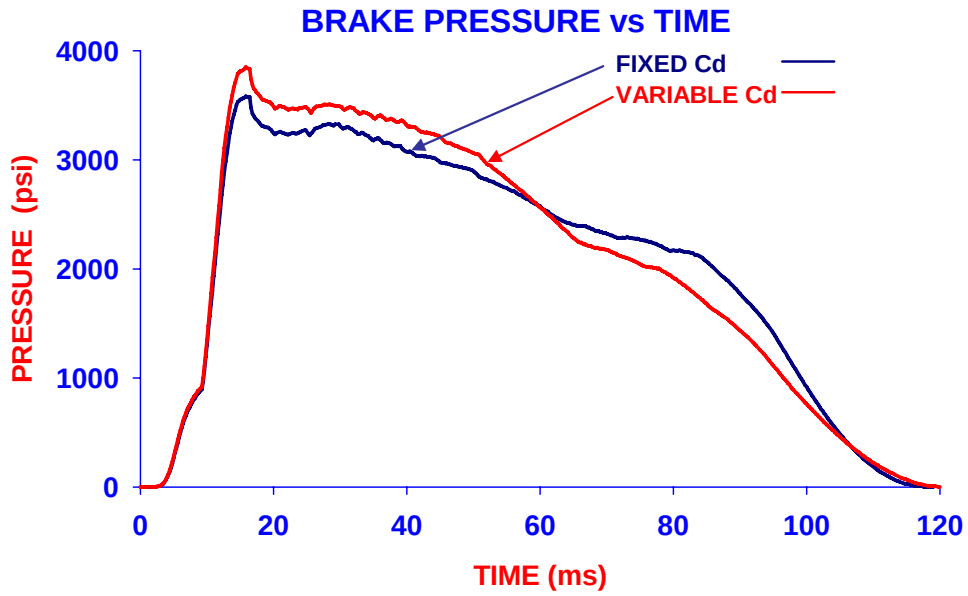

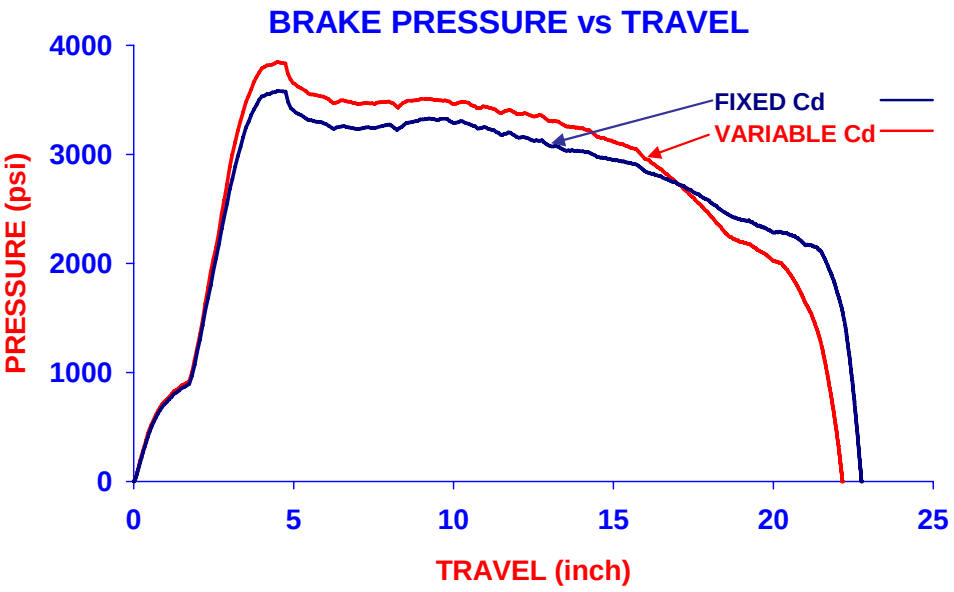

Figure 35. Simulated Brake Pressure Comparison for M831A1 Round

Brake pressures for the M831A1 round are shown on Figure 35. The upper plot shows pressure versus time whereas the lower plot presents pressure versus travel. The blue line is the response for a fixed value of C_d , whereas the red line is the response for variable C_d values. Peak pressure values for both are about 3550 to 3850 psi. During the initial state of recoil (time < 15ms; travel < 3 inches), both responses track each other. From this point, the variable C_d model diverges quickly and overshoots the fixed model by about 300 psi. This occurs just short of 18 ms at a travel value of 5 inches. This response separation continues up to about 60 ms and 17.0 inches of travel. At this point, the pressure responses cross each other and the variable model predicts pressure values that are up to 400 psi lower than the fixed model. Total recoil stroke for the variable model is about 0.6 inches shorter than the same for the fixed model, whereas the timing difference is negligible. C_d values are plotted against time and travel for the M831A1 round on Figure 36. The fixed value of 0.95 is shown along with the values determined within the dynamics analysis loop in the recoil analysis routine. The variable C_d response starts quite low but then rises quickly to its peak value of 0.94 within 10 ms of shot initiation and 2 inches of travel. At its peak, the C_d variation between fixed and variable is only 0.01. The C_d reduces slightly at 17 ms (4 inches of travel) and remains at this level until about 30 ms (10 inches of travel). From this time and travel location, the C_d reduces very slowly to about 0.85 at 55 ms and 16 inches of travel. It then reduces rapidly eventually to a value of 0.45 at 120 ms which is not shown on the plot.

Brake pressures for the M865 round are shown on Figure 37. The upper plot shows pressure versus time whereas the lower plot presents pressure versus travel. The blue line is the response for a fixed value of C_d, whereas the red line is the response for variable C_d values. Peak pressure values for both are about 2150 to 2350 psi. During the initial state of recoil (time < 12ms; travel < 3 inches), both responses track each other. From this point, the variable C_d model diverges quickly and overshoots the fixed model by about 200 psi. This occurs just short of 19 ms at a travel value of 5 inches. This response separation continues up to about 75 ms and 17.0 inches of travel. At this point, the pressure responses cross each other and the variable model predicts pressure values that are up to 200 psi lower than the fixed model. Total recoil stroke for the variable model is about 0.1 inches shorter than the same for the fixed model whereas the timing difference is 1.5 ms. C_d values are plotted against time and travel for the M831A1 round on Figure 38. The fixed value of 0.95 is shown along with the values selected within the

LW120 XM36 RECOIL SYSTEM SIMULATED RESPONSE
RECOIL STROKE: 23.5 inch; ROUND: M831A1 (AMB)
FIXED and VARIABLE Cd

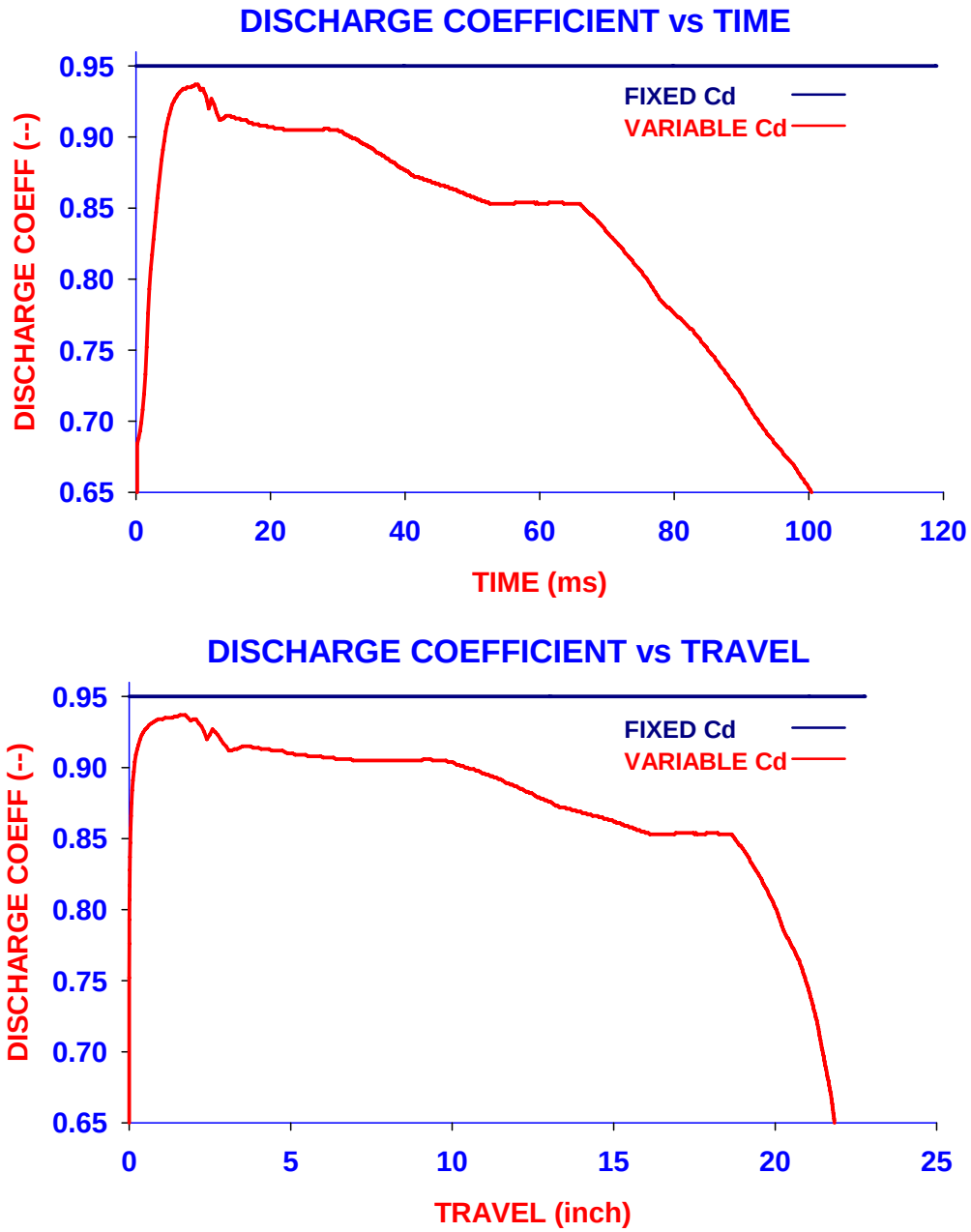

Figure 36. Simulated Discharge Coefficient Comparison for M831A1 Round

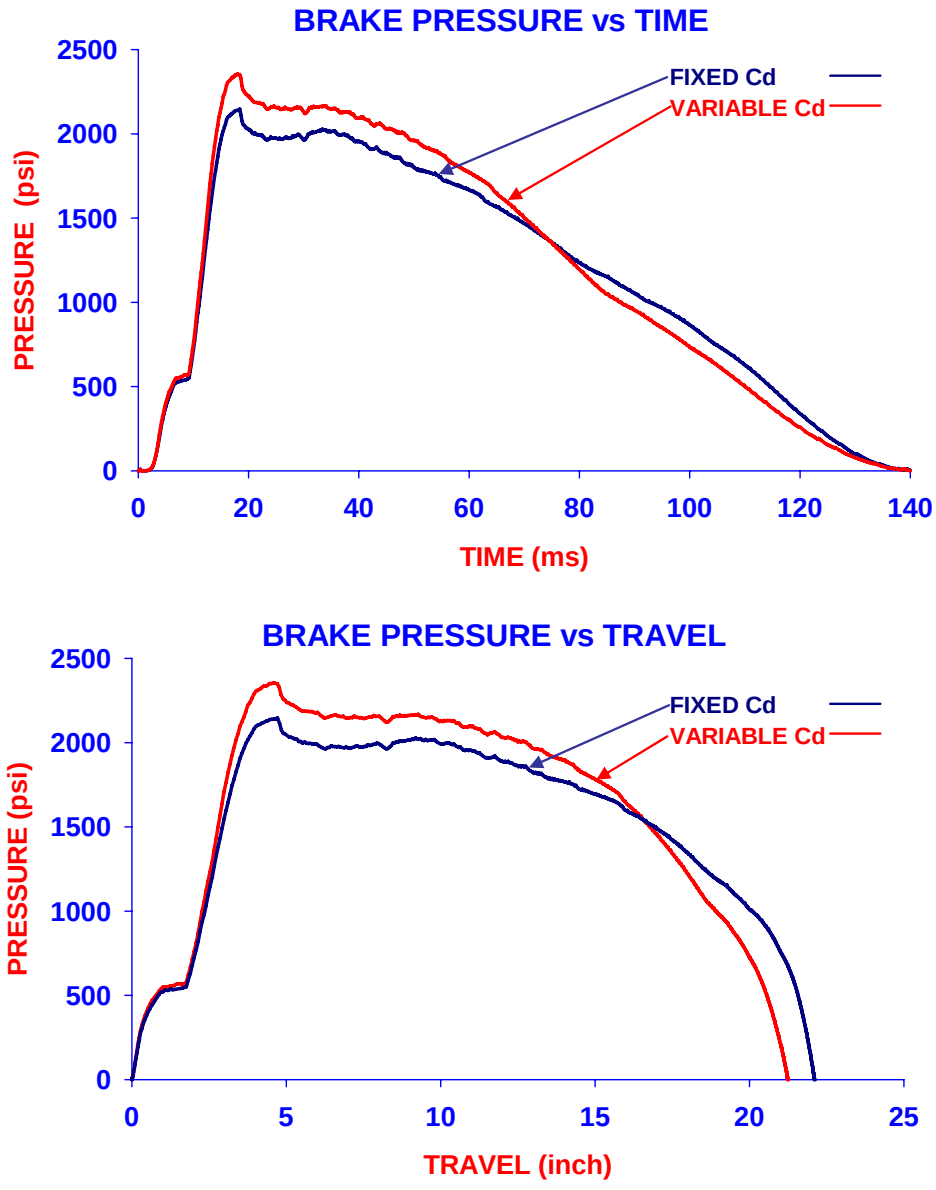

Figure 37. Simulated Brake Pressure Comparison for M865 Round

LW120 XM36 RECOIL SYSTEM SIMULATED RESPONSE
RECOIL STROKE: 23.5 inch; ROUND: M865 (AMB)
FIXED and VARIABLE Cd

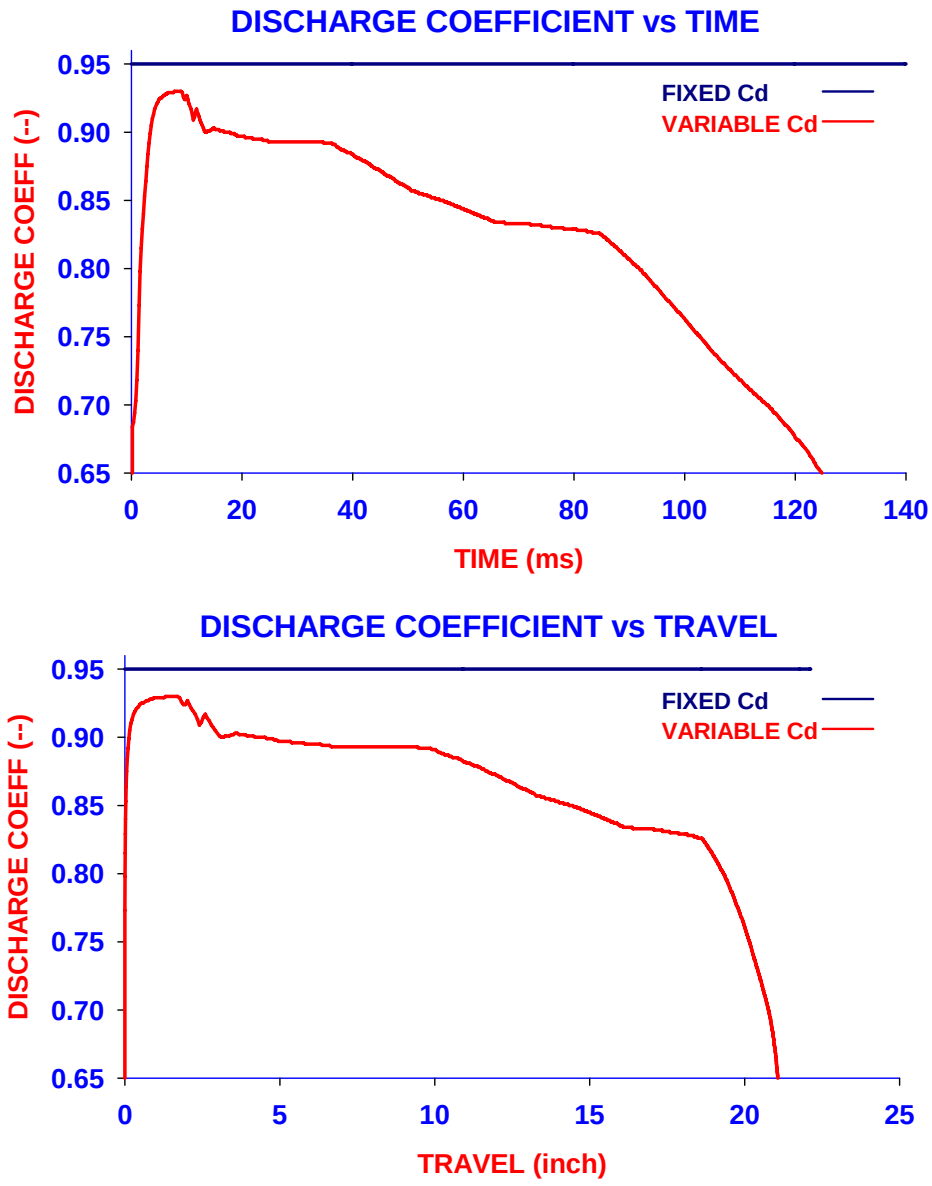

Figure 38. Simulated Discharge Coefficient Comparison for M865 Round

dynamics analysis loop in the recoil analysis routine. The variable C_d response starts quite low but then rises quickly to its peak value of 0.93 within 8 ms of shot initiation and 2 inches of travel. At its peak, the C_d variation between fixed and variable is only 0.02. The C_d reduces slightly to about 0.90 at 17 ms (4 inches of travel) and remains at this level until about 38 ms (10 inches of travel). From this time and travel location, the C_d reduces very slowly to about 0.83 at 65 ms and 17 inches of travel. It then reduces rapidly eventually to a value of 0.45 at 140 ms which is not shown on the plot.

In general, the comparison between the fixed and variable models was consistent for all three round types considered. The variable model produced peak pressure values slightly greater than the fixed. The pressure response for the variable model exceeded the same for the fixed for about one-half of the recoil cycle in time and three-quarters in travel. Subsequently, the variable model's response was less than the fixed. The maximum C_d value for the variable model was slightly less than the expected value of 0.95 and reduced in a similar manner as time and recoil stroke progressed. The final values for C_d always became quite small as recoil speed decreased and area ratio increased.

Comparison of Test Data to Predictions from Simulations

In order to determine the benefit in using this new analysis algorithm, we shall compare results against brake pressure data collected during firing. During the various ATD tests of the XM360 weapon there were occasions during which several shots were fired in a relatively short period of time. For example, the Target Impact Dispersion (TID) test dictated that the firing cadence be as quick as possible. As a norm, these tests usually required the firing of at least 10 rounds to get meaningful data. During the ATD-1 tests three round types were fired in this manner during a 2 day period. We shall use these results to assess the worth of the variable C_d as compared to a fixed C_d analysis model. As an indication of the robustness of the recoil system, we shall compare brake pressure data for several rounds on a single plot and superimpose the average response of the rounds.

The first of these is shown on Figure 39 on which the brake pressure data response for 9 shots of the M829A3 round. The upper plot contains the data for the upper left brake whereas the lower plot has the data for the lower right brake. The 'dust particle' plot (points only) is the data results for all 9 shots whereas the heavy line plot is the average of the 9 shots. The similarity of the response for each brake is

LW120 XM36 ATD #1 RECOIL SYSTEM TEST RESPONSE
TEST ROUNDS #28-36 (8/04/04); M829A3 ROUND

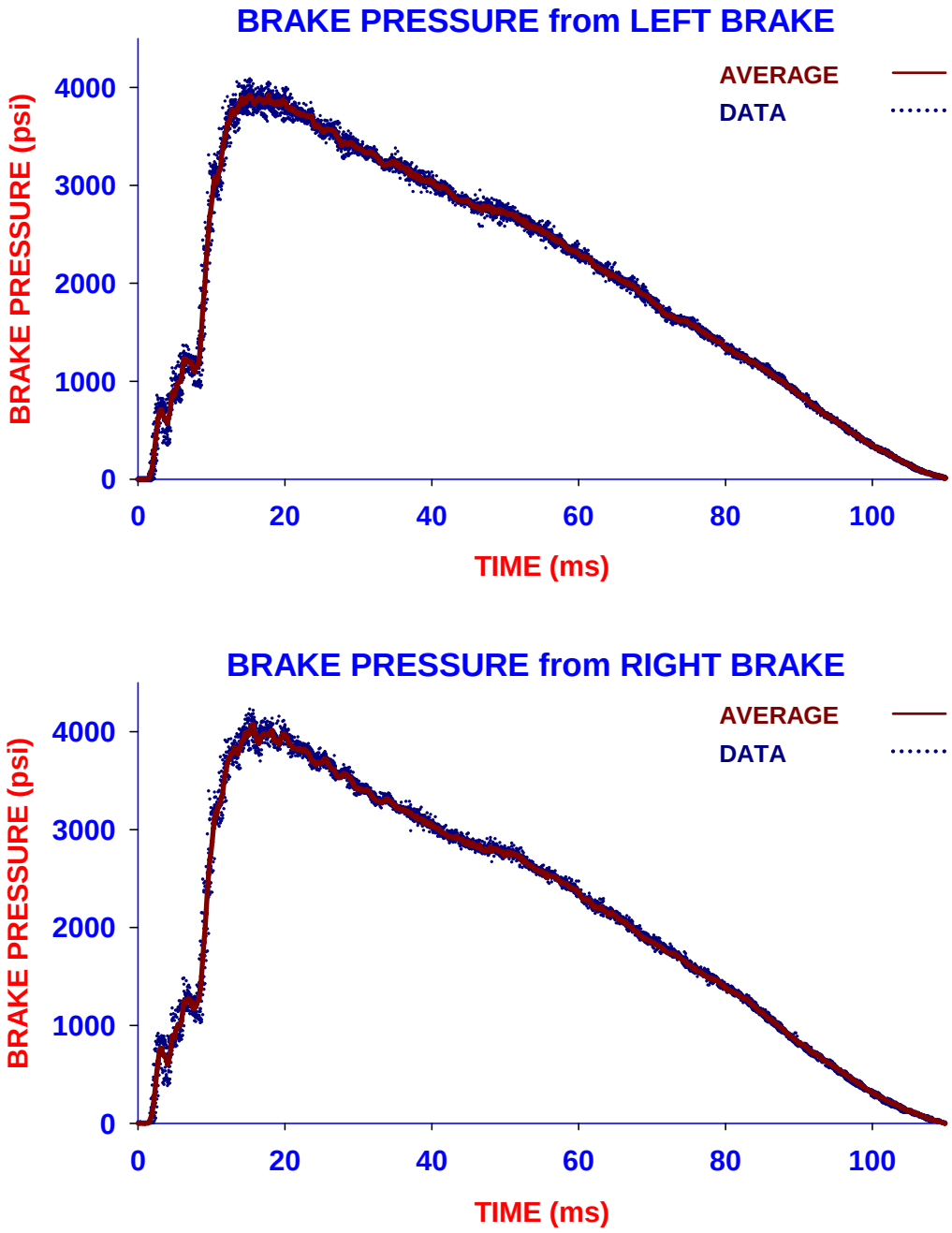

Figure 39. ATD-1 Test Results Brake Pressure M829A3

noteworthy. Additionally, the variation from shot to shot is minimal indicating stability in the design of the components. The meandering of the 'dust particles' from the average is only indicated during the early portions of the response and just beyond the peak level. Subsequent to this, pressure values from the individual responses are indeterminable from the average. Figures 40 and 41 contain the same type of data for the M831A1 and M865 rounds. For these rounds, the within round variation in the pressure response is slightly larger, especially early in the cycle. However, the shot to shot stability is quite good. The average data for these round types will be used as comparison with the simulation runs.

These test firings were conducted in August of 2004 at Aberdeen Test Center where the ambient temperature range is usually between 90^{o}F and 100^{o}F. Since we do not have fluid nor brake cylinder temperature data for these tests, a reasonable estimate would be between 100^{o}F to 125^{o}F and possibly higher depending upon the intensity and duration of radiant solar heat. One would think that this would produce a marginal change in results, but the fact is the viscosity of the fluid at 100^{o}F is about 60 percent of its value at 75^{o}F. The density change, however, is negligible. An initial set of simulations and comparisons were completed using the 'data' from the C_d tables developed using a fluid temperature of 75^{o}F and the results were not bad but the peak pressure was over-predicted by 200 to 700 psi depending upon round type.

At this point in the project, we decided to reevaluate the C_d calculations at an elevated temperature of 100^{o}F to determine its sensitivity to temperature. The complete list of CFD models were rerun at a fluid temperature of 100^{o}F and the results collected for comparison. The CFD results for area ratios of 23.5 and 12.7 are shown on Figure 42. On this figure C_d is plotted against flow rate for the fluid temperature values of 75^{o}F and 100^{o}F. As indicated the distribution for the higher fluid temperature model is slightly to significantly greater than the lower temperature. For the smaller area ratio value (12.7) which would occur early in the cycle at high flow rate values, the C_d values are 0.01 to 0.03 units greater at the higher temperature. At the larger area ratio (23.5) the C_d values are greater at the higher temperatures but eventually converge at the highest flow rates. The additional benefit gleaned from running this additional CFD analysis was that we could extrapolate to other proximate temperatures without the need

LW120 XM36 ATD #1 RECOIL SYSTEM TEST RESPONSE
TEST ROUNDS #47-56 (8/05/04); M831A1 ROUND

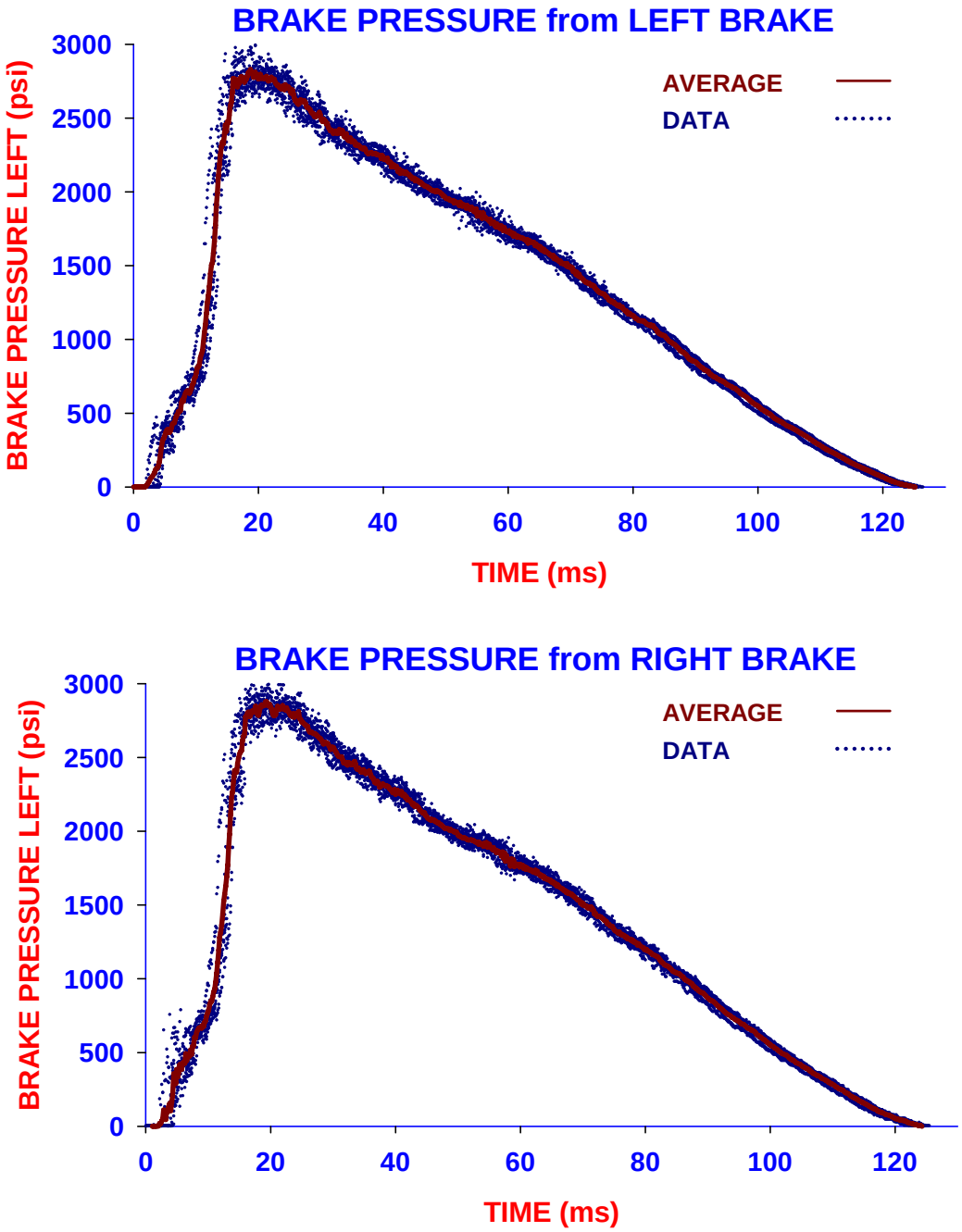

Figure 40. ATD-1 Test Results Brake Pressure M831A1

LW120 XM36 ATD #1 RECOIL SYSTEM TEST RESPONSE
TEST ROUNDS #38-46 (8/05/04); M865 ROUND

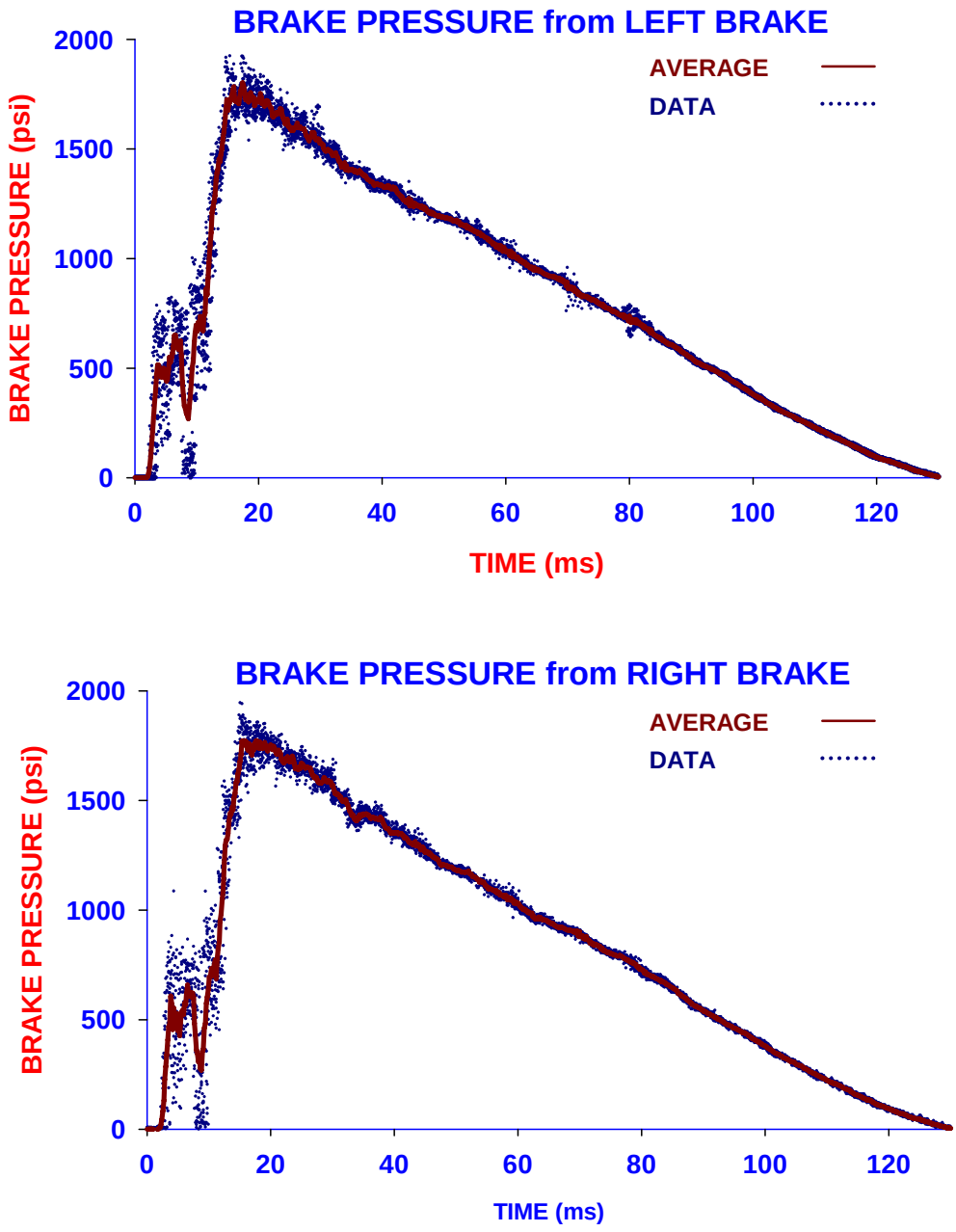

Figure 41. ATD-1 Test Results Brake Pressure M865

CFDesign ANALYSIS OF RECOIL CYLINDER / ORIFICE FLOW
FLUID: HYDRAULIC BRAKE @ 75°F & 100°F

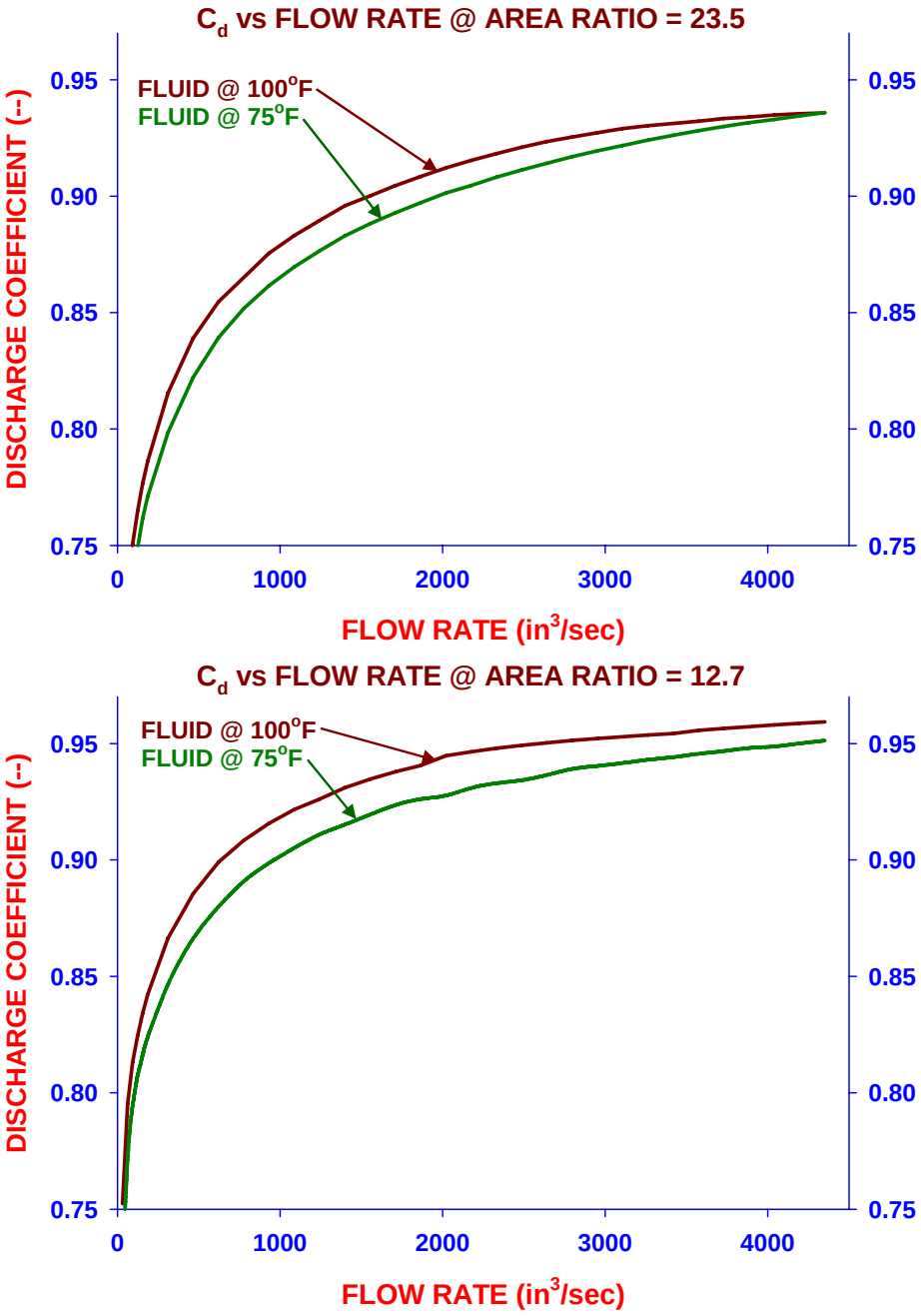

Figure 42. CFD Calculations @ Various Fluid Temperatures

to run the complete CFD model at the expected temperature. For the comparisons detailed below, we extrapolated the C_d values to 125°F using the CFD 'data' from the two temperature dependent runs (75ºF and 100ºF) and assumed a linear response beyond the temperature range. We cannot justify the linear extrapolation until additional analyses are conducted, however, for this exercise this should be acceptable.

Figures 43 through 45 contain graphical results comparing the test data and simulations. The graphs on these figures present brake pressure versus time in the upper plot and pressure versus travel in the lower plot. Within each, three graphs entitled TEST DATA, VARIABLE C_d @ 125°F and FIXED C_d @ 125°F are indicated. The assumed value for the fluid temperature was 125°F, thus the table of C_d values had to be extrapolated to 125°F using the values at 75°F and 100°F. The test data used for comparison is the average response for the series of shots as indicated previously. The C_d value used for the fixed model was 0.95.

Results for the M829A3 round are shown on Figure 43. As indicated, the simulated responses for either fixed or variable C_d are quite similar. Before peak pressure is reached (up to 17ms and 5 inches of travel) the results from both models are essentially superimposed. However, at peak pressure the variable model predicts a pressure value that is slightly less than its fixed C_d counterpart. Additionally, the "sharpness factor" which is the plateau-type flat is characteristic for both models. Early in the cycle, test data indicates a response that is greater than either model. However, at peak pressure the data response is slightly lower than either, its timing somewhat later (20 ms and 6 inches) and its duration much broader without the "sharpness factor" that is indicated in the simulations. Beyond peak pressure and up to 60 ms and 15 inches of travel, both models over predict the data by as much as 300 to 500 psi depending upon the model. The response from the variable C_d model is more consistent with the data than the fixed C_d model during this portion of the cycle. At 90 ms, both simulation models and the data converge at about 800 psi and the end of cycle occurs at 110 ms for both models and the data. Maximum travel for variable model exceeds the data by about one-half inch, whereas for the fixed model the difference is about one inch.

LW120 XM36 ATD #1 RECOIL SYSTEM TEST RESPONSE
SHOT #28-36 (8/4/04) M829A3
AVERAGE TEST RESPONSE & SIMULATION

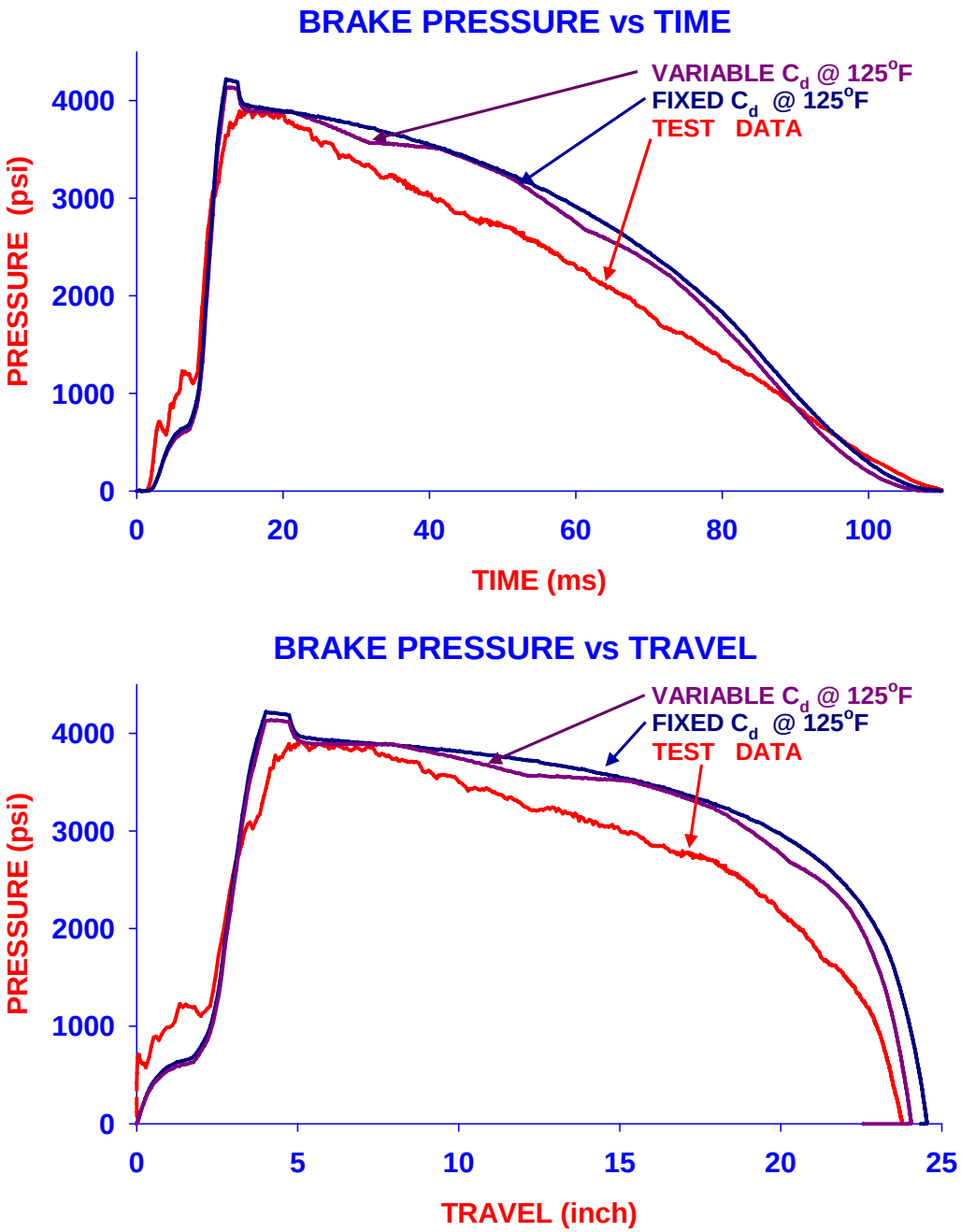

Figure 43. Comparison of Brake Pressure for M829A3 Round

LW120 XM360 ATD-1 RECOIL SYSTEM TEST RESPONSE
SHOTS #47-56 (8/5/04) M831A1
AVERAGE TEST RESPONSE & SIMULATION

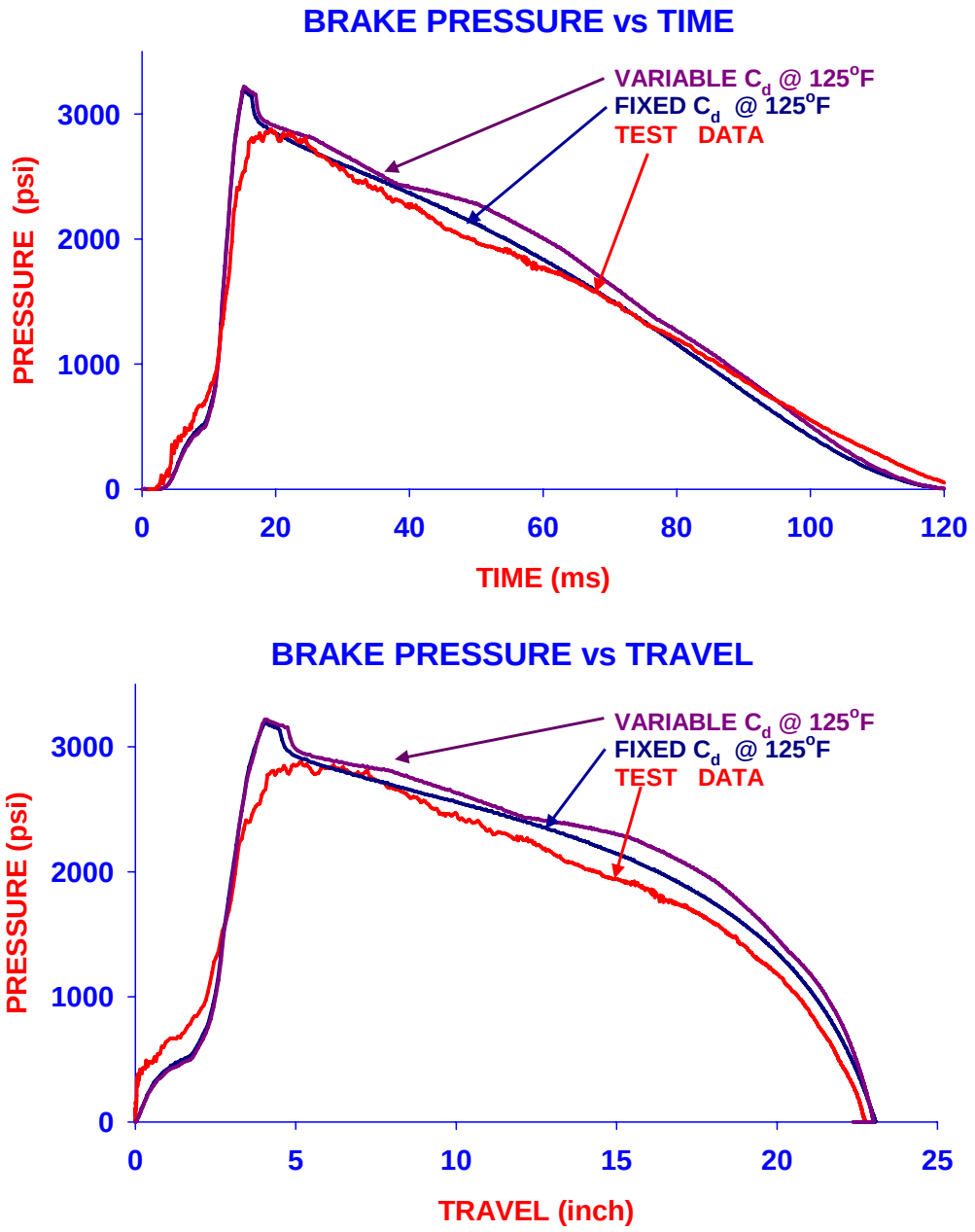

Figure 44. Comparison of Brake Pressure for M831A1 Round

LW120 XM36 ATD-1 RECOIL SYSTEM TEST RESPONSE
SHOTS #38-46 (8/5/04) M865
AVERAGE TEST RESPONSE & SIMULATION

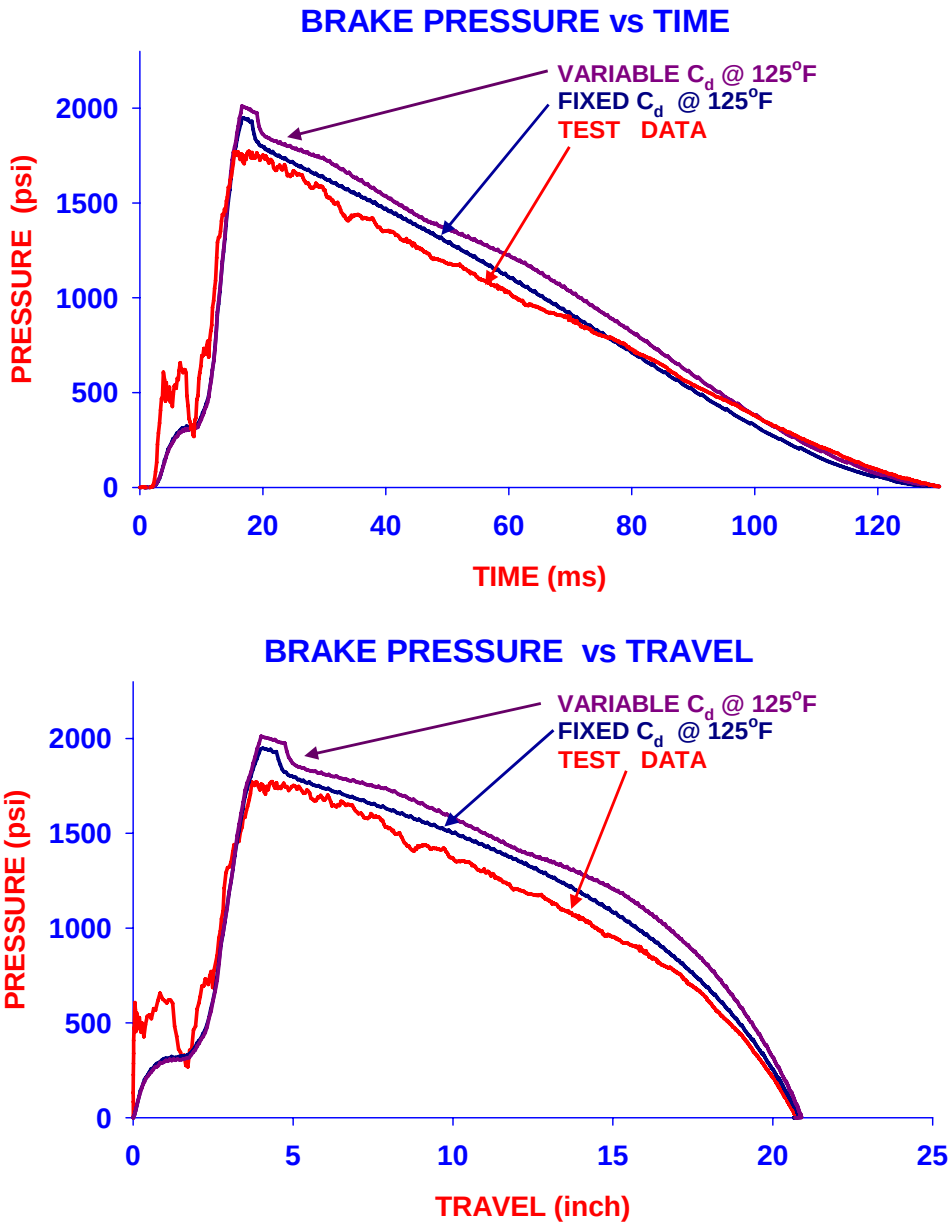

Figure 45. Comparison of Brake Pressure for M865 Round

Results for the M831A1 round are shown on Figure 44. In a manner that is similar to the previous round, the simulated responses for either fixed or variable C_d are quite similar. Both track exactly prior to the achievement of the peak pressure value. The “sharpness factor” exists at peak pressure with a value that exceeds the data by about 400 psi. The prediction from the variable C_d model is slightly greater than for the fixed. During certain portions in the cycle beyond peak pressure, the prediction from variable model exceeds the fixed model by a few hundred psi. During the decay portion both simulation responses converge at 100 ms. The total cycle time for both models and the data is around 120ms. The results plotted against travel indicate the same trends as reported above. Both simulation models slightly over predict pressure for the complete length of travel. In addition, the predicted maximum travel slightly exceeds that of the data by about one-half inch.

Results for the M865 round are shown on Figure 45. With the exception of the first 15 ms of data, the similarities and discrepancies indicated in the previous results are the same for this round. Both simulation models over predict the data by at most a few hundred psi with the differences from variable model slightly greater than the fixed. However, maximum travel as predicted by both models is the same as the data. Regarding the early portion of the cycle and recalling that the data and average for the 10 M865 rounds were shown on Figure 42, the ‘dust’ plots of the individual shots during this portion of the cycle were rather ‘chaotic’. This resulted in an average that captured the erratic nature of the data as well.

On Figure 46 the calculated C_d values (determined from the flow rates in recoil analysis code) for all three round types as well as the value for the fixed C_d model are presented. The upper plot contains these values potted against time whereas on the lower plot these results are plotted against travel. The range of values for the variable C_d is 0.50 to 0.98. As indicated, the C_d values achieve their maximum of 0.98 early in the recoil cycle. For the first 4 inches of travel and 20 ms in time, these sustained levels are greater than the previously assumed value of 0.95. Subsequently, the trend decreases from their maximum values to a sustained level ranging from 0.91 to 0.93 for a significant portion of the cycle. An abrupt ‘knee’ in all three plots is shown to occur towards the end of the cycle when 20 to 22 inches of travel has been achieved. Overall, the C_d distribution contains areas of distinct oscillations. This is most likely due to the nature of the fitting function used for finding the C_d values between independent variable

LW120 XM36 ATD #1 RECOIL SYSTEM TEST RESPONSE
C_d VALUES from SIMULATION CALCULATIONS

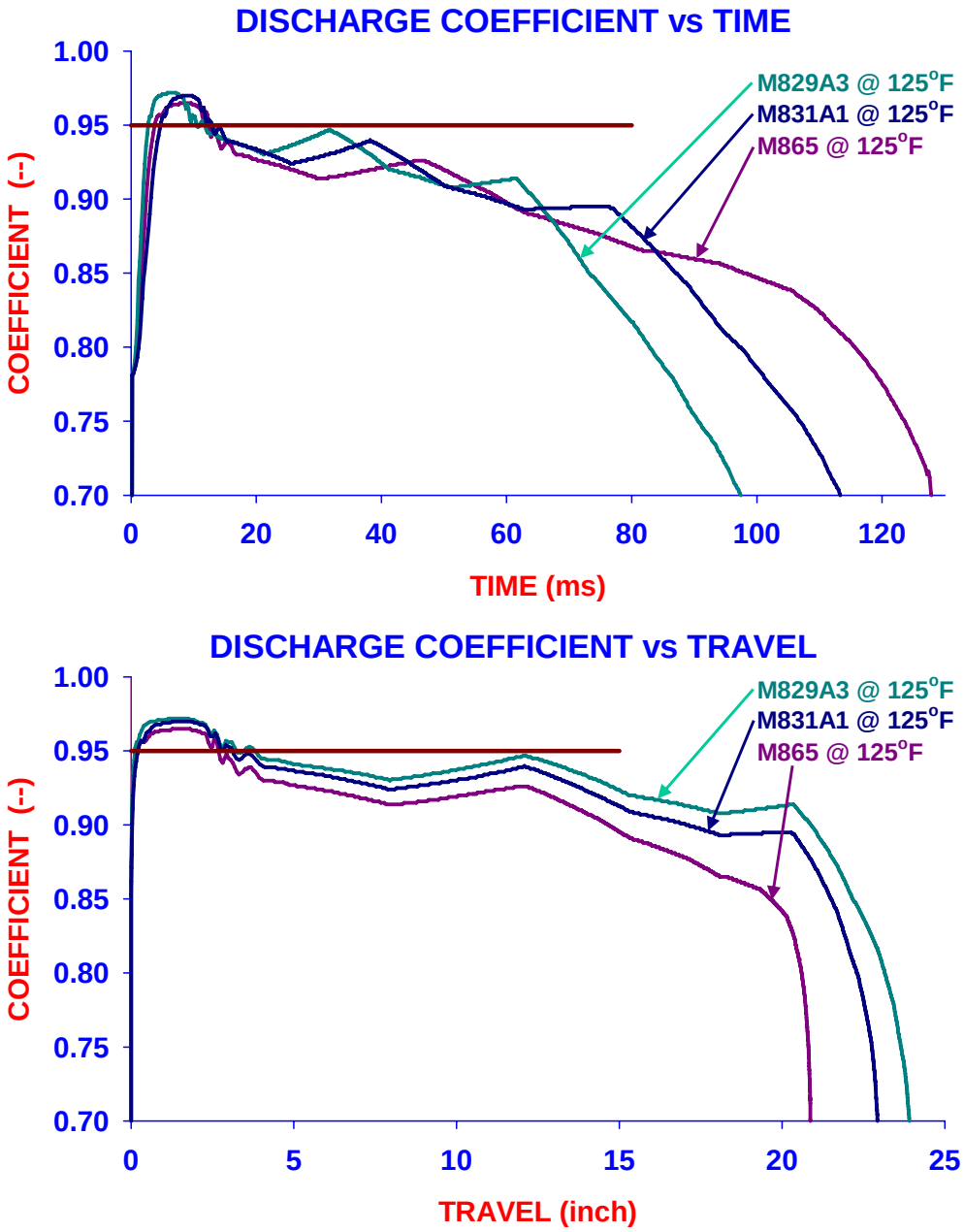

Figure 46. Comparison of Calculated C_d Values

points. Recalling Figure 28, on which the C_d response as a function of area ratio is shown, the trend is linear on the semi-logarithmic plot, however, the individual 'data' points meander above and below the trend line. The fitting function used in the analysis uses a linear fit between area ratio points thus the C_d value would tend to oscillate above and below the trend line. The remedy would be to use the trend line to predict the C_d values or reduce the number of area ratio points in the table of values.

Discussion of the Significance of the Fixed and Variable Discharge Coefficient Method

Although the results did not indicate predictive capabilities that are much better than we currently have using an assumed and fixed C_d, we did demonstrate that the using off-line CFD results as 'data' to the recoil analysis simulations does lend itself to results that are comparable to our current capabilities. Since we have been conducting recoil design and analysis for at least 25 years at Benét Labs, we possess the experience needed to estimate appropriate C_d values from the myriad of test data and simulation runs generated during this time. Since the characteristics of the flow path from the annular chamber of the brake and through the orifice is similar to all previous models that have been built and tested, the choice of a C_d value of 0.95 for the XM360 system is consistent and renders very accurate predictions of test results. In addition, when the C_d values from CFD analysis and dynamic simulations are compared to the extrapolated values from firing data (Figures 16 – 18), the distribution is similar. The C_d value is large during early phases of recoil (0 to 5 in), and then decreases slowly as recoil stroke approaches its maximum value.

However, there are still other considerations. For example, the accuracy of the test data is questionable, especially during the early portion of the cycle when speeds, flow rates and area ratios are changing rapidly. The data from Figures 43 through 45 indicated a rather benign peak in the pressure response whereas the simulations show a sharp and distinct peak. Data was extracted from a gage located in the brake cylinder's the fill port which is not embedded directly in the fluid and at a 90º offset from the direction of flow, thus the recorded data may not be commensurate with the average pressure in the stream. Another possible contributor is the elastic response of the cylinder structure that may have affected the accuracy of the recorded pressure. Currently, this is our best method for determining pressure response and may continue to be for some time.

The real worth of this exercise may be in determining the relationship between pressure and flow rate for flow paths and orifice geometries that are not consistent with our current models. For example, in counter recoil, the main orifice contributes to the generation of counter recoil forces in a manner that is similar to recoil, however, the orifice shape that is presented to the reverse flow is 'flange-like' with a sharp taper to the throat. This feature is much different than in the recoil direction. Again we have been using C_d values derived from firing data (albeit, we could not get reasonable force nor kinematics data until the XM360 program) and have found the value to be somewhat lower than it is in the recoil direction. However, by using the same CFD models developed for the recoil direction, the C_d values in counter recoil may be determined by reversing the inlet and outlet boundaries and the direction and magnitude of flow rate. The Bernoulli Equation and the calculation of C_d values in spirit is the same in counter recoil as it is in recoil. Also, the flow from the buffer chamber in counter recoil is considerably more complicated than in recoil, moreover, it has been shown through unsteady CFD analysis that cavitation bubbles that form during recoil collapse, and in some cases pass over the buffer plug and into the rear cavity [8]. So, in a manner similar to the methods presented in this work, we may use CFD analysis to predict the relationship between flow rate and fluid pressure in the counter recoil direction for flows emanating from the buffer chamber.

Discussions and Conclusions

Summary of Analysis Philosophy and Results

As detailed in the introduction, the motivation driving the conduction of this study is the need to more accurately model the flow variables within the chambers of recoil brakes in a dynamic environment. Since the recoil brake provides greater than ninety percent of the retarding force in recoil, it is essential that the most accurate method of modeling this component is employed. Prior to this work, several assumptions regarding the efficiency of the brake's main orifice were taken from published values for restrictors of similar geometry. Neither the fluid characteristics nor the flow regime was factored into these values. In addition, a method of 'backing out' these values from field generated test data proved to be somewhat subjective as well. We concluded that a better method could be devised by combining the results of an off-line and more detailed CFD analysis to the simplified recoil brake model currently used for analysis. There have been attempts at using a full-blown CFD dynamic analysis model of recoil brake

performance but due to the 3D nature of the flow and the need for fine grid meshing, a real-time analysis is quite difficult to achieve. However, the use of parallel processing and higher speed super computers should dramatically speed up analysis turn-around times. We devised a method of modeling the intricate flow paths within a recoil brake and calculate the orifice efficiency using a CFD flow model, the results of which were tabulated against flow areas and rates. Although this required several CPU hours and weeks to conduct these studies, once completed the results were used repeatedly as 'data' for the one degree of freedom Benét Labs recoil model.

Unfortunately, the viscosity value of the fluid (being a strong function of fluid temperature) greatly influenced the C_d values calculated in the CFD analysis. A new table of values had to be generated in order to best model the firing data since the fluid temperature of the data was approximately 110°F to 125°F and not the 75°F used in the initial CFD analysis. One may postulate that a better independent variable may be the Reynolds Number of flow through the orifice since fluid properties (at any temperature), flow rate and geometric structure are intrinsic to this value. To determine the worth of this hypothesis we conducted a cursory CFD analysis for a single area ratio (12.12) with fluid at various temperatures and the same list of flow rates expected during actual firing of the weapon. Seven values for fluid temperature along with their comparable values for specific gravity and dynamic viscosity were used along with sixteen flow rates. Thus, 112 separate runs comprise this mini analysis. The results are presented on Figure 47 in the form scatter plots of C_d versus Reynolds Number using two axes types. In the upper plot the C_d values are plotted on a linear scale whereas the Reynolds Number is shown on a common logarithm scale. In the lower plot both C_d and Reynolds Number values are shown on a common logarithm scale. The structure of these results is quite striking and indicates extreme tractability in that the results tend to meld into each other as the analysis transitions from one temperature to another. The grey symbols are results at fluid temperature of -50ºF for which the Reynolds number range is ~5 to ~300. The cyan symbols at the other extreme are for a temperature of 250ºF for which the Reynolds number range is ~8500 to ~600,000. Thus, the entire range for Reynolds Number is 5 to 600,000. The results as presented on the Log-Log plot indicates more linearity for the lower values of Reynolds Number as well a flatter response at upper values. All in all, it is the same set of data and the reason for presenting on both axes is to show that a rather benign fitting function could be devised to extrapolate values between 'data'

points, yielding very acceptable results. We shall continue exploring this idea at different area ratios. In fact, we may discover that since area ratio is mildly contained in the Reynolds Number (i.e. the hydraulic radius is contained in the numerator), all models may meld together. This would quite serendipitous, in that a single 'data' file of C_d values with only Reynolds Number as the independent variable could be devised. Since the Benét Labs recoil model requests fluid temperature the Reynolds Number may be calculated within the dynamic loop and the appropriate C_d value found. The burden would only be the time needed to set up and extract results from the bank of runs (which is minimal) and the CPU time needed to conduct these runs (which for some geometries is quite extensive).

When applied to current data from XM360 gun firings, this variable C_d method proved to be as good a predictor of the brake pressure data as the previous fixed C_d model. For some regimes of the flow, the variable model more accurately predicted pressure values than did the fixed and vice versa for other regimes. In any event, both models predict pressure values that are quite close to reality, however, if we use the variable model we no longer need to 'guess' at C_d values which has always been problematic at best. In fact, several other restrictor geometries for which C_d data is unavailable could be analyzed prior to the incorporation into brake design or simulation. The only downside is the need for detailed CFD analysis to determine C_d values prior to conducting recoil simulations.

Model Enhancement for Future Endeavors

Since this methodology proved to be useful for the recoil portion of the cycle it would seem lucrative to conduct similar studies for the counter recoil portion. The main flow orifice which controls brake pressure in recoil does the same in counter recoil. However, the geometry and cross section area are not the same nor is the range of flow rates. (In counter recoil the velocity barely reaches 100 in/sec whereas in recoil the maximum speed is ~700 in/sec.) A separate table of values for C_d would have to be included in the recoil model but the method for its incorporation and use is the same as it is for recoil.

In addition, there are other restrictive flow paths through which the fluid flows in counter recoil. The flow from the buffer pocket over and through the buffer plug is quite complicated. There are two parallel paths through which the flow is apportioned. Currently, we use several coefficients to model abrupt entrance and exit effects as well as a dedicated Moody Diagram to determine friction factors along

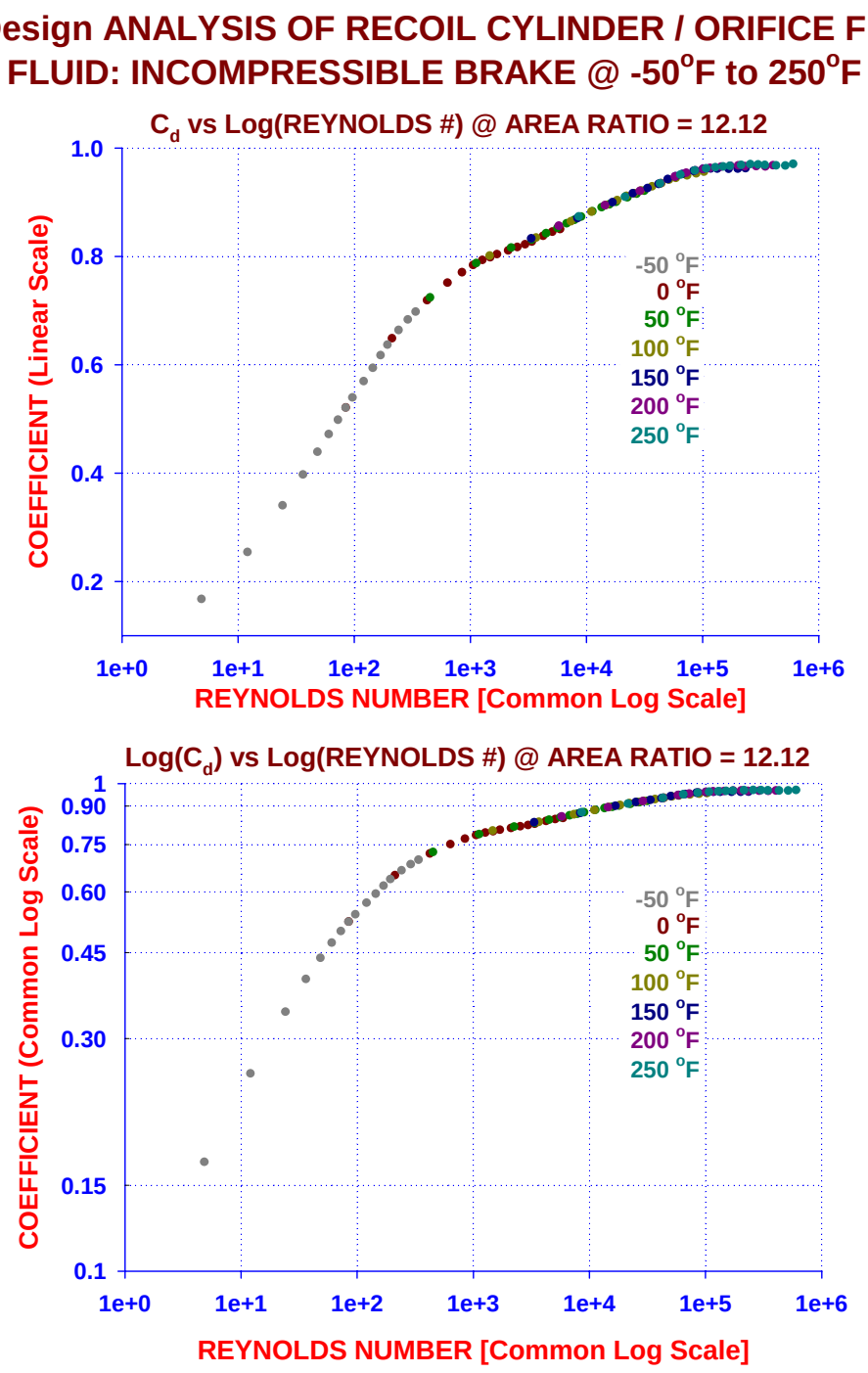

Figure 47. C_d vs Reynolds Number @ Various Fluid Temperatures

the flow length between the external profile of the buffer plug and the circumferential surface of the throttling sleeve. This path has tapers and abrupt changes in diameter as well as circumferential grooves to control the back pressure in the buffer pocket. In fact, it is our experience that modeling flow in these regions is quite a bit more difficult than in the recoil direction. The various entrance and exit coefficients used in the current model have been determined based upon the results of test data in counter recoil and have been set to best match the data. Since the total recoil time is a highly sensitive value for the XM360 program and the fact that counter recoil time comprises the bulk of cycle time it would be quite beneficial to be able to model flow in this regime as well as predicting terminal velocity and total cycle time prior to test firing.

Recommendations for Future Work

As with most comprehensive analyses, the initial findings usually beget the question of how accurate are the results or the fidelity of the models to reality. Earlier we set the ground rules for the CFD analysis to be axisymmetric, incompressible and steady state. We choose these characteristics since the flow equations during any time step within the dynamics loop of the recoil model are those for quasi-steady state conditions. In addition, these model characteristics allowed the conduction of manageable and cost effective analyses from which timely results were extracted. As a follow-on, it may be beneficial to reproduce the pressure and flow rate relationships using another more detailed CFD code namely Fluent©. In addition, the non included characteristics of asymmetry, compressibility, and unsteady motion could be modeled using both CFDesign© and Fluent© to determine their effect. In addition, Fluent© could be used to model multi-phase cavitated flow and more complicated fluid properties that vary as a function of temperature.

Since there are flow paths in the counter recoil direction which are more complicated than those in recoil, the application of the CFD analysis for these paths should be conducted and the results used in the recoil analysis code. However, the results may take on a different flavor. For the recoil direction, the CFD ‘data’ was applied to the steady-state flow equation to determine C_d values used in the recoil analysis code. In counter recoil, since there are flow lengths as well as tapered restrictors, it may be

easier to use the pressure versus flow rate results directly in the recoil model. Currently, we use entrance coefficients and a modified Moody Diagram to determine orifice efficiency and flow length friction factors to achieve the pressure drop along any restrictive path. A direct table of values relating flow rate and recoil position to back pressure would alleviate the need to use the friction diagrams and artificial entrance coefficients.

As recounted earlier, the time required to have a representative set of meaningful data from the CFD models was quite extensive. This was due to many factors. First, the use of the CFDesign© code required an initial 'learning curve' since these authors had no experience in its use. Second, a priori knowledge in the expected results dictated a conservative approach to the grid meshing of the flow regime as well as the number and spacing of independent variable values. Since we now have considerable knowledge in these issues, design of experiments (DOE) techniques may be employed for future use of this methodology. DOE can be used in a sequential approach, starting with simple models and adding (augmenting) as needed. This could have reduced the number of runs required. DOE has built in capabilities within the ANOVA tool sets to tell you if you need more data to get a better fit.

Currently, the design of a brake system begins with the use of a simple spreadsheet code, the input of which comprises operating characteristics along with other fixed and limiting values for geometric structure and fluid. The orifice coefficient is one of the fixed values required. We have always used an appropriate value determined from experience. Output from the design code contains the remaining geometry values for brake and recuperator diameters and lengths as well as a tabulation of the control rod diametrical profile. We treat this table of values as a starting point for the design. The analysis code uses these values to 'refine' the profile for optimization across several operating parameters and dimensional tolerances. Prior to this step and after the basic design of the brake is known, the detailed CFD analysis would be used to determine expected C_d values. In the very least, basic research in this area should continue irrespective of any design program. Several different restrictor characteristics could be modeled to determine the most efficient and optimum regarding the size and weight tradeoff which is always at the forefront of any weapon design. Additionally, our modeling capabilities in recoil would rise to the next level.

REFERENCES

1. Gast, R.G., “Exploitation of the T-62 Recoil System’s Operational Characteristics”, ARCCB-TR-88007, February 1988.

2. Sneck, H.J., “Analysis of a Schneider-Type Recoil Mechanism for the 120mm XM256 Tank Gun”, ARLCB-TR-82017, June 1982.

3. “Recoil Systems”, Military Handbook, DOD HDBK 778 (AR), July 1988.

4. Burden, R.L., Faires, J.D., Reynolds, A.C., Numerical Analysis, 2nd Edition, Prindle, Weber and Schmidt, Boston MA 1981.

5. Giles, R.V., Fluid Mechanics and Hydraulics, Schaum, New York, NY, 1962.

6. Sneck, H.J., Recoil Mechanism Orifice Coefficient Experiment, Informal proposal for experimental work, Benét Labs, May 1991.

7. Bell, K.J., Bergelin, O.P, “Flow-Through Annular Orifices,” Transactions of the ASME, Volume 79, 1957, pp 593 – 604.

8. Cler, Daniel L., “A Simplified 2-D Axi-Symmetric Recoil Brake Unsteady Computational Fluid Dynamics Analysis”, To Be Published.

9. CFdesign home page www.cfdesign.com, February 2007.

APPENDIX

Matlab© C_d Calculator Routine

```
%
%.... Initial code to Determine Cd from data (1/30/07)
%.... This version computes Reynolds #
%.... load 1: Input test data from firing test
%.... load 2: Brake geometric data from drawing
%.... load 3: Travel / Velocity 'DATA' from Sigma Plot Analysis
%
%.... Contains O/P for SP plotting
%
load Rnd_113.dat;
load BL_46569.dat;
%
%.... Set poly order for poly fits for data
%
Nx = 3;
Np = 20;
%
%.... O/P file for SP plotting
%
filename1 = 'Rnd_113_L_R.dat';
%
%
%.... set data into local vectors
%
t    =  Rnd_113(:,1);
x    =  Rnd_113(:,2);
pl    =  Rnd_113(:,3);
pr    =  Rnd_113(:,4);
X_Fit = Rnd_113(:,5);
V_Fit = Rnd_113(:,6);
%.... Brake Geometry Data
Axi =   BL_46569(:,1);
Dia =   BL_46569(:,2);
AreaB = BL_46569(:,3);
%
%.... Set constant values for brake geometry and fluid properties
%
gg = 386.4;
P_test = pr;
wH2O = 62.4/1728;
w = 0.853*wH2O;
nu = .000111646;
mu = nu*(gg/w);
Cyl_ID = 3.312;
ThS_OD = 1.748;
AreaA = (pi/4.)*(Cyl_ID^2 - ThS_OD^2);
Orif = 1.13;
Disc = 0.70;
%
%.... Calculate variable orifice area
%
AreaO = (pi/4.)*(Orif^2 - Dia.*Dia);
```

```
Wperm = pi*(Orif + Dia);
Hyd_Rad = 4*AreaO./Wperm;

%
%.... Calculate poly fits for data
%
Cpl = polyfit(t,P_test,Np);
P_Fit = polyval(Cpl,t);
%
%.... Interpolate all calculations to travel
%
PX_Fit = P_test;
VX_Fit = V_Fit;
AO_Fit = interp1(Axi,AreaO,X_Fit);
AB_Fit = interp1(Axi,AreaB,X_Fit);
Hyd_R = interp1(Axi,Hyd_Rad,X_Fit);
%
%.... Determine flow rate from Annular Chamber
%
Qdot = AreaA.*VX_Fit;
%
%.... Calculate terms used in equation #4
%
T1 = 2*gg/w;
T2 = (Disc.*AreaA.*AB_Fit).*(Disc.*AreaA.*AB_Fit);
T3 = AreaA.*AreaA - (Disc.*AB_Fit).*(Disc.*AB_Fit);
QdotB = sqrt((T2./T3).*T1.*PX_Fit);
%
%.... Calculate terms used in equation #6
%
QdotO = Qdot - QdotB;
%
%.... Calculate terms used in equation #5
%
AreaR = AreaA.*(1./AO_Fit);
V2 = AreaA*VX_Fit;
Reyn = (1/mu)*(V2.*Hyd_R);
T5 = AreaA^2*T1*PX_Fit./(QdotO.*QdotO);
CdO = real(AreaR./(sqrt(T5 + 1)));
%
%.... Reject CdO values above 1.0
%
%for j = 1:size(CdO)
%     if CdO(j) > 1.0
%        CdO(j) = 1.0;
%     end
%end
ho = figure;
plot(t,x,'b:',t,X_Fit,'g-')
%axis([0 120 0 25])
title({'XM360 RECOIL TRAVEL DATA & FIT','ATD-4 TEST ROUND: 104','AMSRD-AAR-
AEW-C','JANUARY 2007'})
xlabel('TIME (m-secs)')
ylabel('TRAVEL (inches)')
grid
plottools
hold
```

```
%
%
%
h1 = figure;
plot(t,P_test,'b-',t,P_Fit,'g-')
title({'XM360 BRAKE PRESSURE DATA & FIT','JANUARY 2007'})
xlabel('TIME (m-secs)')
ylabel('PRESSURE (psi)')
grid
plottools
hold
%
%
%
h2 = figure;
plot(X_Fit,CdO)
%axis([5 20 .8 1.000])
title({'XM360 CALCULATED VALUE FOR Cd from BRAKE DATA','JANUARY 2007'})
xlabel('TRAVEL (inches)')
ylabel('DISCHARGE COEFFICIENT (--)')
grid
plottools
hold
%
%
%
h3 = figure;
plot(V_Fit,CdO)
%axis([100 450 .8 1.000])
title({'XM360 CALCULATED VALUE FOR Cd from BRAKE DATA','AMSRD-AAR-AEW-
C','JANUARY 2007'})
xlabel('VELOCITY (in/sec)')
ylabel('DISCHARGE COEFFICIENT (--)')
grid
plottools
hold
%
%
%
h4 = figure;
plot(AreaR,CdO)
%axis([0 120 0 6000])
title({'XM360 CALCULATED VALUE FOR Cd','JANUARY 2007'})
xlabel('AREA RATIO (--)')
ylabel('DISCHARGE COEFFICIENT (--)')
grid
plottools
hold
%
%
%
h5 = figure;
plot(t,V_Fit)
%axis([0 1 0 600])
title({'XM360 RECOIL VELOCITY FROM DERIVED FIT','JANUARY 2007'})
xlabel('TIME (m-secs)')
ylabel('VELOCITY (in/sec)')
```

```
grid
plottools
hold
%
%
%
h6 = figure;
plot(Reyn,CdO)
%axis([0 120 0 6000])
title({'XM360 CALCULATED VALUE FOR Cd','JANUARY 2007'})
xlabel('REYNOLDS NUMBER (--)')
ylabel('DISCHARGE COEFFICIENT (--)')
grid
plottools
hold
%
%
%

%
%.... O/P data for SP plotting
%
A_Out = [t,x,X_Fit,P_test,P_Fit,V_Fit,AreaR,CdO];
dlmwrite(filename1,A_Out,'delimiter','\t','precision','%.6f');
```

FORTRAN© Subroutine of the Variable C_d Model

```
C....Cdfind:  This routine is used to determine the dynamic discharge
C             coefficient thru the maim orifice of the Schneider-Type
C             recoil brake. It is emperical in nature in that it uses
C             recults from a series of steady state CFDesign runs in
C             which the flow speed and area ratio was varied.
C
C...        ORIGINAL DATE: 01/01/2007
C...        PROGRAMMER: R. G. GAST
C
C.... COMMON BLOCKS: None
C
C
C.... INPUT VARIABLES:
C        Qdot: Volumetric flow rate (in^3/s)
C        Arat: Area ratio of flow resevoir to restrictive orifice (--)
C
C           Cd: Velocity discharge coeficient used in Bernoulli eqn (--))
C
C
C.... OTHER ROUTINES CALLED: NONE
C
C.....................................................................
C
      SUBROUTINE Cdfind(Qdin,Arin,Cd)
C
C.... SET SPECIFICTIONS, DEFINE COMMON AREAS, DIMENSION MATRICES
C
            implicit real*8 (A-H,O-Z)
            dimension QQ(100),AA(100),CC(100,100)
            DATA ktrip /1/
c
c.... initial excursion read data
c
            If(ktrip .eq. 1) then
c
c.... Read area ratio values and save as common logarithm
c
             do 15 Ka = 1,100
              read(28,*)Aval
              if (Aval .GE. 0.0) then
               AA(Ka) = log10(Aval)
              else
               KA_fin = Ka - 1
               go to 17
              end if
 15          continue
 17          continue
c
c.... Read flow rate values
c
             do 10 Kq = 1,100
              read(28,*)Qval
              if (Qval .GE. 0.0) then
               QQ(Kq) = Qval
```

```
            else
             KQ_fin = Kq - 1
             go to 12
            end if
 10        continue
 12        continue
c
c.... Read discahrge coefficient values
c

            do 20 Ka = 1,KA_fin
             do 20 Kq = 1,KQ_fin
              read(28,*)CC(Ka,Kq)
 20        continue
           ktrip = 2
          end if
c
c.... Reset to local variables and adjust to be within bounds of data
c
          Arat = log10(Arin)
          Qdot = Qdin
c
          if(Arat .LT. AA(1)) then
           Arat = AA(1)
          else if (Arat .GE. AA(KA_fin)) then
           Arat = AA(KA_fin) -.0001*(AA(KA_fin) - AA(KA_fin-1))
          end if
          if(Qdot .LT. QQ(1)) then
           Qdot = QQ(1)
          else if (Qdot .GE. QQ(KQ_fin)) then
           Qdot = QQ(KQ_fin) -.0001*(QQ(KQ_fin) - QQ(KQ_fin-1))
          end if
C
c.... Search algorithm for Q & A bounds
c
          do 30 ka = 1, KA_fin - 1
           if(Arat .GE. AA(ka) .AND. Arat .LT. AA(ka+1))then
            KA_low = ka
            A1 = AA(ka)
            A2 = AA(ka+1)
            go to 35
           end if
 30        continue
 35        continue
          do 40 kq = 1, KQ_fin - 1
           if(Qdot .GE. QQ(kq) .AND. Qdot .LT. QQ(kq+1))then
            KQ_low = kq
            Q1 = QQ(kq)
            Q2 = QQ(kq+1)
            go to 45
           end if
 40        continue
 45        continue
c
c.... Linear search algorithm for Cd value
c
```

```
      delQ = Q2 - Q1
      delA = A2 - A1
      W1 = sqrt(((Arat-A1)/delA)**2 + ((Qdot-Q1)/delQ)**2)
      W2 = sqrt(((Arat-A2)/delA)**2 + ((Qdot-Q2)/delQ)**2)
      Wtot = W1 + W2
      W22 = W1/Wtot
      W11 = W2/Wtot
      C11 = CC(KA_low,KQ_low)
      C12 = CC(KA_low,KQ_low+1)
      C21 = CC(KA_low+1,KQ_low)
      C22 = CC(KA_low+1,KQ_low+1)
c
      dC1dQ = (C12-C11)/delQ
      dC2dQ = (C22-C21)/delQ
c
      dC1dA = (C21-C11)/delA
      dC2dA = (C22-C12)/delA
c
      Cd1 = C11 + dC1dA*(Arat-A1) + dC1dQ*(Qdot-Q1)
      Cd2 = C22 + dC2dA*(Arat-A2) + dC2dQ*(Qdot-Q2)
      Cd = W11*Cd1 + W22*Cd2
c
c****
c
    RETURN
    END
```